UPPSALA
UNIVERSITET

Digital Comprehensive Summaries of Uppsala Dissertations from the Faculty of Science and Technology 1694

Plasma environment of an intermediately active comet

Evolution and dynamics observed by ESA's Rosetta spacecraft at 67P/Churyumov-Gerasimenko

ELIAS ODELSTAD

ACTA
UNIVERSITATIS
UPSALIENSIS
UPPSALA
2018

ISSN 1651-6214
ISBN 978-91-513-0386-4
urn:nbn:se:uu:diva-356426

Dissertation presented at Uppsala University to be publicly examined in Ångström 80101, Lägerhyddsvägen 1, Uppsala, Friday, 14 September 2018 at 13:15 for the degree of Doctor of Philosophy. The examination will be conducted in English. Faculty examiner: Professor of Physics Andrew Coates (University College London (UCL)).

Abstract
Odelstad, E. 2018. Plasma environment of an intermediately active comet. Evolution and dynamics observed by ESA's Rosetta spacecraft at 67P/Churyumov-Gerasimenko. *Digital Comprehensive Summaries of Uppsala Dissertations from the Faculty of Science and Technology* 1694. 90 pp. Uppsala: Acta Universitatis Upsaliensis. ISBN 978-91-513-0386-4.

The subject of this thesis is the evolution and dynamics of the plasma environment of a moderately active comet before, during and after its closest approach to the Sun. For over 2 years in 2014-2016, the European Space Agency's Rosetta spacecraft followed the comet 67P/Churyumov-Gerasimenko at distances typically between a few tens and a few hundred kilometers from the nucleus, the longest and closest inspection of a comet ever made. Its payload included a suite of five plasma instruments (the Rosetta Plasma Consortium, RPC), providing unprecedented in-situ measurements of the plasma environment in the inner coma of a comet.

In the first two studies, we use spacecraft potential measurements by the Langmuir probe instrument (LAP) to study the evolving cometary plasma environment. The spacecraft potential was mostly negative, often below -10 V and sometimes below -20 V, revealing the presence of warm (around 5-10 eV) coma photoelectrons, not effectively cooled by collisions with the relatively tenuous coma gas. The magnitude of the negative spacecraft potential depends on the electron density and traced heliocentric, cometocentric, seasonal and diurnal variations in cometary outgassing, consistent with production at or inside the cometocentric distance of the spacecraft as the dominant source of the observed plasma.

In the third study, we investigate ion velocities and electron temperatures in the diamagnetic cavity of the comet, combining LAP and Mutual Impedance Probe (MIP) measurements. Ion velocities were generally in the range 2-4 km/s, well above the expected neutral velocity of at most 1 km/s. Thus, the ions were (at least partially) decoupled from the neutrals already inside the diamagnetic cavity, indicating that ion-neutral drag was not responsible for balancing the outside magnetic pressure. The spacecraft potential was around -5 V throughout the cavity, showing that warm electrons were consistently present inside the cavity, at least as far in as Rosetta reached. Also, cold (below about 0.1 eV) electrons were consistently observed throughout the cavity, but less consistently in the surrounding region, suggesting that while Rosetta never entered a region of efficient collisional cooling of electrons, such a region was possibly not far away during the cavity crossings. Also, it reinforces the idea of previous authors that the intermittent nature of the cold electron component was due to filamentation of this cold plasma at or near the cavity boundary, possibly related to an instability of this boundary.

Finally, we report the detection of large-amplitude, quasi-harmonic density-fluctuations with associated magnetic field oscillations in association with asymmetric plasma and magnetic field enhancements previously found in the region surrounding the diamagnetic cavity, occurring predominantly on their descending slopes. Typical frequencies are around 0.1 Hz, i.e. about ten times the water and half the proton gyro-frequency, and the associated magnetic field oscillations, when detected, have wave vectors perpendicular to the background magnetic field. We suggest that they are Ion Bernstein waves, possibly excited by the drift-cyclotron instability resulting from the strong plasma inhomogeneities this region.

Elias Odelstad, Swedish Institute of Space Physics, Uppsala Division, Box 537, Uppsala University, SE-75121 Uppsala, Sweden. Department of Physics and Astronomy, Space Plasma Physics, 516, Uppsala University, SE-751 20 Uppsala, Sweden.

ISSN 1651-6214
ISBN 978-91-513-0386-4
urn:nbn:se:uu:diva-356426 (http://urn.kb.se/resolve?urn=urn:nbn:se:uu:diva-356426)

Dedicated to my parents, Lena and Jan,
for their never-ending love and support

List of papers

This thesis is based on the following papers, which are referred to in the text by their Roman numerals.

I *Evolution of the plasma environment of comet 67P from spacecraft potential measurements by the Rosetta Langmuir probe instrument*

E. Odelstad, A. I. Eriksson, N. J. T. Edberg, F. Johansson, E. Vigren, M. André , C.-Y. Tzou, C. Carr, and E. Cupido
Geophysical Research Letters, Volume 42, Issue 23, Dec 2015, Pages 10,126-10,134
DOI:10.1002/2015GL066599

II *Measurements of the electrostatic potential of Rosetta at comet 67P*

E. Odelstad, G.Stenberg-Wieser, M. Wieser, A. I. Eriksson, H. Nilsson, F. L. Johansson
Monthly Notices of the Royal Astronomical Society, Volume 469, Issue Suppl_2, 21 July 2017, Pages S568–S581
DOI:10.1093/mnras/stx2232

III *Ion velocity and electron temperature inside and around the diamagnetic cavity of comet 67P*

E. Odelstad, A. I. Eriksson, F. L. Johansson, E. Vigren, P. Henri, N. Gilet, K. L. Heritier, X. Vallières, M. Rubin, and M. André
Journal of Geophysical Research: Space Physics, 123
Article published in Early View on 25 July, 2018
DOI:10.1029/2018JA025542

IV *Plasma density and magnetic field fluctuations in the ion gyro-frequency range near the diamagnetic cavity of comet 67P*

E. Odelstad, A. I. Eriksson, M. André, D. Graham, H. Breuillard, C. Goetz, E. Vigren, K. Masunaga, H. Nilsson and P. Henri
Manuscript in preparation

Reprints were made with permission from the publishers.

Papers not included in the thesis

Johansson, F. L., **Odelstad, E.**, J. J. P. Paulsson, S. S. Harang, A. I. Eriksson, T. Mannel, E. Vigren, N. J. T. Edberg, W. J. Miloch, C. Simon Wedlund, E. Thiemann, F. Eparvier, and L. Andersson (2017). "Rosetta photoelectron emission and solar ultraviolet flux at comet 67P". MNRAS 469, S626–S635. DOI: 10.1093/mnras/stx2369.

Stenberg Wieser, G., **Odelstad, E.**, M. Wieser, H. Nilsson, C. Goetz, T. Karlsson, M. André, L. Kalla, A. I. Eriksson, G. Nicolaou, C. Simon Wedlund, I. Richter, and H. Gunell (2017). "Investigating short-time-scale variations in cometary ions around comet 67P". MNRAS 469, S522–S534. DOI: 10.1093/mnras/stx2133.

André, M., **Odelstad, E.**, D. B. Graham, A. I. Eriksson, T. Karlsson, G. Stenberg Wieser, E. Vigren, C. Norgren, F. L. Johansson, P. Henri, M. Rubin, and I. Richter (2017). "Lower hybrid waves at comet 67P/Churyumov-Gerasimenko". MNRAS 469, S29–S38. DOI: 10.1093/mnras/stx868.

Karlsson, T., A. I. Eriksson, **Odelstad, E.**, M. André, G. Dickeli, A. Kullen, P.-A. Lindqvist, H. Nilsson, and I. Richter (2017). "Rosetta measurements of lower hybrid frequency range electric field oscillations in the plasma environment of comet 67P". Geophys. Res. Lett. 44, pp. 1641–1651. DOI: 10.1002/2016GL072419.

Galand, M., K. L. Héritier, **Odelstad, E.**, P. Henri, T. W. Broiles, A. J. Allen, K. Altwegg, A. Beth, J. L. Burch, C. M. Carr, E. Cupido, A. I. Eriksson, K.-H. Glassmeier, F. L. Johansson, J.-P. Lebreton, K. E. Mandt, H. Nilsson, I. Richter, M. Rubin, L. B. M. Sagnières, S. J. Schwartz, T. Sémon, C.-Y. Tzou, X. Vallières, E. Vigren, and P. Wurz (2016). "Ionospheric plasma of comet 67P probed by Rosetta at 3 au from the Sun". MNRAS 462, S331–S351. DOI: 10.1093/mnras/stw2891.

Edberg, N. J. T., A. I. Eriksson, **Odelstad, E.**, E. Vigren, D. J. Andrews, F. Johansson, J. L. Burch, C. M. Carr, E. Cupido, K.-H. Glassmeier, R. Goldstein, J. S. Halekas, P. Henri, C. Koenders, K. Mandt, P. Mokashi, Z. Nemeth, H. Nilsson, R. Ramstad, I. Richter, and G. S. Wieser (2016a). "Solar wind interaction with comet 67P: Impacts of corotating interaction regions". J. Geophys. Res. Space Physics 121, pp. 949–965. DOI: 10.1002/2015JA022147.

Edberg, N. J. T., A. I. Eriksson, **Odelstad, E.**, P. Henri, J.-P. Lebreton, S. Gasc, M. Rubin, M. André, R. Gill, E. P. G. Johansson, F. Johansson, E. Vigren, J. E. Wahlund, C. M. Carr, E. Cupido, K.-H. Glassmeier, R. Goldstein, C. Koenders, K. Mandt, Z. Nemeth, H. Nilsson, I. Richter, G. S. Wieser, K. Szego, and M. Volwerk (2015). "Spatial distribution of low-energy plasma around comet 67P/CG from Rosetta measurements". Geophys. Res. Lett. 42, pp. 4263–4269. DOI: 10.1002/2015GL064233.

Yang, L., J. J. P. Paulsson, C. S. Wedlund, **Odelstad, E.**, N. J. T. Edberg, C. Koenders, A. I. Eriksson, and W. J. Miloch (2016). "Observations of high-plasma density region in the inner coma of 67P/Churyumov-Gerasimenko during early activity". MNRAS 462, S33–S44. DOI: 10.1093/mnras/stw2046.

Gunell, H., H. Nilsson, M. Hamrin, A. Eriksson, **Odelstad, E.**, R. Maggiolo, P. Henri, X. Vallieres, K. Altwegg, C.-Y. Tzou, M. Rubin, K.-H. Glassmeier, G. Stenberg Wieser, C. Simon Wedlund, J. De Keyser, F. Dhooghe, G. Cessateur, and A. Gibbons (2017). "Ion acoustic waves at comet 67P/Churyumov-Gerasimenko. Observations and computations". A&A 600, A3, A3. DOI: 10.1051/0004-6361/201629801.

Eriksson, A. I., I. A. D. Engelhardt, M. André, R. Boström, N. J. T. Edberg, F. L. Johansson, **Odelstad, E.**, E. Vigren, J.-E. Wahlund, P. Henri, J.-P. Lebreton, W. J. Miloch, J. J. P. Paulsson, C. Simon Wedlund, L. Yang, T. Karlsson, R. Jarvinen, T. Broiles, K. Mandt, C. M. Carr, M. Galand, H. Nilsson, and C. Norberg (2017). "Cold and warm electrons at comet 67P/Churyumov-Gerasimenko". A&A 605, A15, A15. DOI: 10.1051/0004-6361/201630159.

Vigren, E., M. Galand, A. I. Eriksson, N. J. T. Edberg, **Odelstad, E.**, and S. J. Schwartz (2015). "On the Electron-to-Neutral Number Density Ratio in the Coma of Comet 67P/Churyumov-Gerasimenko: Guiding Expression and Sources for Deviations". ApJ 812, 54, p. 54. DOI: 10.1088/0004-637X/812/1/54.

Hajra, R., P. Henri, X. Vallières, M. Galand, K. Héritier, A. I. Eriksson, **Odelstad, E.**, N. J. T. Edberg, J. L. Burch, T. Broiles, R. Goldstein, K. H. Glassmeier, I. Richter, C. Goetz, B. T. Tsurutani, H. Nilsson, K. Altwegg, and M. Rubin (2017). "Impact of a cometary outburst on its ionosphere. Rosetta Plasma Consortium observations of the outburst exhibited by comet 67P/Churyumov-Gerasimenko on 19 February 2016". A&A 607, A34, A34. DOI: 10.1051/0004-6361/201730591.

Engelhardt, I. A. D., A. I. Eriksson, G. Stenberg Wieser, C. Goetz, M. Rubin, P. Henri, H. Nilsson, **Odelstad, E.**, R. Hajra, and X. Vallières (2018). "Plasma density structures at comet 67P/Churyumov-Gerasimenko". MNRAS 477, pp. 1296–1307. DOI: 10.1093/mnras/sty765.

Vigren, E., K. Altwegg, N. J. T. Edberg, A. I. Eriksson, M. Galand, P. Henri, F. Johansson, **Odelstad, E.**, C.-Y. Tzou, and X. Valliéres (2016). "Model-Observation Comparisons of Electron Number Densities in the Coma of

67P/Churyumov-Gerasimenko during January 2015". AJ 152, 59, p. 59. DOI: 10.3847/0004-6256/152/3/59.

Nilsson, H., G. S. Wieser, E. Behar, H. Gunell, M. Wieser, M. Galand, C. Simon Wedlund, M. Alho, C. Goetz, M. Yamauchi, P. Henri, **Odelstad, E.**, and E. Vigren (2017). "Evolution of the ion environment of comet 67P during the Rosetta mission as seen by RPC-ICA". MNRAS 469, S252–S261. DOI: 10.1093/mnras/stx1491.

Vigren, E., M. André, N. J. T. Edberg, I. A. D. Engelhardt, A. I. Eriksson, M. Galand, C. Goetz, P. Henri, K. Heritier, F. L. Johansson, H. Nilsson, **Odelstad, E.**, M. Rubin, G. Stenberg-Wieser, C.-Y. Tzou, and X. Vallières (2017). "Effective ion speeds at ∼200-250 km from comet 67P/Churyumov-Gerasimenko near perihelion". MNRAS 469, S142–S148. DOI: 10.1093/mnras/stx1472.

Broiles, T. W., J. L. Burch, K. Chae, G. Clark, T. E. Cravens, A. Eriksson, S. A. Fuselier, R. A. Frahm, S. Gasc, R. Goldstein, P. Henri, C. Koenders, G. Livadiotis, K. E. Mandt, P. Mokashi, Z. Nemeth, **Odelstad, E.**, M. Rubin, and M. Samara (2016). "Statistical analysis of suprathermal electron drivers at 67P/Churyumov-Gerasimenko". MNRAS 462, S312–S322. DOI: 10.1093/mnras/stw2942.

Edberg, N. J. T., M. Alho, M. André, D. J. Andrews, E. Behar, J. L. Burch, C. M. Carr, E. Cupido, I. A. D. Engelhardt, A. I. Eriksson, K.-H. Glassmeier, C. Goetz, R. Goldstein, P. Henri, F. L. Johansson, C. Koenders, K. Mandt, C. Möstl, H. Nilsson, **Odelstad, E.**, I. Richter, C. S. Wedlund, G. Stenberg Wieser, K. Szego, E. Vigren, and M. Volwerk (2016b). "CME impact on comet 67P/Churyumov-Gerasimenko". MNRAS 462, S45–S56. DOI: 10.1093/mnras/stw2112.

Heritier, K. L., K. Altwegg, H. Balsiger, J.-J. Berthelier, A. Beth, A. Bieler, N. Biver, U. Calmonte, M. R. Combi, J. De Keyser, A. I. Eriksson, B. Fiethe, N. Fougere, S. A. Fuselier, M. Galand, S. Gasc, T. I. Gombosi, K. C. Hansen, M. Hassig, E. Kopp, **Odelstad, E.**, M. Rubin, C.-Y. Tzou, E. Vigren, and V. Vuitton (2017). "Ion composition at comet 67P near perihelion: Rosetta observations and model-based interpretation". MNRAS 469, S427–S442. DOI: 10.1093/mnras/stx1912.

Acknowledgements

While a doctoral thesis is formally a single-author publication, real-world processes rarely lend themselves to such simplified, idealized descriptions. This thesis relies on the work and support of many people. An exhaustive list of all contributors would soon become intractable. I would like to express my sincere gratitude to all my colleges at IRF and in the Rosetta Plasma Consortium for their kindness and help. I mention here only a few people who have been particularly instrumental to and supportive of my work, during my time at IRF in general and on Rosetta in particular.

First and foremost, I would like to thank my main supervisor, Anders Eriksson, without whom none of this would have been possible. Always eager to partake in scientific discussions, which were often of great benefit to my work (and sometimes just digressions out of general scientific curiosity), his perpetually good spirit and enthusiasm made working with him these past years a pure delight. Having such an accommodating supervisor regularly available a few doors down the hall has been an invaluable privilege, one which I could scarcely have managed without. Thus, I owe most of my academic achievements during this time, and this thesis in particular, to him and his generous and skillful supervision.

I am also very grateful for the advice and contribution of my second supervisor, professor Mats André. With a steady and and watchful eye, he has overseen my work, often providing a fresh perspective and never afraid to ask the hard questions. With his knowledge of plasma waves, he has in particular been very helpful in the work on Paper IV.

Among my IRF colleagues, I also want to give special credit to Fredrik Leffe Johansson, who in addition to doing great and vital work on the archiving and analysis of LAP data, that enabled any science to be done at all, was also a great scientific collaborator and brother-in-arms in the quest to conquer the sometimes bewildering nature of the Rosetta Langmuir probe data.

I would also like to express my great appreciation to the ICA team, especially Hans Nilsson, Gabriella and Martin Wieser, for their wonderful hospitality during my visits in Kiruna, our rewarding collaboration and their generous support, especially during my time working on the LAP/ICA cross-calibration study (Paper II of this thesis).

A special thanks also to Erik Vigren for many interesting discussions on how the comet ionosphere does (and does not) work, especially in the last months of my thesis work. His sensible, measured approach to research has been a great inspiration to me for my future work in this field.

I also want to thank Niklas Edberg, for valuable collaboration and good company during many trips and meetings, especially in the earlier part of my PhD studies.

Many thanks to Erik Johansson, for good work and smooth cooperation on the Rosetta archive. And a special thanks for taking charge of organizing the weekly game nights at IRF over the last couple of months (helping me not go completely insane during my thesis work).

I would also like to give a special thanks to Andris Vaivads, who took me under his wings when I first came to IRF as a prospective degree project student. Even though the project I was interested in had already been given to another student, he came up with an angle for me to work on it as well. Thus, he is in many ways responsible for bringing me into this field and introducing me to IRF.

A great thanks also to my fellow IRF PhD students, in particular Elin, Andreas, Ilka, Oleg and Mika, for great collaboration on course work and pleasant company during trips and conferences. Thanks also to Daniel Graham, for valuable help with plasma wave physics in general and Paper IV in particular.

Many thanks also to my colleagues outside of IRF, in the Rosetta Plasma Consortium. For example, Charlotte Götz (TU Braunschweig), for great company during many meetings and conferences, and much interesting discussion, particularly on the diamagnetic cavity and related issues. And also Pierre Henri, Xavier Vallières, Luca Bucciantini, Hugo Breuillard, Nicolas Gilet, Rajkumar Hajra and the rest of the MIP team at LPC2E, Orléans, for great collaboration and hospitality.

I would also like to thank Björn Davidsson (then Uppsala University, at present JPL) for his enduring efforts at teaching me and some of my fellow PhD students the ins and outs of comet physics. Learning about the more general aspects of comet physics, how it fits into the broader field of planetary science and how it contributes to unravelling the mystery of how the solar system was formed, was one of the most interesting and fascinating parts of my PhD studies.

Finally, my sincerest gratitude and appreciation goes out to my family, in particular my parents, Lena and Jan, for their enduring support and encouragement, without which I would not be where I am today.

Contents

1. Introduction

The subject of this thesis is the evolution and dynamics of the cometary plasma environment of a moderately active comet before, during and after its closest approach to the Sun. For over two years in 2014 – 2016, the European Space Agency's Rosetta spacecraft followed the Jupiter Family comet 67P/Churyumov-Gerasimenko at distances typically between a few tens and a few hundred kilometers from the nucleus surface, the longest and closest inspection of a comet ever made. Its payload included a suite of five plasma instruments (the Rosetta Plasma Consortium, RPC), providing unprecedented in-situ measurements of the plasma environment in the inner coma of a comet. Two of the plasma instruments, the Ion Composition Analyzer (RPC-ICA) and the Langmuir Probe instrument (RPC-LAP) were provided and operated by the Swedish Institute of Space Physics (IRF) in Kiruna and Uppsala, respectively. In this thesis, data from these instruments and other instruments of RPC (as well as the Rosetta Orbiter Spectrometer for Ion and Neutral Analysis, ROSINA) are used to study the characteristics and evolution of the cometary plasma environment.

1.1 Thesis outline

The thesis is structured as follows: The rest of this chapter (1.2) presents some background and motivation to cometary plasma science in general and this thesis in particular. Chapter 2 gives a brief overview of the Rosetta mission and payload. Chapter 3 presents an overview of cometary plasma physics, beginning with the neutral coma (Section 3.1) followed by production and transport in the cometary ionosphere (Section 3.2), interaction with the solar wind (Section 3.3) and an overview of the plasma observed by Rosetta at 67P (Section 3.4). The chapter is concluded with a comprehensive review of the structure of the cometary plasma environment (Section 3.5) based on a comparison between the models pre-dating Rosetta and results obtained during the mission. A general summary and outlook is given in Capter 4 and Chapter 5 contains summaries of the four papers included in the thesis. Chapter 6 contains a slightly more popularized summary in Swedish.

1.2 Background and motivation

From the point of view of space plasma physics, comets differ from planets in two important respects. First, in contrast to planets with their roughly circular

orbits, typical comets have ever changing distances to the Sun and therefore see strongly varying influx of solar energy, typically varying by at least a factor ten. Second, comets are small bodies not able to gravitationally retain their atmospheres, which thus blow away into space and are lost if not replenished by sublimation of volatiles from the cometary nucleii. Taken together, these characteristics mean that the space environment of a comet changes drastically from aphelion to perihelion.

The environment of a planet is determined by a set of boundary conditions, such as the distance to the central star (the Sun), the planet size, its atmosphere, rotation and magnetic field, stellar properties like mass, absolute magnitude, activity, magnetic field and stellar wind, among others. The study of planetary plasma environments, i.e. magnetospheres and ionospheres, can be done in detail only on the finite sample of planets available in our solar system, each characterized by its particular values of the parameters above. As astrophysical techniques evolve, exoplanets may offer an increased sample in the future, but it is safe to say that there will be nothing to match the possibilities for detailed investigation of comets offered by in-situ measurements in our own solar system in the near future. The flow of knowledge is therefore in the other direction: we learn from our own solar system to understand others. While there are e.g. seasonal variations on the planets as well as long- and short-term changes in the boundary conditions set by the Sun, e.g. its ultraviolet flux and the solar wind, each planet essentially occupies a small region in the space of parameters determining the character of its environment. Comets are here unique (at least in our solar system) in that one of the most important parameters, the distance to the central star, changes over a wide range of values. A study of a comet thus offers the possibility to observe not only a small region in the environment parameter space, but an elongated volume with large coverage of at least this parameter. While most other parameters are about as fixed as for any other object, this variation gives a strong advantage for identifying and studying universal phenomena among all peculiarities set by particular parameter values.

One particular example is the bow shock forming in front of any body capable of significantly obstructing a supersonic flow. As our solar system is permeated by a supersonic flow of tenuous plasma from the Sun, the *solar wind*, collision-less bow shocks form at all the planets. A plethora of bow shocks have also been observed around other astrophysical objects, particularly stars of various character (van Buren, 1993). The by far best studied example is of course the terrestrial bow shock, which has many similarities with the shocks around the giant planets. The shocks at Mars and Venus differ by being much closer to the planets themselves, because these planets have no intrinsic magnetic field that can form a proper magnetosphere to fend off the solar wind at large distances. Hence they have their shocks inside their exospheres, resulting in continuous mass loading of newly ionized plasma to the solar wind, strongly changing the character of the shock. The shocks at

Venus and Mars in turn differ by their scale lengths: above the ion gyro-radius for Venus, making for a rather fluid-like interaction quite symmetric along the solar wind flow direction, but below the ion gyro-radius at Mars, giving a more intricate pattern with a broken symmetry. These are the available samples of planetary bow shocks, all more or less continuously existing (see e.g. Russell (2013) and Balogh and Treumann (2013a) for recent reviews of planetary bow shocks). For a comet passing the frost line into the inner solar system the situation is quite different: initially, there is no bow shock at all, only a weak Mach cone becoming stronger as the outgassing increases with the solar heating, and eventually transforming to a bow shock whose character continues to evolve (Koenders et al., 2013; Bagdonat and Motschmann, 2002). No planet, nor indeed the complete set of planets in the solar system, can offer a similar variation.

In addition to the universal character of space plasma phenomena, there is a scientific interest in the particular details of the comet-plasma interaction. As an example, models and measurements at comet 1P/Halley show the existence of several plasma boundaries and regions around the comet, among them the diamagnetic cavity with no known direct counterpart in other solar system plasmas (although it is somewhat reminiscent of the induced magnetosphere of Venus, (Elphic et al., 1980) the extensive mass-loading makes comets a special case). Investigating the nature and physics of this boundary, particularly its development and stability, is of high interest. Previous missions to comets carrying plasma instruments (von Rosenvinge et al., 1986; Reinhard, 1986; Hirao and Itoh, 1987; Sagdeev et al., 1987; Grensemann and Schwehm, 1993; Richter et al., 2011) have all been fast flybys, passing hundreds or thousands of kilometers from the nucleus at relative speeds of tens of kilometers per second. Rosetta spent more than two years within a few hundred kilometers from the nucleus, moving around it at a relative speed on the order of one meter per second (yes, *meter* per second, not kilometer). One should stay away from superlatives in a scientific description, but this does open for a truly enormous evolution in our knowledge of the cometary nucleus and its environment, and opportunities for studying the evolution of the cometary plasma and physical processes in it orders of magnitude better than ever before. The pre-Rosetta picture of the cometary plasma environment and its evolution was based on very few in-situ measurements, of which Giotto's observations at comet 1P/Halley in 1986 still stand out as the most complete, and modeling efforts by theoretical and numerical means (e.g. Gombosi, 2015). Theoretical models can only address simplified situations, and the numerical modeling is quite challenging for an object with as diverse scale lengths as a comet, where the nucleus has a size of a few kilometers, pickup ions have gyro-radii of thousands of kilometers, and the exosphere extends for millions of kilometers (Gombosi, 2015). As previous observations are few, and the Rosetta dataset yet far from completely analyzed, the uncertainties are large, partic-

ularly regarding dynamics. A sample of unknowns that have been, and are being addressed is:

1. What boundaries are actually found at the comet, and how do they evolve? Neither theoretical considerations nor experimental evidence have settled questions on the existence of an inner shock, where the outflowing gas and plasma from the nucleus is slowed down to subsonic speed before mixing with the solar wind (Balogh and Treumann, 2013b). This can be compared to the situation at the heliopause, where an inner shock (the termination shock) has been observed by the Voyager spacecrafts but the existence of an outer shock (the heliospheric bow shock) has been called into doubt by measurements of energetic neutral atoms by the IBEX mission (McComas et al., 2012). Also, the transition from a Mach cone to a fully developed bow shock is not known at any level of detail; comets provide unique setting for studying this process. And how stable are the boundaries? In general, plasma boundary stability is one of the core topics in space plasma physics, where e.g. reconnection at the Earth's magnetopause changes the otherwise closed nature of its boundary. Previous measurements at brief flybys could not provide answers and the theoretical uncertainties are large. Our long term investigation at walking speed provided an opportunity to directly observe boundaries like the diamagnetic cavity boundary and its dynamics, whether it be externally imposed or internally generated.

2. The electron temperature near the comet, T_e, is poorly constrained except for the case of a strongly outgassing comet with high collision frequency with the neutral gas, like 1P/Halley. This is an important parameter influencing among other things the charging of dust grains, and hence the dust dynamics, but also plasma recombination and electron impact ionization rates. The possible T_e range runs from the values collisional models predict (few hundred K) to the levels typically found in solar system plasmas with UV ionization (10^3-10^5 K, Eberhardt and Krankowsky, 1995; Gan and Cravens, 1990). With Rosetta, we were able to constrain T_e and its evolution as the coma developed during the mission for improved environmental models.

3. The velocity and flow regime of the ions near the comet is similarly poorly known. This is of vital importance for understanding the formation and dynamics of the boundaries in point 1 above, in particular the diamagnetic cavity and possible inner shock. It is also crucial for modeling the cometary ionosphere and, together with the electron temperature discussed in point 2 above, sets the stage for many chemical processes in the coma. Our in situ observations of the ion velocity in the inner coma do not seem to fit with the Halley paradigm, where the

cometary ions were collisionally coupled to the neutral gas in the inner coma. This suggests the need for a reevaluation of the processes governing the formation and dynamics of the cometary ionosphere in general and the diamagnetic cavity and inner shock in particular.

4. Instabilities, waves and turbulence play an important role for the energetics in any plasma, redistributing energy e.g. by means of wave-particle and wave-wave interactions, possibly reshaping the plasma environment of the comet. The extensive interaction region between the cometary atmosphere and the solar wind provides a rare opportunity to study such processes in detail over many spatial and temporal scales.

5. The process of mass-loading of a plasma, in which extraneous mass is implanted and incorporated into a high-speed flowing magnetized plasma, e.g. due to continuous ionization and accommodation of background neutral particles, is a common phenomenon in space plasmas (Szegö et al., 2000). Comets are one of the most formidable examples of this, due to the vast amounts of cometary neutral gas that evaporate from the nucleus surface during its active phase. Other examples include the interaction of the solar wind with planetary atmospheres and exospheres or the interaction of ions from the local interstellar medium with the solar wind plasma. Rosetta's prolonged stay at 67P has enabled much new data to be gathered and insights to be gained on how this process works at the comet and how it contributes to shaping its plasma environment and affect the chemistry therein.

The studies included in this thesis primarily investigate aspects of points 1 – 4 above. Much time and effort still remains before the vast amount of Rosetta data is properly processed and digested. More insight and new interesting questions are sure to follow.

Finally, we note that ESA's decision to fly the Jupiter Icy Moons Explorer (Grasset et al., 2013) ensures that icy bodies of the solar system (like comets and some Jovian moons) and their plasma environments will be a strong research area for a long time to come, so this topic will have long term future relevance.

2. Rosetta: Mission and payload

2.1 Rosetta: Mission and payload

The European Space Agency's Rosetta mission (Glassmeier et al., 2007b; Taylor et al., 2017) was the closest and longest investigation of a cometary nucleus ever, and the first to deploy a lander on the surface. The primary objective of the mission was to study the structure, composition and morphology of the nucleus, with the eventual goal of learning more about the formation and early evolution of the solar system from this potentially primordial body. Supplementary goals included the development of cometary activity, dynamics and interaction of gas and dust in the cometary coma, and processes in the cometary plasma environment and its interaction with the solar wind. For these purposes, the spacecraft carried a payload of 11 different instruments (c.f. Figure 2.1 and Table 2.1) and a lander, Philae, with a payload of 10 additional instruments (not shown).

Rosetta arrived at comet 67P/Churyumov-Gerasimenko on August 6, 2014, at a heliocentric distance of 3.6 AU. It deployed the lander Philae on November 12, 2014, and subsequenntly followed the comet through perihelion on August 13, 2015, at cometocentric distances mostly on the order of a few tens to a few hundreds of kilometers. It continued to follow the comet as it moved away from the Sun, until September 30, 2016, when the mission ended with a touchdown on the nucleus surface. An overview of Rosetta's journey is shown in Figure 2.2.

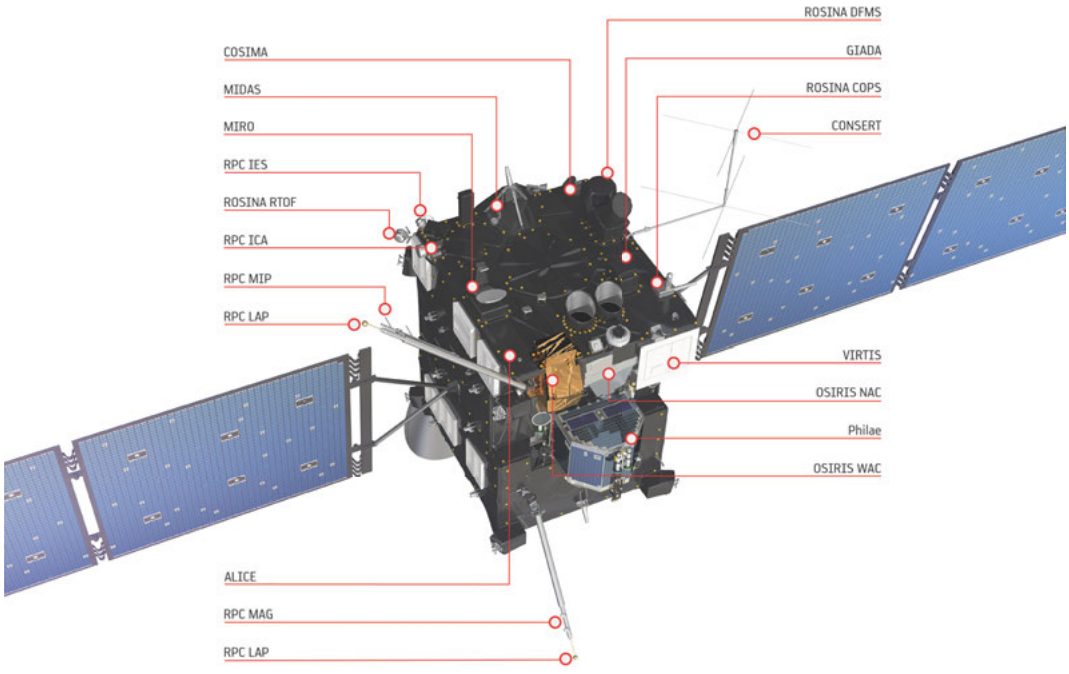

Figure 2.1. Rosetta orbiter instruments. *(Image credit: ESA/ATG medialab)*

Alice	Ultraviolet Imaging Spectrometer	Stern et al. (2007)
CONSERT	**Co**met **N**ucleus **S**ounding **E**xperiment by **R**adio wave **T**ransmission	Kofman et al. (2007)
COSIMA	**Co**metary **S**econdary **I**on **M**ass **A**nalyser	Kissel et al. (2007)
GIADA	**G**rain **I**mpact **A**nalyser and **D**ust Accumulator	Colangeli et al. (2007)
MIDAS	**M**icro-**I**maging **D**ust **A**nalysis **S**ystem	Riedler et al. (2007)
MIRO	**M**icrowave **I**nstrument for the **R**osetta **O**rbiter	Gulkis et al. (2007)
OSIRIS	**O**ptical, **S**pectroscopic and **I**nfrared **R**emote **I**maging **S**ystem	Keller et al. (2007)
-NAC	**N**arrow **A**ngle **C**amera	
-WAC	**W**ide **A**ngle **C**amera	
ROSINA	**R**osetta **O**rbiter **S**pectrometer for **I**on and **N**eutral **A**nalysis	Balsiger et al. (2007)
-COPS	**Co**metary **P**ressure **S**ensor	
-DFMS	**D**ouble **F**ocussing Mass **S**pectrometer	
-RTOF	**R**eflection **T**ime of **F**light mass spectrometer	
RPC	**R**osetta **P**lasma **C**onsortium	Carr et al. (2007)

Table 2.1. *Rosetta instrument full names and references to instrument descriptions.*

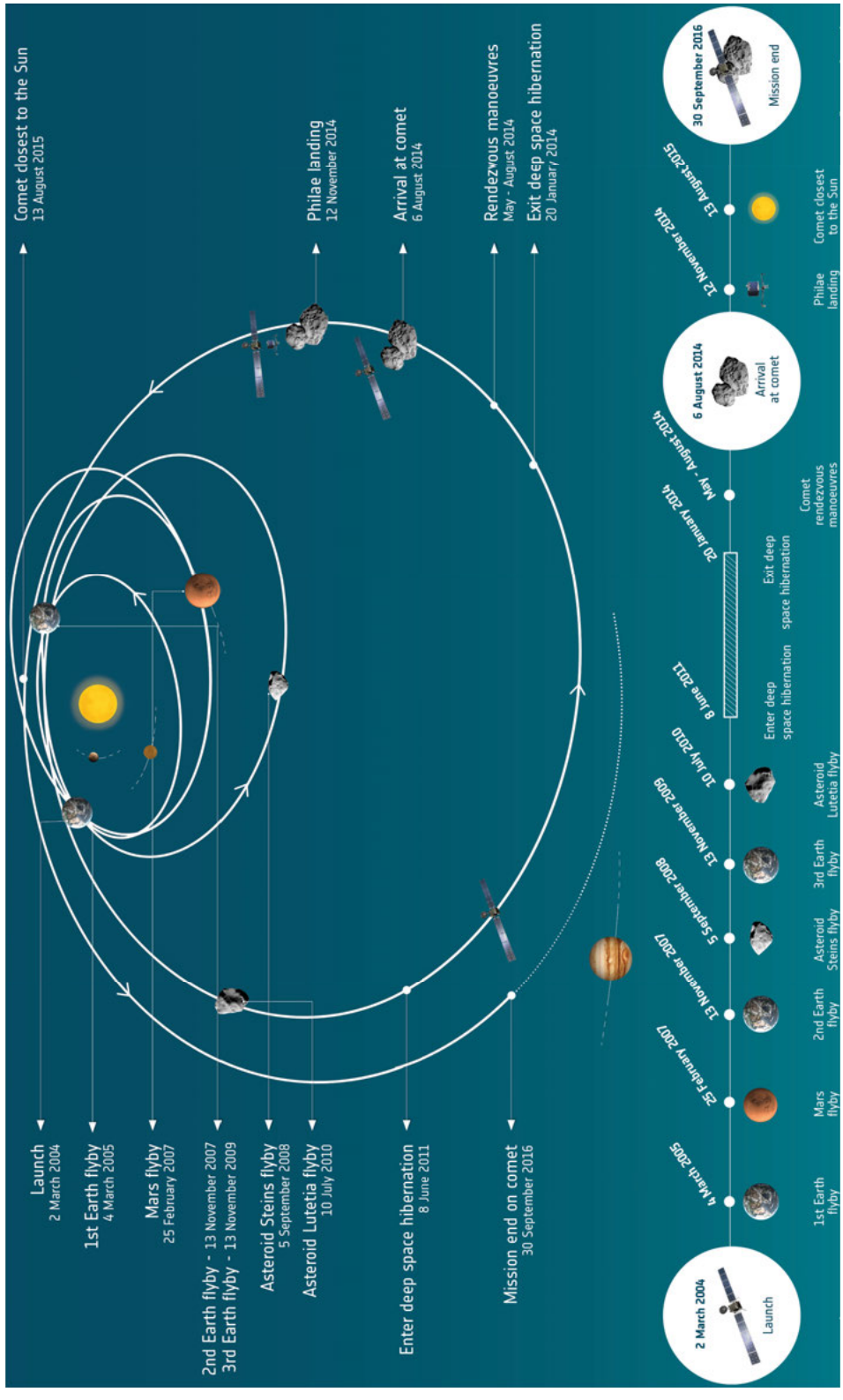

Figure 2.2. Rosetta's journey. *(Image credit: ESA)*

2.2 Comet 67P/Churyumov-Gerasimenko

Rosetta's target comet, 67P/Churyumov-Gerasimenko (hereafter 67P), is a Jupiter family comet (i.e. a short-period [$\lesssim$20 years] comet dynamically dominated by Jupiter) discovered in 1969. It was put on its current orbit, with an orbital period of 6.5 years and perihelion and aphelion distances of 1.2 AU and 5.6 AU, respectively, by a close encounter with Jupiter in 1959. Its nucleus is bilobed (c. f. Figure 2.3), approximately 4 km across and has a rotation period of 12.4 hours with a spin axis right ascension of 69 degrees and declination of 64 degrees (Sierks et al., 2015). The shape and spin axis orientation of the nucleus produces great diurnal and seasonal variations of the outgassing and activity as the solar insolation varies over the nucleus surface (Hässig et al., 2015).

67P is typically described as an intermediately active comet; its peak activity (18 – 22 days after perihelion) was $(3.5 \pm 0.5) \times 10^{28}$ molecules s^{-1} (Hansen et al., 2016). In comparison, comet 1P/Halley had an activity of 6.9×10^{29} s^{-1} when it was encountered by multiple spacecraft in 1986 (Krankowsky et al., 1986), and comet C/1995 O1 Hale–Bopp reached production rates of $\sim 10^{31}$ s^{-1} near perihelion (Dello Russo et al., 2000).

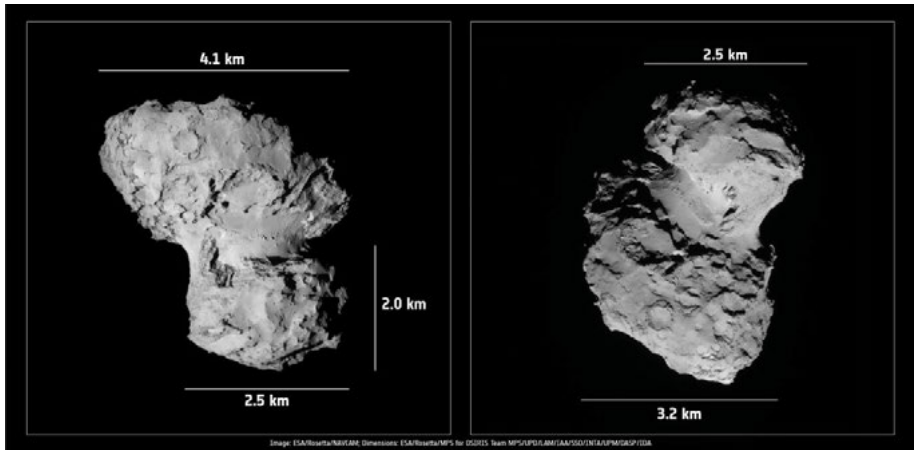

Figure 2.3. The nucleus of Rosetta's target comet, 67P/Churyumov-Gerasimenko. *(Image credit: ESA)*

2.3 The Rosetta Plasma Consortium

The Rosetta Plasma Consortium (RPC) included 5 instruments designed to probe the cometary plasma environment (see Figure 2.4):

- The **I**on **C**omposition **A**nalyser (RPC-ICA), a combined electrostatic and magnetic momentum analyzer for ions. Measured the three-dimensional distribution of positive ions in the energy-per-charge range 5 eV/q – 40 keV/q, with an energy resolution of $dE/E = 0.07$ for $E > 30$ eV, changing up to $dE/E = 0.30$ for $E < 30$ eV, a time resolution of 192 s for 3D measurements (4 s possible for 2D measurements), and a mass resolution good enough to resolve the major ion species, e.g. H, He, H_2O etc. (Nilsson et al., 2007; Stenberg Wieser et al., 2017).

- The **I**on and **E**lectron **S**ensor (RPC-IES), consisting of two electrostatic analyzers, one for ions and one for electrons. Measured the three-dimensional distributions of ions (including negative) and electrons, covering an energy-to-charge range of 4.3 eV/q – 18 keV/q with an energy resolution of $dE/E = 0.08$ and a time-resolution of (at best) 128 s (Burch et al., 2007; Broiles et al., 2016).

- The **La**ngmuir **P**robe instrument (RPC-LAP), consisting of two spherical 2.5-cm diameter Langmuir probes mounted on the edges of booms at 2.24 m and 1.62 m distances outside the orbiter, respectively. Possible measurements included plasma density (1 – 10^6 cm^{-3}), electron temperature ($\sim$10 meV – 10 eV), plasma flow velocity ($\lesssim$10 km/s), spacecraft potential ($\pm$40 V), electric field fluctuations ($\lesssim$8 kHz) and integrated EUV flux (for $n_e \lesssim 1000$ cm^{-3}) (Eriksson et al., 2007; Eriksson et al., 2017).

- The Fluxgate **Mag**netomter (RPC-MAG), a tri-axial fluxgate magnetometer mounted on a 1.5 m boom outside the orbiter. Measured magnetic fields in three dimensions in the frequency range 0 – 10 Hz (Glassmeier et al., 2007a).

- The **M**utual **I**mpedance **P**robe (RPC-MIP), consisting of two receiving and two transmitting electrodes on a 1-m long bar, mounted on one of the spacecraft booms. Measured the electron density, temperature, plasma drift velocity and wave activity from the mutual impedance frequency response (Trotignon et al., 2007; Gilet et al., 2017), for Debye lengths of 0.5 – 200 cm.

This thesis primarily makes use of data from RPC-LAP (hereafter LAP), which was designed and operated by the author's home institute, the Swedish

Figure 2.4. The Rosetta Plasma Consortium (RPC). The Langmuir probe instrument (LAP), provided and operated by the Swedish Institute of Space Physics in Uppsala, is the main instrument of use in this thesis. *(Image credit: STFC / Imperial College London)*

Institute of Space Physics[1] (IRF) in Uppsala, Sweden. In Papers I and II, LAP is used to probe the cometary plasma environment and monitor its evolution by means of measurements of the electrostatic potential of the spacecraft (see also Sections 5.1 – 5.2). For details on LAP instrument design, operation and characteristics with regards to these measurements, see Sections 2 – 3 in Paper I and Section 2.1 in Paper II. In Paper II, we also use RPC-ICA (hereafter ICA) to compare and calibrate the spacecraft potential measurements. For details of how ICA works in this context, see Section 2.1 of Paper II and Stenberg Wieser et al. (2017). In Paper III, LAP is used in conjunction with RPC-MIP (hereafter MIP) to determine ion velocities and estimate the electron temperature in the inner coma. For details on how LAP and MIP work with respect to these measurements, see Sections 2.1 and 2.2 of Paper III, respectively. In Paper IV, we also use data from RPC-MAG, which is described in some detail in Section 2.2 of that paper. Finally, a non-RPC instrument, the Rosetta Orbiter Spectrometer for Ion and Neutral Analysis Cometary Pressure Sensor

[1]With important contributions from the Royal Institute of Technology (KTH) in Stockholm, Sweden, the Finnish Meteorological Institute (FMI) in Helsinki, Finland, and the University of Oslo, Norway.

(ROSINA-COPS), was also used in Papers I and III to provide neutral density measurements as context for our plasma observations. For details on this instrument, the reader is referred to the instrument description by Balsiger et al. (2007).

3. The cometary plasma environment

3.1 The cometary coma

Cometary nuclei consist of a mixture of volatile and refractory materials, as first suggested by Whipple (1950). The volatiles are dominated by H_2O, CO, CO_2 (Bockelee-Morvan et al., 2004) and, as it turns out, molecular oxygen, O_2 (Bieler et al., 2015). The refractories mostly consist of silicates and organics (Hanner and Bradley, 2004). While on long-period orbits in the outer parts of the solar system, the volatiles remain frozen in the form of ices, but for comets that have been injected into the inner solar system the increased insolation brings about sublimation of the near-surface volatiles. The sublimating gas expands into the surrounding space and forms a coma enveloping the comet nucleus.

The sublimation of volatiles from the nucleus of an active comet provides an enduring source of gas for the cometary coma. Cometary nuclei are so small and light that there is no significant gravitational force on the gas, which therefore expands freely into the surrounding space. The resulting gas envelope is referred to as the coma, deriving from the Greek word "kome", just as the word comet itself. Terms like atmosphere or exosphere, while usually reserved for cases where the particles are gravitationally bound to the parent body, can occasionally be found in the scientific literature as well. The free expansion of the gas means that, while tenuous, the coma generally extends very far from the nucleus, on the order of 10^5 km or more. Here follows a brief overview of the dynamics of the neutral coma gas and a comparison with the case of a gravitationally bound planetary atmosphere.

The neutral gas envelope around a body in space obeys the continuity equation, which in the absence of ionization loss and production from extended sources (sublimation from dust) takes the form

$$\frac{\partial n}{\partial t} + \nabla \cdot (n\mathbf{u}) = 0, \tag{3.1}$$

and the fluid equation of motion (Euler momentum equation)

$$mn\left(\frac{\partial \mathbf{u}}{\partial t} + (\mathbf{u}\cdot\nabla)\mathbf{u}\right) = -\nabla\cdot\mathbf{P} + mn\mathbf{g}. \tag{3.2}$$

Here, m is the particle mass, n is the number density, $\mathbf{u}$ is the fluid velocity, $\mathbf{P}$ is the the pressure tensor and $\mathbf{g}$ is the gravitational acceleration. In the presence

of a non-negligible gravitational term, Equation (3.2) allows a solution under static equilibrium $\mathbf{u} = 0$ by simply equating the pressure and gravitational terms. In this case, Equation (3.1) is trivially satisfied. Also, local thermodynamic equilibrium can be assumed, reducing the pressure tensor to the scalar pressure p given by

$$p = nk_{\mathrm{B}}T, \tag{3.3}$$

where k_{B} is Boltzmann's constant and T is the temperature of the gas. The static equilibrium solution is thus characterized by the balance of the pressure gradient and gravitational forces:

$$\nabla p = mn\mathbf{g}. \tag{3.4}$$

The static, durable nature of this state also makes it possible, if not likely, for the gas to attain global thermal equilibrium, with uniform temperature of the gas, allowing the pressure gradient to be written as

$$\nabla p = k_{\mathrm{B}}T\nabla n. \tag{3.5}$$

Introducing a coordinate system with the z-axis antiparallel to the gravitational force (altitude) so that $\mathbf{g} = -g\hat{\mathbf{z}}$ then gives

$$k_{\mathrm{B}}T\frac{dn}{dz} = -mng, \tag{3.6}$$

which can be solved with a boundary condition $n = n_0$ at $z = 0$ to give

$$n = n_0 \exp\left\{-\frac{mgz}{k_{\mathrm{B}}T}\right\} = n_0 \exp\left\{-\frac{z}{H}\right\}, \tag{3.7}$$

where the e-folding of the density $H = k_{\mathrm{B}}T/mg$ is called the *scale height*. Thus, in the case of a gravitationally bound atmosphere, there exists a static equilibrium given by the balance of the thermal pressure gradient and the gravitational force that produces an exponential decay of the atmospheric density with altitude.

In the case of a comet, the gravitational term in Equation (3.2) is negligible and no static equilibrium solution with $\mathbf{u} = 0$ exists. However, there is a stationary solution with $\partial\mathbf{u}/\partial t = 0$, for which the continuity equation reads

$$\nabla \cdot (n\mathbf{u}) = 0. \tag{3.8}$$

Assuming radial outflow $\mathbf{u} = u\hat{\mathbf{r}}$, Equation (3.8) takes the form

$$\frac{\partial}{\partial r}(r^2 n(r,\theta,\phi)u(r,\theta,\phi)) = 0, \tag{3.9}$$

where r, θ, ϕ are the spherical radial, polar and azimuthal coordinates, respectively. Integrating Equation (3.9) w.r.t. r gives

$$r^2 n(r,\theta,\phi)u(r,\theta,\phi) = C(\theta,\phi), \tag{3.10}$$

where C is constant w.r.t. r but generally depends on θ and ϕ, unless the boundary conditions have spherical symmetry. Cometary activity is usually expressed in terms of the *outgassing rate* Q, which is the total number of molecules coming off the surface of the nucleus per second. In the case of spherical symmetry, this gives an inner boundary condition at the surface of $4\pi R^2 n(R)u(R) = Q$, from which C can be determined to be $Q/4\pi$, giving

$$n(r) = \frac{Q}{4\pi r^2 u(r)}. \tag{3.11}$$

If the outflow velocity is constant, $u(r) = u$, Equation (3.11) yields a neutral density profile that falls of with the inverse square of the radial distance r. That $du/dr \approx 0$ is not obvious, e.g. radiational and collisional processes and (photo-)chemistry can affect the energetics and dynamics of the gas. However, kinetic Digital Simulation Monte Carlo (DSMC) models including such effects (Tenishev et al., 2008), applied to comet 67P with parameters representative of several different stages of the Rosetta mission, predicted a virtually constant outflow velocity ($\sim$700 m/s) beyond a few nucleus radii (for a more detailed discussion of likely outflow velocities at 67P, see Paper III, section 1.3, and references therein). If the outgassing is not spherically symmetric, but the outflow is still strictly radial (which in this case requires the gas to be cold and collisionless), solving Equation (3.10) for n gives

$$n(r,\theta,\phi) = \frac{C(\theta,\phi)}{r^2 u(r,\theta,\phi)}. \tag{3.12}$$

This also gives a $1/r^2$ density profile if u is constant w.r.t. r, although the integration constant C can now vary in the polar and azimuthal directions and is related to the fractional outgassing rate from the respective parts of the nucleus surface rather than the total outgassing rate Q. Thus, in the case of a cometary coma, the fact that the gas is not gravitationally bound to the nucleus produces a different density profile than in the planetary atmosphere described above. Instead of decreasing exponentially, the density will fall off as $1/r^2$, even in the absence of spherical symmetry (although then only along radial trajectories), provided only that the outflow is radial at constant velocity.

The assumption of strictly radial outflow velocity can be motivated by a geometrical argument: any particle trajectory off of the surface, even if initially highly non-radial, will approach the radial direction at distances much larger than the maximum radius of the (possibly non-spherical) nucleus. In other words, at sufficiently large distances, the active nucleus is indistinguishable from a point source.

3.2 The cometary ionosphere

3.2.1 Introduction

The cometary plasma environment is sculpted by the interaction between newly formed cometary ions and the flowing plasma of the solar wind. In fact, it was in order to explain the pointing direction of cometary tails that the existence of the solar wind and the interplanetary magnetic field was first inferred (Biermann, 1951; Alfven, 1957). The main body of knowledge presently available on the cometary plasma environment derives from the spacecraft encounters with Comets 1P/Halley, 21P/Giacobini-Zinner and 26P/Grigg-Skjellerup in the 1980s and early 1990s. The picture obtained from the encounter with the highly active Halley has become something of a standard template for the cometary plasma environment, that has so far fit quite well also to less active comets like Grigg-Skjellerup, at least in terms of the main features and with with the few, brief observations available. In this section an overview of this picture is presented. It is important to note that, in addition to its target being a much weaker comet than Halley, Rosetta was *much* closer to it than any previous mission, frequently within a few tens of kilometers compared a minimum distance of 600 km of the Giotto spacecraft at Halley. Thus, deviations from the Halley case are to be expected, and will be pointed out where appropriate.

3.2.2 Ionization processes

The gas of the cometary coma is subject to three main ionization processes: photoionization by solar EUV, electron impact ionization by supra-thermal electrons in the solar wind or the photoelectrons resulting from photoionization, and charge exchange processes with ions in the the solar wind. The probability of an ionization reaction occurring is typically quantified in terms of the *cross section*, σ, for the process, which is the ratio of ions produced per exposed neutral particle to the incident flux I of ionizing radiation or particles. The cross section for a given reaction typically varies with the energy of the incident ionizing particle and the species of the neutral target. For each incident energy and target species, there are generally multiple possible reactions, giving rise to different ion species. For example, the production rate of ions of species j due to photoionization is given by summing over all target species k, of density n_k, the integral over of the product of partial cross sections σ_k^j and I over all incident photon wavelengths λ,

$$P_{j,\mathrm{ph}} = \sum_k n_k \int \sigma_k^j(\lambda) I(\lambda) d\lambda \quad . \tag{3.13}$$

In the case of photoionization, if the coma is not optically thin, the intensity $I(\lambda)$ will decrease exponentially with optical depth τ, which depends on the radial distance from the nucleus as well as the densities and absorption cross

sections of the various coma species. More on optical depth can be found in Schunk and Nagy (2009), along with photoionization and absorption cross sections for the relevant species. An important property of photoionization is that, due to conservation of momentum, nearly all the excess energy at ionization gets imparted on the electrons rather than the much heavier ions. Thus photoionization tends to produce rather warm electrons ($\sim 10-15$ eV) wheres the produced ions typically remain at the same temperature as the neutral gas (see also Section 5.1 and Papers I and II).

Electron impact ionization can be treated in a similar manner, replacing the photon flux by the supra-thermal electron flux. Some relevant cross sections for water can be found in Itikawa and Mason (2005).

Charge exchange processes in the form of electron transfer from neutral coma molecules to solar wind ions may also contribute to the ionization of gas in the coma. There are two main processes: a neutral water molecule in the coma may transfer one of its electrons to a solar wind major ion, H^+, producing a neutral hydrogen atom and an H_2O^+ ion, or a cometary neutral (not necessarily water) may transfer one of its electrons to a solar wind minor ion in a high charge state (e.g. O^{5+}, O^{6+}, C^{5+}, C^{6+}, N^{7+}). The latter process generally results in an ion in an excited state and for large enough initial charge states, the de-excitation results in the emission of X-rays that can be observed from Earth, thus providing a means of studying the cometary plasma environment by remote sensing (Lisse et al., 2004).

An important property of the charge exchange process between cometary H_2O molecules and solar wind H^+ ions is that the resulting neutral hydrogen keeps most of the energy that the fast solar wind H^+ ion had, while the H_2O^+ ion added to the plasma remains about as slow as the its parent H_2O molecule. Thus, this charge exchange process effectively cools the plasma.

3.2.3 Ionospheric transport

Transport equations

The continuity equation for particles of species s with bulk drift velocity $\mathbf{u}_s$ and number density n_s is

$$\frac{\partial n_s}{\partial t} + \underbrace{\nabla \cdot (n_s \mathbf{u}_s)}_{\text{transport}} = \overbrace{S_s}^{\text{net source}}, \tag{3.14}$$

where, S_s is the net source of particles of species s per unit volume. The momentum equation for particles of species s is given by (Cravens, 2004)

$$m_s n_s \left(\frac{\partial \mathbf{u}_s}{\partial t} + (\mathbf{u}_s \cdot \nabla)\mathbf{u}_s \right) = \underbrace{n_s q_s (\mathbf{E} + \mathbf{u}_s \times \mathbf{B})}_{\text{Lorentz force}} \overbrace{- \nabla \cdot \mathbf{T}_s}^{\text{pressure gradient force}} + \ldots$$
$$\ldots - \underbrace{\sum_{t \neq s} m_s n_s \nu_{s \to t} (\mathbf{u}_s - \mathbf{u}_t)}_{\text{inter-species collisions}} + \underbrace{\sum_{t \neq s} (m_t \mathbf{u}_t - m_s \mathbf{u}_s) P_{t \to s}}_{\text{chemical transformations}} . \quad (3.15)$$

Here, m_s, q_s and $\mathbf{T}_s$ are the mass, charge and pressure tensor of particle species s (denoted here by $\mathbf{T}$ to avoid confusion with the production P), $\nu_{s \to t}$ is the momentum transfer collision frequency from particles of species s to particles of species t, $\mathbf{E}$ and $\mathbf{B}$ are the electric and magnetic fields, and $P_{t \to s}$ is the chemical production rate of particles of species s from particles of species t. The first three terms on the right-hand side are the familiar Lorentz force on charged particles in electric and magnetic fields, the pressure gradient force due to transfer of momentum between different parts of the fluid made up particles of species s by microscopic motions of such particles under a nun-uniform particle distribution, and the transfer of momentum from species s to t by means of binary collisions between particles of different species. The last term, the "mass-addition" or "mass-loading" term, accounts for the change of momentum of the fluid of species s by a net change of mass of the fluid due to chemical reactions producing particles of species s from particles of species t. This term is perhaps less familiar to many readers; for a discussion of why it looks the way that it does, and why the corresponding loss term is not present, the reader is referred to Cravens (2004, Chapters 2.4.2 and 2.4.4.).

Ionosphere in photochemical equilibrium

Consider a fluid consisting of ions of species j in the cometary plasma. The characteristic timescales of chemical loss and transport are quantified in terms of the *chemical life time* $\tau_c = 1/L_j$ and *transport time* $\tau_{trans} = \ell/u_j$, where ℓ is the characteristic scale length of the plasma and L_j is the chemical loss rate of ions of species j. If the transport time is much larger than the chemical life time of ions of this species ($\tau_{trans} \gg \tau_c$), which is expected close enough to a sufficiently active comet, the transport term in Equation (3.14) can be neglected and a steady state ($\partial n_j/\partial t \equiv 0$) density profile can be obtained under photochemical equilibrium:

$$P_j - L_j n_j = 0 \qquad \Rightarrow \qquad n_j = P_j/L_j. \quad (3.16)$$

Here, P_j is the production rate of ions of species j and it is directly proportional to the neutral density n_n and the ionization frequency ν_j, thus $P_j = \nu_j n_n$. For loss through recombination, the loss rate is proportional to the electron density

n_e and the recombination coefficient α_j, thus $L_j = \alpha_j n_e$. If ion species j is the dominant species, so that $n_j \approx n_i \approx n_e$ (quasi-neutrality), Equation (3.16) gives

$$n_j = \frac{\nu_j n_n}{\alpha_j n_j} \qquad \Rightarrow \qquad n_j = \sqrt{\frac{\nu_j Q}{4\pi u_n \alpha_j}} \cdot \frac{1}{r} \quad , \tag{3.17}$$

where Equation (3.11) was used for the neutral density. Thus, if the dominant ion species is photochemically controlled and the chemical loss is dominated by recombination, the cometary plasma will have a density profile that falls of with the inverse of the radial distance r to the comet. Note however that any radial dependence of the ionization frequency (e.g. photo-absorption of solar EUV radiation by the neutral coma in the case of photoionization) has here been neglected, and could, if significant, cause deviations from a $1/r$ profile.

Transport-dominated ionopshere

If instead the chemical life time of an ion species j is much larger than the transport time ($\tau_{trans} \ll \tau_c$), as may well happen at low activity or large distances where reaction rates are low, the loss term in Equation (3.14) can be neglected and the steady state density profile is determined by the balance of production and transport:

$$\nabla \cdot (n_j \mathbf{u}_j) = P_j. \tag{3.18}$$

For transport predominantly in the radial direction, $\mathbf{u}_j = u_j \hat{\mathbf{r}}$, Equation (3.18) becomes

$$\frac{1}{r^2}\frac{d}{dr}(r^2 n_j u_j) = \frac{\nu_j Q}{4\pi u_n r^2}. \tag{3.19}$$

Integrating Equation (3.19) and solving for n_j gives

$$n_j = \frac{\nu_j Q}{4\pi u_n u_j r} + \frac{C}{r^2 u_j}, \tag{3.20}$$

where C is an integration constant. If we take the inner boundary to be the nucleus surface (at $r = R$) with $n_j = 0$, C becomes $-\nu_j Q R/4\pi u_n$, giving

$$n_j = \frac{\nu_j Q}{4\pi u_n u_j}\left(\frac{1}{r} - \frac{R}{r^2}\right) = \frac{\nu_j Q}{4\pi u_n u_j r}\left(1 - \frac{R}{r}\right). \tag{3.21}$$

In the general case, u_j depends on r, thus an explicit density profile cannot be obtained without knowledge of the radial velocity profile. This requires invoking the fluid momentum equation (3.15) for ion species j which, neglecting collisions (and chemistry) between different ion species (and assuming a single neutral species n), takes the form:

$$m_j n_j \left(\frac{\partial \mathbf{u}_j}{\partial t} + \mathbf{u}_j \cdot \nabla \mathbf{u}_j \right) = \underbrace{n_j q_j (\mathbf{E} + \mathbf{u}_j \times \mathbf{B})}_{\text{Lorentz force}} - \overbrace{\nabla \cdot \mathbf{T}_j}^{\text{pressure gradient force}} - \underbrace{m_j n_j \nu_{jn}}_{\text{ion-neutral collisions}} + \ldots$$
$$\ldots + \underbrace{(m_n \mathbf{u}_n - m_j \mathbf{u}_j) P_{n \to j}}_{\text{mass-loading}}, \quad (3.22)$$

where the parameters indexed j and n have the meanings described in connection with Equation (3.15), with $s = j$ and $t = \mathrm{n}$. The ion-neutral momentum transfer collision frequency ν_{jn} is directly proportional to n_n through a rate coefficient k_{jn} (Cravens, 1986; Cravens, 1987). The importance of ion-neutral collisions therefore increases with neutral density, and hence with comet activity, and decreases with radial distance. Close enough to a sufficiently active comet there will thus be a region where the ion and neutral velocities are closely coupled by frequent ion-neutral collisions so that $\mathbf{u}_j \approx \mathbf{u}_n$. This is a great simplification of the momentum equation and is especially useful since the neutral velocity is generally constant w.r.t. the radial distance (c.f. Section 3.1). For distances much greater than the nucleus radius, $r \gg R$ (but still smaller than the ion-neutral decoupling distance R_{jn}, to be calculated below), we then again get a density profile that falls off with the inverse of the radial distance, although with a different dependence on the outgassing Q:

$$n_j = \frac{\nu_j Q}{4\pi u_n^2 r} \left(1 - \frac{R}{r} \right) \xrightarrow{r \gg R} \frac{\nu_j Q}{4\pi u_n^2 r}. \quad (3.23)$$

Note that here there was no need to assume j to be the dominant species in the plasma, Equation (3.23) thus also holds for minor ion species in the coma.

Ion-neutral decoupling distance

An estimate of the ion-neutral decoupling distance R_{jn} is often obtained (e.g. Gombosi, 2015) by equating the ion-neutral coupling time scale, $\tau_{jn} = 1/\nu_{jn}$, with the characteristic transport time τ_{trans}. As the plasma density goes as $1/r$, it is clear that ℓ, the characteristic scale length of the plasma, is given by r. Since ion-neutral coupling is presumed to hold out to R_{jn}, $\mathbf{u}_j = \mathbf{u}_n$ inside R_{jn}, the characteristic transport time $\tau_{\mathrm{trans}} = r/u_n$. Using Equation (3.11) for the neutral density then gives the ion-neutral decoupling distance (for ion species j) as

$$R_{jn} = \frac{k_{jn} Q}{4\pi u_n^2}. \quad (3.24)$$

For a neutral outflow velocity of $\lesssim$1 km/s (Tenishev et al., 2008), an outgassing rate $\sim 10^{28}$ s -1, typical of 67P at perihelion, and a rate coefficient $k_{in} = 1.1 \cdot 10^{-9}$ cm^{-1} for a major ion species (i) of H_3O^+ in a water-dominated

coma (Cravens, 1986; Cravens, 1987), this gives $R_{\text{in}} \approx 900$ km. This distance is much larger than typical cometocentric distances of Rosetta around perihelion ($\gtrsim$150 km, see e.g. Paper III, Figure 5 for an overview plot containing outgassing rate and spacecraft radial distance throughout Rosetta's stay at the comet). Yet, in Paper III, we found that the cometary ions were not strongly collisionally coupled to the neutral gas, even in the inner-most part of the coma (the so called *diamagnetic cavity*, c.f. Section 3.5.5) but had typical outflow velocities of 2 – 4 km/s (see also Vigren et al., 2017). Thus Equation (3.24) appears to be off here. The problem lies in the simplified approach taken when calculating the characteristic transport time τ_{trans} above, which included the assumption that the ions were collisionally coupled out to R_{in} (i.e. $\mathbf{u}_{\text{i}} = \mathbf{u}_{\text{n}}$). This is only true in a statistical sense; in fact some ions will undergo early collisions and some will not collide until much later. In the absence of external forces to substantially accelerate the ions between collisions this matters little, but if an electric field is present (e.g. an ambipolar field in the presence of warm electrons, see e.g. Papers I — III and Sections 5.1 – 5.3) ion acceleration between collisions can be significant, decreasing their effective transport time and, consequently, their effective decoupling distance (Vigren and Eriksson, 2017). Since the ion-neutral momentum transfer collision frequency ν_{in} decreases with the neutral density as $1/r^2$, the effective decoupling distance given by Equation (3.24) may be severely overestimated (Vigren and Eriksson, 2018, submitted).

Transport and chemistry

When the chemical life time and transport time are comparable ($\tau_{\text{trans}} \sim \tau_{\text{c}}$) and both radial transport and recombination must be included, the steady state continuity equation becomes

$$\frac{1}{r^2}\frac{d}{dr}(r^2 n_j u_j) = \frac{\nu_j Q}{4\pi u_{\text{n}} r^2} - \alpha_j n_{\text{e}} n_j. \tag{3.25}$$

Again assuming ion-neutral collisional coupling, an analytical solution can be obtained also in this case. The expression, not to mention the calculations required to obtain it, is rather involved in the general case with a finite size nucleus (see Beth et al., 2018), but for distances much greater than the nucleus radius, $r \gg R$ (but still smaller than the ion-neutral decoupling distance $R_{j\text{n}}$) it simplifies to (Gombosi, 2015)

$$n_j \approx \left(\sqrt{1+\frac{Q}{Q_0}}\right)\frac{u_{\text{n}}}{2\alpha_j r}, \tag{3.26}$$

where

$$Q_0 = \frac{\pi u_{\text{n}}^3}{\nu_j \alpha_j}. \tag{3.27}$$

Thus, for radial distances much greater than the nucleus radius, we again get a density profile that falls off with the inverse of the radial distance r.

Transport and ambipolar electric field

Even if the electron and ion gases have the same temperature, their thermal speeds will differ by a factor equal to the square root of the mass ratio, i.e. about 180 for water ions. Around the comet nucleus, there is a strong inward density gradient in the neutral gas which is the source for the charged particles. The much faster motion of the electrons would in the absence of an electric field lead to a 180 times higher outward flux of electrons than ions, which of course rapidly violates quasineutrality. In consequence, an outward electric field known as the *ambipolar field* forms to maintain the charge balance, accelerating ions outward and retaining electrons. If the ion velocity is constrained to equal the neutral gas velocity by strong ion-neutral collisional coupling, the resulting field magnitude can be shown (by balancing the pressure gradient and electric field terms in the electron fluid equation of motion) to be KT_e/er for distances large compared to the nucleus size, assuming isothermal electrons and spherical symmetry. Furthermore, Vigren et al., 2015 showed that a $1/r$ electric field also provides a self-consistent solution if the ions are free to move under the action of this field, under the same assumptions on isothermal electrons and spherical symmetry. The ambipolar field is weaker in this situation, but its form is still $1/r$. The only plasma simulations yet able to self-consistently model it are particle-in-cell (PIC) simulations by Deca et al. (2017). Despite insufficient spatial resolution for handling the near-nucleus region, the ambipolar field can in these simulations be seen to retain cometary electrons and accelerate solar wind electrons toward the innermost region.

As this ambipolar field influences also the ions, it is of high interest for understanding the behaviour of the innermost coma. In Paper III, we will attribute the elevated ion speeds we find mainly to this field. It should be noted that ambipolar fields are well known also from the terrestrial ionosphere, and they also turn up as the pressure gradient term in the generalized Ohm's law used to interpret data and simulations of reconnection in the terrestrial magnetosphere.

Observations

Empirical observations of cometary plasma density profiles were e.g. reported from Halley's comet by Balsiger et al. (1986), derived from the sum of ion mass spectrometer count rates for masses 16-19 and 32, observed during the Giotto flyby in 1986, and shown in Figure 3.1(a). The plasma density followed a close to $1/r$ dependence out to about 10^4 km from the nucleus, in agreement with the derivations in this Section. Further out, the density profile changed to an inverse square law, consistent with constant radial expansion in the absence of production (and chemical loss), as was discussed in the context of the neutral gas coma in Section 3.1. It may be concluded that in the outer parts

of the coma, the neutral gas was too tenuous for ionization of it to effectively replenish the expanding plasma, whose density profile therefore approached the $1/r^2$ dependence prescribed by simple radial expansion.

Unlike the fast Giotto flyby of comet Halley, Rosetta at 67P mostly followed a steady trajectory in the terminator plane with only very slow variations in radial distance. Thus, radial density variations could not easily be disentangled from long-term variations due to changing heliocentric distance and activity of the comet. However, a radial density profile was nevertheless obtained from Rosetta Langmuir probe observations at 67P by Edberg et al. (2015), during two close flybys of the nucleus in February 2015, when the spacecraft came within 6 km of the nucleus and went out to a maximum of ∼260 km, see Figure 3.1(b). The cometary plasma at 67P was highly variable and exhibited strong dynamics on short timescales, thus the measurements have a large scatter (grey dots, the red dots show mean values computed in altitude intervals of 5 km). Yet, the average profile exhibited a close to $1/r$ dependence (black line). In fact, a least squares fit of a power law to the median values produced an altitude dependence $1/r^{1.06}$.

It may be noted that while a $1/r$ dependence is consistent with the assumptions behind Equation (3.25), it does not imply them. For example, Vigren et al. (2015) showed that for collisionless ions and a radial electric field $E \sim 1/r$, the density still follows $1/r$.

3.3 Interaction of the cometary plasma with the solar wind

3.3.1 Ion pickup by the solar wind

An important process driving much of the dynamics in the cometary plasma environment is the pick-up of newly produced cometary ions by the solar wind convective electric field. Consider an ion of mass m and charge q created in the solar wind. In the comet reference frame, the solar wind is a flowing plasma with velocity $\mathbf{v}_{\rm sw}$ permeated by the interplanetary magnetic field $\mathbf{B}_{\rm IMF}$. In this reference frame, the ion will be accelerated by a convective electric field

$$\mathbf{E} = -\mathbf{v}_{\rm sw} \times \mathbf{B}_{\rm IMF}, \tag{3.28}$$

giving

$$\frac{d\mathbf{v}_{\rm i}}{dt} = \frac{q}{m}(\underbrace{\mathbf{E}}_{-\mathbf{v}_{\rm sw}\times\mathbf{B}_{\rm IMF}} + \mathbf{v}_{\rm i} \times \mathbf{B}_{\rm IMF}) = \frac{q}{m}(\mathbf{v}_{\rm i} - \mathbf{v}_{\rm sw}) \times \mathbf{B}_{\rm IMF}. \tag{3.29}$$

For simplicity, assume $\mathbf{B}_{\rm IMF} \perp \mathbf{v}_{\rm sw}$ and let $\mathbf{v}_{\rm sw} = v_{\rm sw}\hat{\mathbf{x}}$ and $\mathbf{B}_{\rm IMF} = B\hat{\mathbf{z}}$. Neglecting ion motion parallel to the magnetic field, we have for the x and y components of $\mathbf{v}_{\rm i}$, v_x and v_y,

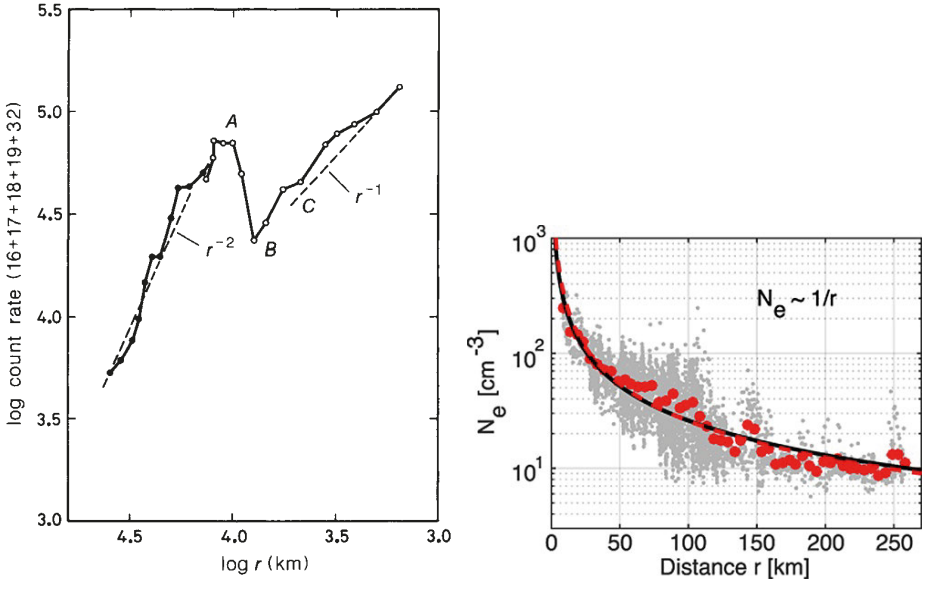

(a) Sum of ion mass spectrometer count rates for masses 16-19 and 32, observed by Giotto during the Halley flyby in 1986. *(Adapted from Balsiger et al., 1986. Reprinted with permission from the publishers.)*

(b) Radial density profile observed by Rosetta during a close flyby in early 2015. *(Reprinted from Edberg et al., 2015, with permission from the publishers.)*

Figure 3.1. In situ observations of cometary ionospheric density profiles.

$$\dot{v}_x - \omega_c v_y = 0 \tag{3.30}$$

$$\dot{v}_y + \omega_c v_x = \omega_c v_{sw} \quad , \tag{3.31}$$

where $\omega_c = \frac{qB}{m}$ is the ion cyclotron frequency and the dot notation is short hand for $\frac{d}{dt}$. Differentiating Equation (3.30), solving for $\dot{v}_y$ and substituting the result for $\dot{v}_y$ in Equation (3.31) gives

$$\dot{v}_y = \frac{\ddot{v}_x}{\omega_c} \tag{3.32}$$

$$\ddot{v}_x + \omega_c^2 v_x = \omega_c^2 v_{sw} \quad . \tag{3.33}$$

Equation (3.33) is a non-homogeneous, linear, second order differential equation, the general solution to which is the sum of the general solution to the corresponding homogenous equation ($v_{x,h}$) and a particular solution to the non-homogenous equation ($v_{x,p}$):

$$v_x = \underbrace{C\cos\omega_c t + D\sin\omega_c t + Et + F}_{v_{x,h}} + \underbrace{v_{sw}}_{v_{x,p}} \quad , \tag{3.34}$$

where C, D, E and F are arbitrary constants. The initial speed of the newly created ion, being of the same order of magnitude as the outflow speed of the neutral gas ($\sim$ 1 km/s), is entirely negligible compared to typical solar wind speeds ($\sim$ 400 km/s), so the ion may be considered to be initially at rest. Given that the solar wind electric field is in the $\hat{\mathbf{y}}$ direction and the Lorentz force vanishes for a particle at rest, the initial acceleration of the ion will be zero in the $\hat{\mathbf{x}}$ direction. Imposing such initial conditions on Equation (3.34) gives $D = E = 0$ and $F = -(C + v_{\rm sw})$. Equation (3.32) now gives

$$\dot{v_y} = -\omega_{\rm c} C \cos \omega_{\rm c} t \quad , \tag{3.35}$$

but we know that the initial acceleration in the $\hat{\mathbf{y}}$ direction is $-\omega_{\rm c} v_{\rm sw}$, thus we have $C = v_{\rm sw}$ and the ion motion becomes

$$v_x = v_{\rm sw}(1 + \cos \omega_{\rm c} t) \tag{3.36}$$

$$v_y = -v_{\rm sw} \sin \omega_{\rm c} t \quad . \tag{3.37}$$

Defining the origin as the starting point of the ion, integration of Equations (3.36) and (3.37) yields

$$x(t) = v_{\rm sw} t + \frac{v_{\rm sw}}{\omega_{\rm c}} \sin \omega_{\rm c} t \tag{3.38}$$

$$y(t) = \frac{v_{\rm sw}}{\omega_{\rm c}} \cos \omega_{\rm c} t \quad . \tag{3.39}$$

The ion thus follows a cycloid motion at the cyclotron frequency, with an effective drift velocity of $v_{\rm sw}$ in the solar wind direction. Such an ion is said to have been *picked up* by the solar wind and is referred to as a *pick-up ion*. Taking the vector product of Equation (3.28) with $\mathbf{B}_{\rm IMF}$ from the right and recalling that $\mathbf{B}_{\rm IMF} \perp \mathbf{v}_{\rm sw}$, $\mathbf{v}_{\rm sw}$ can be solved for, giving

$$\mathbf{v}_{\rm sw} = \frac{\mathbf{E} \times \mathbf{B}_{\rm IMF}}{B_{\rm IMF}^2} \quad , \tag{3.40}$$

where $B_{\rm IMF}$ is the magnitude of $\mathbf{B}_{\rm IMF}$. Equation (3.40) is the well-known expression for $\mathbf{E} \times \mathbf{B}$ drift of a plasma in the presence of an electric field parallel to the background magnetic field. Thus, the phenomenon of ion pick-up can be viewed in the cometary reference frame as $\mathbf{E} \times \mathbf{B}$ drift of the cometary ions in the convective electric field of the solar wind.

The pick-up ion population, being continuously replenished by newly created ions in different phases of their gyro-motion, forms a ring distribution in phase space. If the magnetic field is not exactly perpendicular to the solar wind velocity, no convective electric field exists in the direction of the component of the solar wind velocity parallel to $\mathbf{B}$. Hence the ions will not be immediately accelerated in this direction, thereby forming an ion beam in the solar

wind frame. Thus, the general phase space configuration of the pick-up ions in the solar wind frame is that of a combined ring-beam distribution (Coates et al., 2015; Coates, 2017). This distribution is highly unstable to a number of different low-frequency wave modes, perhaps the most important one being ion cyclotron waves (Tsurutani, 1991). While such waves were detected by Giotto at Halley, no sign of such waves has yet been reported from the Rosetta data, probably because the pick-up process is not complete in the case of 67P, with its much smaller interaction region. This will be discussed in some detail at the end of Section 3.3.2 below.

3.3.2 Mass loading of the solar wind

The pick-up process described in the previous section clearly imparts momentum to the initially stationary cometary ions. Conservation of momentum requires that this come from somewhere; in fact, an equal amount of momentum is removed from the solar wind, causing it to decelerate. The continual influx of non-decelerated solar wind plasma from upstream of the ion pick-up region leads to a compression and densification of the decelerating plasma, a process known as *mass loading*. In the previous section, such feedback on the solar wind from the pick-up ions was neglected, assuming that the solar wind conditions remain unchanged throughout the ion pick-up process. While this may be valid in the limit of small densities of cometary ions, it certainly does not hold once this density becomes appreciable compared to the solar wind. Indeed, most of the large scale processes in the plasma environment of an active comet derive in one way or another from the mass loading process.

The physical mechanisms responsible for the momentum transfer are rather complicated when examined in detail (Coates and Jones, 2009). However, a simplified macroscopic model can be obtained on temporal and spacial scales relevant for the ion dynamics (Omidi et al., 1986). Then, the much lighter and more mobile electrons essentially behave as a massless fluid that immediately moves to cancel out any electrostatic fields in the plasma rest frame. Neglecting resistive effects, any currents in the plasma will also be canceled out by electron motions. Charge neutrality and the zero-current condition then give (in the comet reference frame where $\mathbf{v}_\mathrm{i} = 0$ to begin with)

$$\rho_\mathrm{e} = n_\mathrm{sw} + n_\mathrm{i} - n_\mathrm{e} = 0 \tag{3.41}$$

$$\mathbf{J} = n_\mathrm{sw}\mathbf{v}_\mathrm{sw} - n_\mathrm{e}\mathbf{v}_\mathrm{e} = 0 \quad , \tag{3.42}$$

where n_sw and $\mathbf{v}_\mathrm{sw}$ are the density and velocity of the undisturbed solar wind, respectively, n_i and v_i the density and velocity of the pick-up ions, and n_e and $\mathbf{v}_\mathrm{e}$ are the density and velocity of the electrons, modeled here as a single fluid since their massless nature means that they will be instantly picked up

and mixed into the combined flow. The equation of motion of the massless electrons ($m_e = 0$) is

$$m_e \frac{d\mathbf{v}_e}{dt} = -e(\mathbf{E} + \mathbf{v}_e \times \mathbf{B}_{IMF}) = 0 \quad , \tag{3.43}$$

while solving Equations (3.41) and (3.42) for $\mathbf{v}_e$ gives

$$\mathbf{v}_e = \frac{n_{sw}\mathbf{v}_{sw}}{n_{sw} + n_i} \quad . \tag{3.44}$$

Thus, the pick-up process will decrease the bulk electron velocity by a factor $n_{sw}/(n_{sw} + n_i)$. The resulting electric field can be obtained by solving for $\mathbf{E}$ in Equation (3.43) and substituting Equation (3.44) for $\mathbf{v}_e$, giving

$$\mathbf{E} = \frac{n_{sw}}{n_{sw} + n_i}\mathbf{v}_{sw} \times \mathbf{B}_{IMF} \quad . \tag{3.45}$$

The $\mathbf{E} \times \mathbf{B}$ drift velocity of the pick-up ions is then

$$\mathbf{v}_{i,final} = \frac{1}{B_{IMF}^2}\frac{n_{sw}}{n_{sw} + n_i}(\mathbf{v}_{sw} \times \mathbf{B}_{IMF}) \times \mathbf{B} = \frac{n_{sw}\mathbf{v}_{sw}}{n_{sw} + n_i} = \mathbf{v}_e \tag{3.46}$$

and the same holds for the original solar wind ions. Hence, the result of the mass loading is a combined flow of solar wind ions, pick-up ions and electrons at a reduced speed given by Equation (3.44).

Intermediately active comet

The pick-up process described above may be complicated in the case of a strongly non-homogeneous ion density. It should hold locally where the ion gyro-radius is sufficiently larger than the gradient scale of the ion density. The latter cannot be longer than the distance to the nucleus (see Equation (3.26)), so in practive the possible applicability of Equation (3.46) will be restricted to distances from the nucleus several times the gyro-radius of a pick-up ion. For typical solar wind parameters of 400 km/s and 1 nT, this means several hundred thousand km. Effects of mass loading and magnetic field compression can decrease this value, but for Rosetta, staying within a few thousand km of the nucleus during the high-activity phase of the comet, and most of the time within a few 100 km, we unsurprisingly did not observe an environment dominated by fully picked up cometary ions (Nilsson et al., 2015a; Behar et al., 2016; Behar et al., 2017). Instead, we observed only the very initial phase of the pick-up process, where solar wind and cometary ions were deflected in opposite directions in each other's convective electric fields, and did not have time to gyrate much before leaving the comet-solar wind interaction region, or at least the part of it probe by Rosetta. Figure 3.2 shows ion velocity distributions of solar wind protons, rotated into a Comet–Sun–Electric field (CSE) frame (Behar et al., 2017), obtained by RPC-ICA during the early phase of

the mission (top row) and later on when activity had increased (bottom row). In low-activity case, the ions have a beam-like distribution centered on the anti-sunward direction (v_x) whereas in the second case, there is substantial deflection from the anti-sunward direction and a partial ring distribution has formed.

3.4 Plasma observed by Rosetta at comet 67P

3.4.1 Electrons

Warm electrons and spacecraft potential

Upon arrival at comet 67 in the fall of 2014, Rosetta encountered a fledgling cometary plasma environment in the early stages of formation (Yang et al., 2016; Nilsson et al., 2015a). Electron cooling was highly inefficient in the tenuous neutral gas of the nascent cometary coma, so the warm coma photoelectrons resulting from photoionization of the neutral gas (c.f. Section 3.2.2) retained temperatures on the order of 5 – 10 eV. This drove the spacecraft potential negative, typically to $\gtrsim$-5 – -10 V (see also Section 5.1 and Paper I). As the comet activity increased during the mission, electron cooling never properly set in in the region probed by Rosetta. Thus the warm electrons persisted, and the negative spacecraft potential increased in magnitude along with the plasma density, to at most $\sim$-20 – -30 V close to perihelion (c.f. Section 5.2 and Paper II). Thus these warm photoelectrons were a ubiquitous feature throughout Rosetta's stay at the comet. They are the focus of Papers I and II in this thesis, and are also of substantial interest in Paper III. More details can be found there, and in the corresponding summaries in Sections 5.1-5.3.

Cold electrons

In addition to the warm un-cooled coma photoelectrons just described, a population of cold electrons, with characteristic energies $\lesssim$0.1 eV, has also been identified in the data from both LAP and MIP (Eriksson et al., 2017; Gilet et al., 2017; Engelhardt et al., 2018). These are characteristically observed as intermittent pulses of cold electrons reaching the LAP probes, typically lasting for a few to a few tens of seconds as seen in the spacecraft frame, see Figure 3.3(b). They are also detected completely independently by MIP in the form of a second resonance peak in their mutual impedance spectra, associated with an electron acoustic wave mode that occurs in a plasma with two distinct electron populations at different temperatures. They presumably obtain their low temperatures from cooling by collisions with neutrals in the densest inner part of the coma (inside of Rosetta's position, as evidenced by the persistently negative spacecraft potential). The reason behind their sporadic occurrences is still unclear, but has been suggested to be due to a filamentation of the cold plasma in the inner coma (Eriksson et al., 2017), analogous to what has been

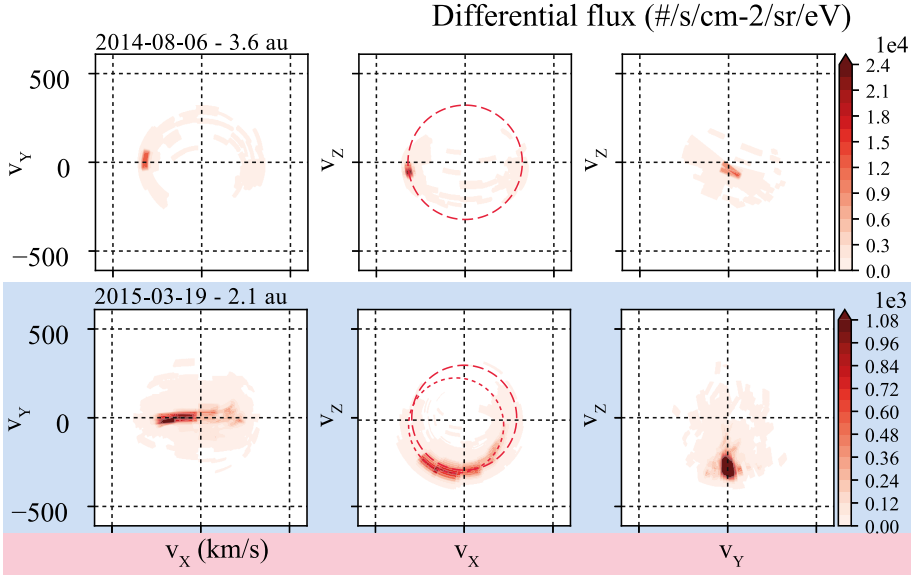

Figure 3.2. Ion distributions observed at 67P by RPC-ICA in (an estimation of the) Comet–Sun–Electric field frame (CSE), which has its x-axis pointing to the Sun, its z-axis along the upstream E-field and the upstream B-field lying in the x-y plane. *(Adapted from Behar et al., 2017. Reprinted with permission from the publishers.)*

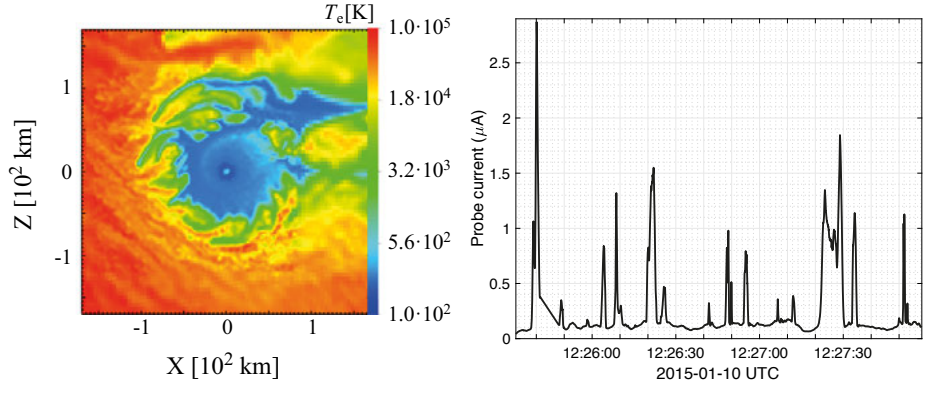

(a) Filamentation of cold-electron plasma in hybrid simulations of the cometary plasma environment. Color indicates electron temperature. The Sun is in the -x direction and the undisturbed interplanetary magnetic field is along the z.axis. *(Adapted from Koenders et al., 2015. Reprinted with permission from the publishers.)*

(b) Intermittent pulses of cold electrons observed in LAP current measurements at fixed bias potential ($\propto n_e/T_e$). The large currents in these pulses cannot be explained by warm plasma alone, without invoking implausibly large densities. Thus, they must include cold ($\lesssim$0.1 eV) electrons.

Figure 3.3. Filamentation of cold plasma, simulations and measurements.

observed in hybrid simulations (Koenders et al., 2015), depicted in Figure 3.3. However, the hybrid simulations cannot distinguish between different electron populations (the warm one and the cold one, in this case) so the relationship, if any, between the filamentation therein and the intermittent cold plasma observed by Rosetta is not clear. The cold electrons are further investigated in Engelhardt et al. (2018), as well as in Paper III of this thesis.

Hot ("supra-thermal") electrons

Supra-thermal electrons accelerated up to several hundreds or thousands of eV, were detected by IES (Clark et al., 2015; Broiles et al., 2016). Their origin is still unclear, but they appeared to become more numerous during periods of stormy solar wind (Edberg et al., 2016b), which might indicate that the responsible heating mechanism was connected to the solar wind energy input. Lower-hybrid waves, which have been observed at the comet (Karlsson et al., 2017; André et al., 2017) have also been suggested as a possible source of at least part of these accelerated electrons. However, these electrons are outside the main scope of this thesis, and will not be discussed further here.

3.4.2 Ions

Types

An example of the different ion populations observed by Rosetta is shown in Figure 3.4(a) (Berčič et al., 2018). They can crudely be divided into three main categories based on the energy range in which they are observed: (pop. 1) high-energy ($\gtrsim$ few hundred eV) ions of solar wind origin (protons, alpha particles and He^+), (pop. 2) intermediate energy (a few tens to a few hundred eV) cometary pickup ions created upstream and accelerated by the convective electric field perpendicular to the solar wind direction (c.f. Section 3.3.1), and (pop. 3) low-energy (a few eV to a few tens of eV, close to the spacecraft potential) "locally produced" cometary ions not yet picked up by the solar wind electric field (denoted "expanding ion population in Figure 3.4(a)). The latter two populations were of cometary origin and are generally considered to be predominantly water group ions (molecular masses 16-19).These were both observed consistently throughout Rosetta's stay at the comet. The observed flux of low-energy ions (pop. 3) was relatively constant throughout this time because the orbit of Rosetta increased with comet activity in order to keep away from the most dust-prone region close to the nucleus for operational reasons. In contrast, the ions of solar wind origin (pop. 1) went completely missing between about mid-April to mid-December 2015, during the time of highest activity of the comet. This was due to deflection of these solar wind ions away from the inner region of the coma and will be discussed in more detail in Section 3.5.2 (see also Behar et al., 2017). The accelerated pickup ions on the other hand, were still observed throughout this time. For more

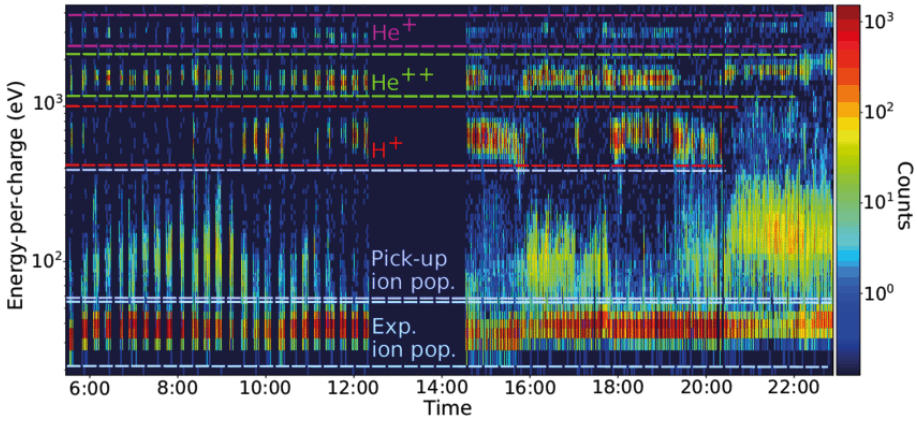

(a) Ions popluations observed by RPC-ICA at 67P (13 January 2015).

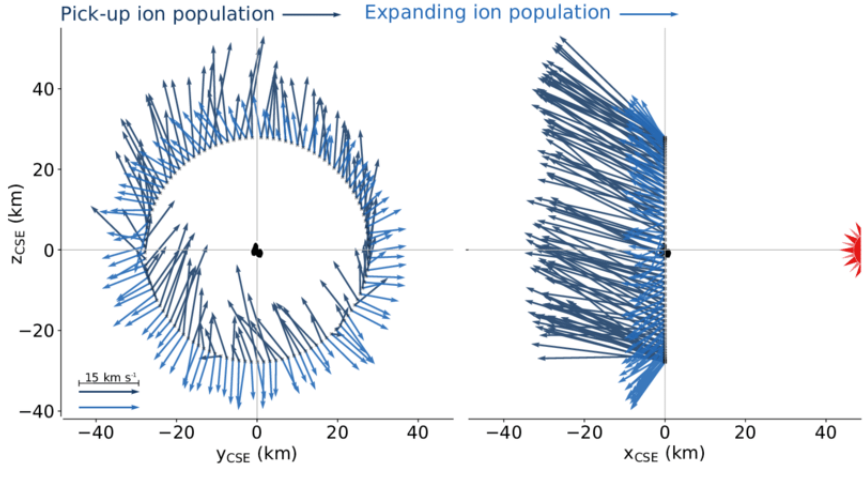

(b) Dynamics of low-energy ions at 67P.

Figure 3.4. Ion flow directions at 67P. *(Adapted from Berčič et al., 2018. Reprinted with permission from the publishers.)*

details on the evolution of the ion environment of 67P during the mission, see Nilsson et al. (2015a), Nilsson et al. (2015b), and Nilsson et al. (2017).

Dynamics

The flow of the picked-up (pop. 2) and low-energy (pop. 3) ion populations observed during the relatively early phase of cometary activity (13 January 2015) is shown in Figure 3.4(b) (Berčič et al., 2018) in the CSE frame (c.f. Figure 3.2). The flow in the terminator plane (left panel in Figure 3.2) is close to radial for the low energy ions (pop. 3), while the pickup ions (pop. 2) is predominantly in the direction of the electric field (the z-axis of the CSE system). Both populations additionally have strong anti-sunward components

(right panel in Figure 3.2), consistent with acceleration along a solar wind convective electric field that has an anti-sunward component due to the deflection of the solar wind (for details, see Berčič et al., 2018, in particular their Figure 6). This well illustrates the picture we have of the cometary ions at 67P, with two dynamically distinct, but not spatially separated populations: one locally produced (pop. 3) flowing (close to) radially outward from the nucleus and one picked-up by the solar wind electric field (pop. 2) flowing (close to) the solar wind electric field direction. The motion of the low-energy cometary ions (pop. 3) during the high-activity phase of the comet has also been investigated by Vigren and Eriksson (2017) and Vigren et al. (2017) and is the main focus of Paper III of this thesis.

3.5 Morphology of the cometary plasma environment

The interaction between plasma of cometary origin and the solar wind produces a highly structured plasma environment characterized by multiple regions of different bulk properties, which are separated by sharp boundaries or broader transition regions. An overview of the resulting morphology will now be given, again starting from the picture obtained from the Halley flybys (the "canonical model") and comparing to hybrid plasma simulations (Koenders et al., 2015) of 67P and observations by Rosetta. The presentation is built around the graphical illustration of the cometary plasma environment of an active comet shown in Figure 3.5, originally published by Mendis (1988).

3.5.1 Bow shock formation

Canonical model

The solar wind constitutes a *supersonic* flow of plasma, in the sense that the bulk (or drift) speed is higher than the speed of the constituent particles in their gyration orbits. For an active comet, the deceleration of the solar wind due to the mass loading process described in the previous section can be strong enough to induce a transition to subsonic flow. This transition gives rise to a *bow shock* (c.f. Figure 3.5), where the the mass-loaded solar wind is abruptly slowed, heated, compressed, and diverted. Due to the tenuous nature of the solar wind, the mean free path of two-body Coulomb collisions is too large for them to affect the formation or energy dissipation of the shock. The cometary bow shock is therefore a collisionless shock, where the dynamics is dominated by wave-particle interactions driven by the instabilities that arise from particles having similar bulk and gyration speeds.

Cometary bow shocks are different from the bow shocks of magnetized bodies like the Earth in that the mass loading takes place on much larger spatial scales than the solar wind-magnetosphere interaction. Analytical one-dimensional fluid models by Biermann et al. (1967) and Flammer and Mendis

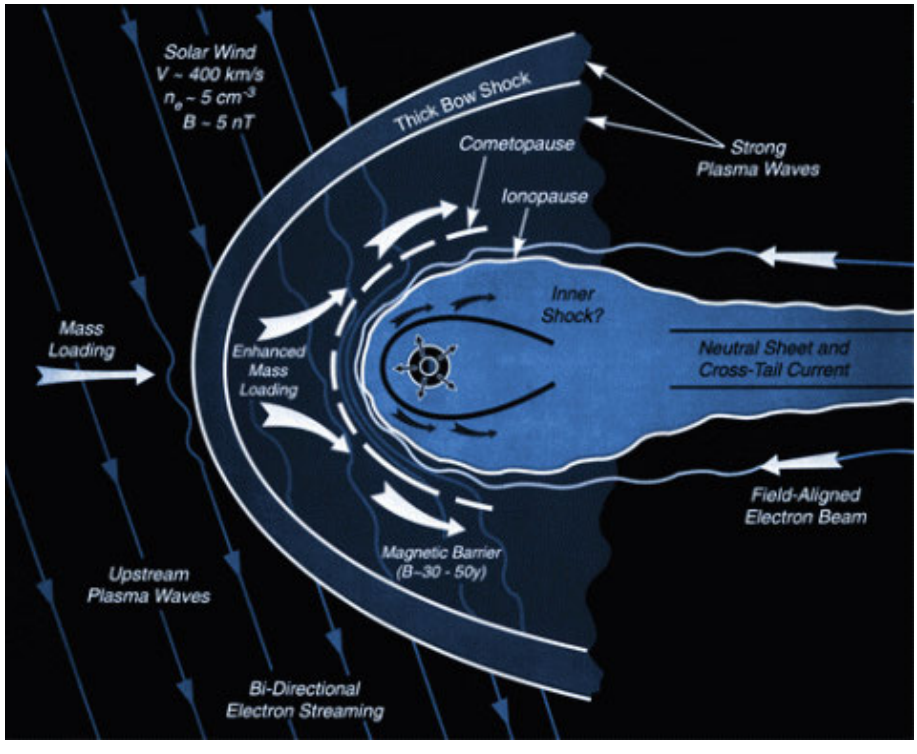

Figure 3.5. Plasma environment of an active comet nucleus. *(Image credit: NASA/JPL)*

(1991) showed that the bow shock would occur at a distance where the mass flux density, which increases as a consequence of mass loading, reaches a critical value which depends on the ratio of specific heats, the dynamic pressure, the magnetic pressure and the thermal pressure in the undisturbed solar wind. Actual stand-off distances can range from $\sim 10^3$ km for weakly outgassing comets (Koenders et al., 2013) to $\sim 10^5$ km (Coates, 1995) for very active comets.

Intermediately active comet

No bow shock has yet been identified in the Rosetta data, which has been attributed to the close distance of Rosetta to the nucleus during the time when the activity was sufficient for a bow shock to form. (See point 7. in Chapter 4 for a further discussion of this.)

3.5.2 Cometopause and collisionopause

Canonical model

Downstream of the bow shock, the mass loading continues at an accelerated rate as the density of cometary ions increases towards the nucleus (c.f. Fig-

ure 3.5). The increased densities of cometary neutrals and ions also mean that collisions become more and more frequent with decreasing cometocentric distance. The distance at which collisions become important for the plasma dynamics is referred to as the *collisionopause*. A more quantitative formulation of this can be obtained by comparing the residence time of the plasma in the region of interest, the characteristic transport time τ_T, to the characteristic collision time τ_c. τ_T is typically taken to be the ratio of the cometocentric distance and local flow speed, while τ_c is the average time between collisions. The collisionopause is the location where $\tau_T \approx \tau_c$. It is important to note that there are many different kinds of collisional processes occurring in the cometary coma, each with its own characteristic time τ_c and therefore also its own separate collisionopause. Examples of collisional processes in the coma include charge exchange, electron cooling and ion-neutral chemistry. The collisionopause for charge exchange between solar wind protons and neutrals, described in Section 3.2.2, is often called the *cometopause* (Cravens, 1991), because it produces a transition (sometimes quite sharp, sometimes rather broad) of the plasma composition from solar wind dominated to cometary dominated.

Intermediately active comet

The situation encountered by Rosetta at comet 67P was quite different. Recall from Section 3.3.2 that we did not see fully picked-up cometary ions at 67P. Instead, the solar wind and cometary ions were deflected in opposite directions in each other's convective electric fields. The deflection increased along with the activity evolution of the comet, see Figure 3.6 where the top panel shows the deflection angle (from the anti-sunward direction) of protons observed by RPC-ICA (Behar et al., 2017). On 28 April 2015, at 1.76 au, the deflection approached 180°, meaning that the solar wind approached Rosetta from a direction opposite to the Sun. After this, the solar wind protons (and alpha particles, not shown) were absent, as shown in the middle panel of Figure 3.6, showing energy spectrograms for solar wind ions (Nilsson et al., 2017). Between 28 April 2015 and 11 December 2015 (at 1.64 au), no solar wind ions were observed (except for a tiny number of events, at least one of which was clearly related to extreme solar wind conditions, in this case a Coronal Mass Ejection (CME) hitting the coma (Edberg et al., 2016a)). When the solar wind was next (consistently) observed, in December 2015, it also had a the deflection angle around 180°, which then gradually decreased following the decrease in comet activity down to close to zero at the end of the mission. A picture thus emerges in which the solar wind ions were entirely deflected away from the inner coma during the comet's most active phase. The mechanism behind this is illustrated in Figure 3.7: The solar wind ions enter the region of interaction with the cometary ionosphere on initially unidirectional anti-sunward trajectories. They are then deflected in the convective electric field of the newly produced cometary ions. Solar wind ions reaching the near-nucleus region will thus not come from directly upstream (such ions will be deflected

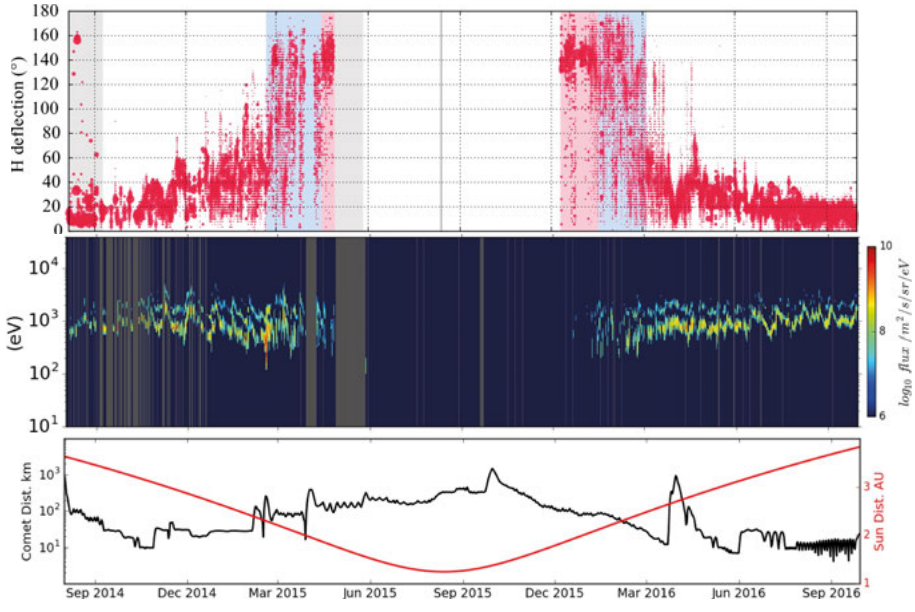

Figure 3.6. Solar wind deflection (top) and solar wind ion flux (middle) at 67P, as observed by RPC-ICA. *(Adapted from Behar et al., 2017 and Nilsson et al., 2017. Reprinted with permissions from the publishers.)*

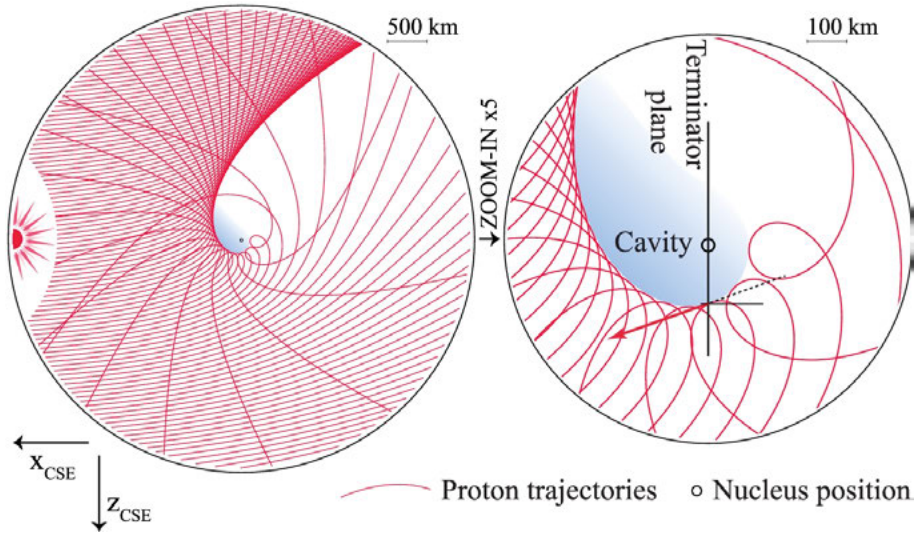

Figure 3.7. Deflection of the solar wind away from the inner coma and the formation of a "solar wind cavity". *(Adapted from Behar et al., 2017. Reprinted with permission from the publishers.)*

away from the nucleus). They will instead originate on trajectories along the flanks, that have been deflected just enough to reach this inner region. The

instantaneous radius of curvature of their trajectories at any point will be their gyro-radius given by the magnetic field at that point. If at any point in the inner coma, the magnetic field is strong enough that the gyro-radius of solar wind ions locally becomes smaller than the distance to the nucleus, there will be a region further inside into which they cannot reach. This is the solar wind cavity. In a sense, the solar wind ions become marginally magnetized just outside the solar wind cavity and start to grad-B drift around it. Only, due to the gradient length of the magnetic field being smaller than their gyro-radii, they will not complete a full gyration but gradually become unmagnetized again during the course of their orbit, as they enter regions of weaker magnetic field.

For an intermediately active comet like 67P, this occurred outward of the charge exchange collisionopause and thus filled a similar function to this in terms of producing a comtopause-like transition from solar-wind to cometary dominated ions, at 67P typically denoted the "solar wind cavity" (not to be confused with the diamagnetic cavity, to be discussed below). However, unlike the broad collisional cometopause at a strongly active comet, which only represents a transition in terms of what ion species are most abundant (solar-wind or cometary ions), the solar wind cavity was bounded by a sharp transition, inside which ions of solar wind origin were *completely absent*. In the Halley case, complete expulsion of solar wind ions only occurred inside the diamagnetic cavity, a region well inside of the cometopause, to be discussed below.

3.5.3 Flow stagnation and magnetic barrier

Canonical model

Inside the cometopause, the solar wind is subject to strong deceleration due to collisions of solar wind ions with cometary neutral molecules, in addition to mass loading. It also cools by charge exchange reactions (c. f. 3.2.2) between solar wind ions, or energetic pick-up ions created upstream, and the cold cometary neutrals. For very active comets, with vast solar wind interaction regions where spatial scales are large, the typical gradient length in the plasma is much greater than the ion gyro-radius. As the magnetic field is frozen into the solar wind, it effectively piles up in front of the comet nucleus as the solar wind decelerates and compresses. Thus, in this region, known as the *magnetic barrier region* (c.f. Figure 3.5), the field strength increases and the magnetic pressure grows, at the expense of solar wind dynamic pressure. As a result, the solar wind eventually almost completely stagnates.

Intermediately active comet

Obviously, this picture needs modification in the case of an intermediately active comet like 67P, where the ions (both solar wind and cometary) were un-magnetized (or at most only very weakly magnetized) and ions of solar

wind origin were completely absent inside the "cometopause", the region also known as the solar wind cavity. Even though ions of solar wind *origin*, such as protons and alpha particles, were absent, cometary pick-up ions still persisted (Nilsson et al., 2017). These are heavier and therefore have larger gyro-radii at a given energy (by a factor $\sim$4), thus they are generally less deflected. Also, they are continuously born and picked-up throughout the comet-solar wind interaction region. Therefore there will always be some pick-up ions born close enough to or inside of the solar wind cavity so as to not yet have been completely deflected. Even though these ions are un-magnetized (even more so than the solar wind ions on account of their larger gyro-radii) the *electrons* are still magnetized, and will carry the solar wind magnetic field (and associated convective electric field) with them. To maintain quasi-neutrality, the electrons must more or less follow the ions, so in effect the magnetic field will still follow the ions as well. Thus the pick-up ions will in a sense play the role of the mass-loaded solar wind in the plasma dynamics inside the solar wind cavity.

It should be noted, however, that the PIC simulations by Deca et al. (2017), which unlike the hybrid simulations can distinguish between different electron populations, showed that close to the nucleus it was in fact the *cometary* electrons that moved to neutralize the solar wind ions, while the *solar wind* electrons moved in the opposite direction, neutralizing the *cometary* ions. Thus the connectivity between the morphology of the magnetic field and the ion motion can be complicated.

While ion-neutral collisions were less important at 67P, the increased mass-loading as the coma became denser and denser further in towards the nucleus can be expected to produce a similar deceleration of the inward ion flow (of pick-up ions), observed as a pile-up of the magnetic field in front of the innermost region of the nucleus. This is illustrated in Figure 3.8 from Koenders et al. (2015), where in Figure 3.8(a) the flow of cometary ions (color denotes flow speed, arrows are velocity vectors) is seen to stagnate in front of the innermost region close to the nucleus (the diamagnetic cavity, to be discussed in Section 3.5.5 below), and to some extent being diverted around it. Note that no qualitative distinction is made between pick-up ions and locally produced cometary ions in this plot (even though the hybrid simulation does of course treat them correctly). However, as will be discussed below, the ion flow outside the diamagnetic cavity in these simulations is dominated by ions picked up upstream and moving inward towards the nucleus, while the ions in the cavity are exclusively produced inside of it. Figure 3.8(b) shows the resulting pile-up of the magnetic field.

These hybrid simulations, while conducted in the context of the Rosetta mission with the aim of predicting and explaining the findings at 67P, appear to actually better depict the case of a strongly active comet such as Halley. For example, while a general increase in the magnetic field in the inner coma of 67P (e.g. Goetz et al., 2017) testified to magnetic pile-up taking place and

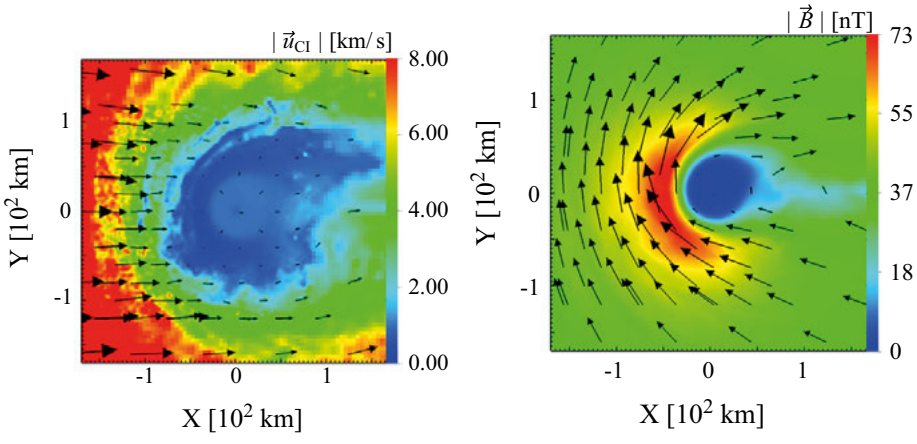

(a) Flow stagnation (b) Magnetic barrier

Figure 3.8. Flow stagnation and magnetic barrier in a hybrid simulation of comet 67P. *(Adapted from Koenders et al., 2015. Reprinted with permission from the publishers.)*

a magnetic barrier (or something like it) forming, ion-neutral collisions was found to play an important role for the deceleration of the pick-up ion flow in these simulations (Koenders et al., 2015) and the almost complete stagnation of the pick-up ion flow outside the diamagnetic cavity is consistent with the picture from Halley, but was was not observed at 67P (although much work still remains to conclusively interpret the ion measurements by Rosetta in this part of the coma).

3.5.4 Magnetic field line draping

Canonical model

The less impeded solar wind to the sides of the inner-most comet-solar wind interaction region moves much faster downstream than the heavily mass-loaded (and in the case of a strongly active comet, strongly collisional) plasma close to the nucleus. The magnetic field being frozen in also to this faster flow (in the case of an intermediately active comet, only into the electrons only), it drags the field lines along downstream, causing them to wrap around the comet, a phenomenon known as *magnetic field line draping*. This was first suggested by Alfven (1957) and is illustrated in Figure 3.9(a). Thus, the magnetic field lines are essentially hung up around the comet. However, this is of course not a stable situation since the continuous flow of solar wind from upstream brings an influx of energy to the piled-up and draped magnetic field. As the field builds up around the comet, the field lines release some of this magnetic energy by slipping around the comet and rejoining the solar wind downstream, in a process called *magnetic slippage*. This is illustrated in Figure 3.9(b) for the

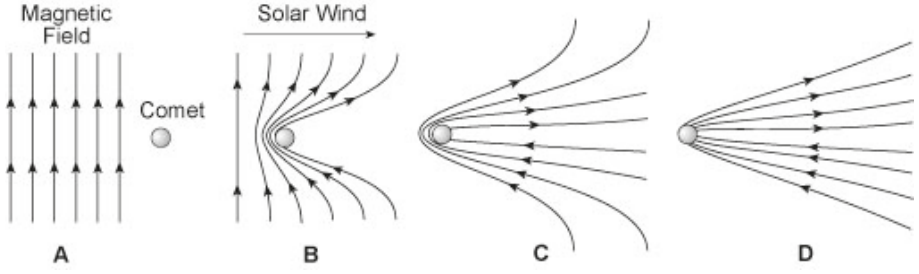

(a) Magnetic field draping around a comet, as first suggested by Alfven (1957). *(Image credit: Professor Kenneth R. Lang, Tufts University.)*

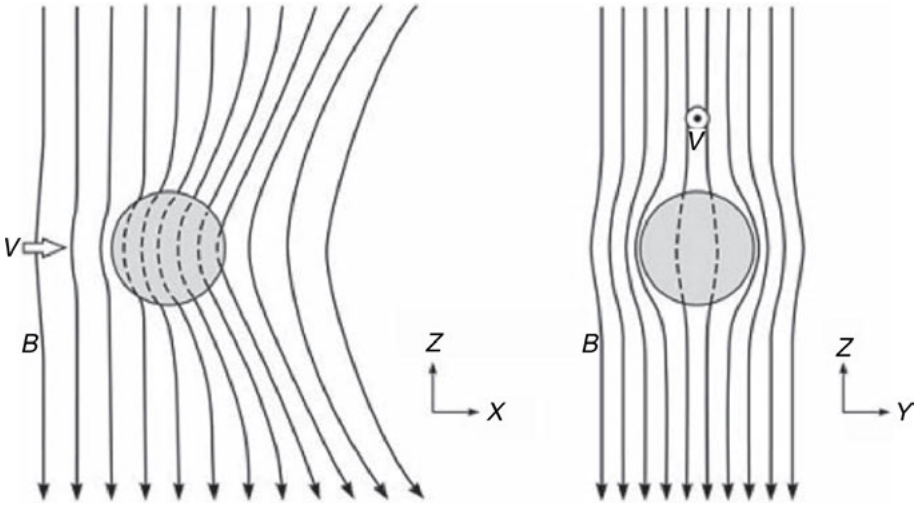

(b) Slippage of magnetic field lines past an obstacle. *(Adapted from Mauk et al., 2009. Reprinted with permission from the publishers.)*

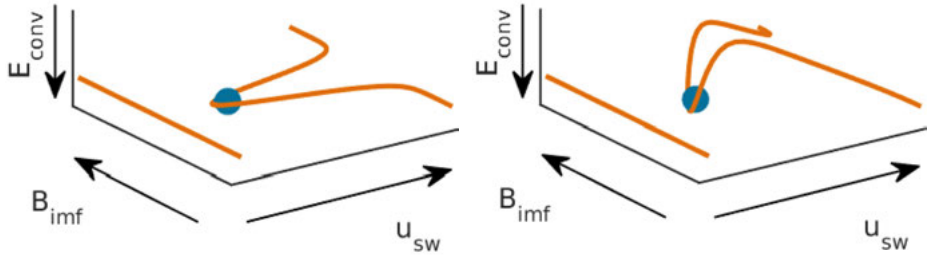

(c) Classical "Alfén" draping around a strongly active comet.

(d) Draping around an intermediately active comet, as deduced from hybrid simulations and Rosetta observations at 67P.

Figure 3.9. Draping of the magnetic field around a comet.*(c) and d) adapted from Koenders et al., 2016. Reprinted with permission from the publishers.)*

case of the much more weakly draped, un-magnetized Kronian moon Enceladus (Mauk et al., 2009).

Downstream, towards the tail of the comet, the magnetic field tends to form two adjacent regions of oppositely directed field lines (c.f. Figure 3.9(a), cartoon D). The resulting curl of the magnetic field is accompanied by a cross-tail current perpendicular to the magnetic field lines in a thin layer between the regions of oppositely directed magnetic field. At the center of this layer, the magnetic field essentially cancels out in a thin sheet called the *neutral sheet*. In case of strong external perturbations like CME impacts or due to internal dynamics in the cometary plasma environment, the cross-tail current may be disrupted, leading to a *tail disconnection* event, analogous to substorms in the terrestrial magnetosphere (Voelzke, 2005; Jia et al., 2009). In this kind of event, a part of the tail breaks off and is accelerated downstream. Also, beams of electrons may shoot back along the field lines into the region of the inner coma, in the form of so-called *field-aligned electron beams* (Russell et al., 1986; Edberg et al., 2016b).

Intermediately active comet

This picture appears to hold quite well also for 67P, although most of the tail processes discussed above would have been out of reach of Rosetta (with the possible exception of field-aligned currents in relation to tail disconnection events, which could affect the inner coma where Rosetta resided, see Edberg et al., 2016b). When the activity was low, little or no magnetic draping was observed, and during the most active phase, draping similar to Figure 3.9(a) was observed (Goetz et al., 2017), albeit not as strongly as in cartoon D, perhaps more like the case in depicted in cartoon B. However, Koenders et al. (2016), using both in situ observations from Rosetta and hybrid simulations, reported a different draping geometry for activity levels in between, when draping was manifest, but only in a region very close to the nucleus ($\lesssim$50 km). Then, the draping was found to be mainly out of the plane containing the (undisturbed) solar wind velocity and interplanetary magnetic field (IMF), as shown in Figure 3.9(d), contrary to the classical picture of planar draping that was confined to this plane (Figures 3.9(c) and 3.9(a)). The explanation offrered was that cometary ions were accelerated along the convective electric field of the solar wind, pointing downwards in Figure 3.9(d). In the innermost region close to the nucleus where mass loading was significant, the solar wind ions were consequently subjected to a convective electric field of the cometary ions, in the opposite direction, i.e. upwards in Figure 3.9(d), in the direction of the observed magnetic field line draping. Thus, this draping geometry, observed in both simulations and in measurements from the comet, is consistent with the magnetic field following the deflected solar wind ions.

3.5.5 Ionopause and diamagnetic cavity

Canonical model

The aforementioned flow stagnation and build-up of a magnetic barrier in front of the comet nucleus culminate with the formation of a *diamagnetic cavity*, into which neither the solar wind, the cometary ions picked up upstream, or the magnetic field they carry, can reach (c.f. Figure 3.5). Here, a tangential discontinuity forms, that separates the mass-loaded solar wind plasma[1] from the purely cometary plasma inside of the discontinuity. This constitutes a compositional boundary generally called the *contact surface*, or cometary *ionopause*. This is illustrated in Figure 3.10, displaying results of hybrid simulations by Koenders et al. (2015). Here the mass-loaded flow of predominantly pick-up ions (purple lines) is diverted around the outside of the contact surface, while the outward-moving cometary ions produced inside are diverted along the inside of this boundary. The magnetic field is expelled from this inner region as well along with the flow of pick-up ions so the region inside the contact surface will be magnetic field free, whence the term diamagnetic cavity.

In the simplest classical picture of a strongly active comet (Cravens, 1986; Cravens, 1987; Ip and Axford, 1987), the density of the outflowing neutral gas at the ionopause is sufficiently large for their collisional drag force on the (radially) stagnant cometary ions to balance the total $\mathbf{j} \times \mathbf{B}$ force of the draped and piled-up magnetic field at the inner edge of the magnetic barrier. Neglecting magnetic tension, this amounts to a pressure balance between the magnetic pressure on the outside of the cavity and the ion-neutral drag on the inside. Subsequent authors have pointed to the contributions of mass loading (Haerendel, 1987) and inertial forces (specifically, the centrifugal force on the diverted flow around the cavity, Israelevich et al., 1992) to maintain this force balance. The reader may tick off the corresponding terms in the momentum equation (3.15, p. 32); ion-neutral collisions and mass loading on the right-hand side and the inertial forces on the left-hand side (the second term). Under spherical or axial (cylindrical) symmetry and stagnation of the *radial* ion flow, the inertial term reduces to the outward radial centrifugal force (Israelevich et al., 1992). The first term on the left-hand side of Equation (3.15) vanishes in steady state. The pressure gradient force term vanishes due to the low temperature of the collisionally cooled ions and electrons. In the first theoretical model of the comet-solar wind interaction (Biermann et al., 1967, well before any in situ measurements were available), energy loss of the cometary plasma was entirely neglected; in this case the contact surface was in fact subtended by the thermal pressure of the plasma, which had average molecular energy $\gtrsim$10 eV, corresponding to the mean surplus energy of the photoionization process (c.f. Section 3.2.2). It turns out, as will be discussed below, that this particular aspect of that model may have some new-found relevance to the

[1] It is not clear how much ions of solar wind origin (e.g. H^+) can still persist this far inside the cometopause; Ip and Axford (1990) suggest none at all.

Figure 3.10. Flow around the contact surface. Purple lines depict the flow of incoming cometary ions which were picked up by the solar wind. Blue lines show the outward flow of ions originating in the inside the diamagnetic cavity. *(Image credit: TU Braunschweig)*

case of the intermediately active 67P (though other aspects of this model are not at all applicable to 67P).

Intermediately active comet

A diamagnetic cavity was first observed at comet Halley by Giotto in 1986 (Neubauer et al., 1986), at a distance of $\sim$4000 km from the nucleus. The magnetic field measurements by the Giotto magnetometer from this event are shown in Figure 3.11(a). A diamagnetic cavity was first detected by Rosetta at 67P in data from 26 July, 2015, shown in Figure 3.11(b). While the Giotto observation of the cavity at Halley consisted of a single cavity crossing, from which emerged the picture of a steady global un-magnetized structure coincident with the contact surface as described above, Rosetta observed many ($\sim$700) brief ($\sim$10 s $-$ $\sim$40 min) cavity crossings. The slow pace at which Rosetta moved about the comet ($\sim$0.5 m/s) implied that these were the result of a highly dynamic cavity boundary moving back and forth past the spacecraft, and *not* of the spacecraft moving in and out of a steady structure. Whether this was the result of an instability at the cavity boundary or a temporal variability of the entire cavity structure is not yet clear.

An important result in this context comes out of Paper III: we observe ion velocities well in excess of the neutral outflow velocity ($\sim$2-4 km/s, vs. $\lesssim$1 km/s for the neutrals), showing that the ions were collisionally decoupled

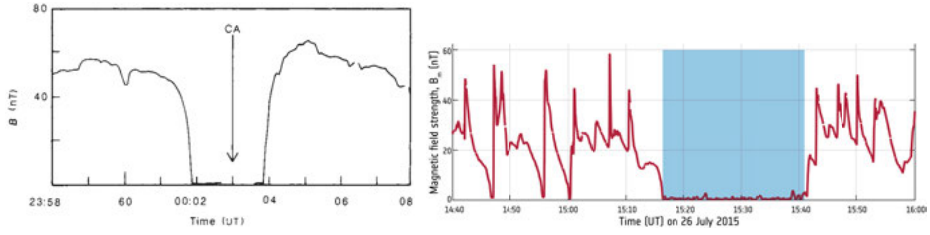

(a) Giotto observation of diamagnetic cavity at Halley's comet. *(Adapted from Neubauer et al., 1986. Reprinted with permission from the publishers.)*

(b) Rosetta detection of a diamagnetic cavity at 67P. *(Adapted from Goetz et al., 2016a. Reprinted with permission from the publishers.)*

Figure 3.11. Diamagnetic cavity observations.

from the neutral gas already well inside of the diamagnetic cavity, meaning that the ion-neutral drag force could not be responsible for balancing the outside magnetic pressure at the cavity boundary. Also, as already mentioned briefly in Section 3.5.3, the stagnation and diversion of the flow at the cavity boundary has not been observed at 67P. While the flow directions outside the cavity remain largely unconstrained at this time (further analysis is in the works), observations of pick-up ions by ICA inside the diamagnetic cavity (Kei Masunaga, private communication, 2018) suggest that the nature of the cavity boundary was *not* that of an ionopause-like contact surface clearly separating two regions of different composition (inward-flowing pickup ions on the outside, outward flowing un-picked-up cometary ions on the inside). Hence, the mechanism behind the formation and extent of the diamagnetic cavity at 67P, and the nature of its boundary surface, cannot be said to be fully understood.

An interesting point here, which to some extent ties back to the early modeling of Biermann et al. (1967) discussed above, is the fact that the observed ion velocities inside the diamagnetic cavity at 67P means that that the dynamic pressure of the ions is in fact of the right order of magnitude to balance the outside magnetic pressure. However, this would require a considerable drop in at least the radial component of the dynamic pressure across the cavity boundary. Plasma densities generally increase substantially in this region, so a radial stagnation of the ions would be required for this explanation to work. Again, this is not observed, but cannot conclusively be ruled out at this time either, due to the uncertainty regarding the ion flow direction outside the cavity.

In addition, the population of warm ($\sim$5 eV) electrons (c.f. Section 3.4.1) has been found to pervade everywhere inside the cavity reached by Rosetta (Paper III). Their thermal pressure would also be more than enough to balance the outside magnetic pressure at the cavity boundary. However, the fact that the density is higher on the outside of the cavity boundary means that a sufficient pressure drop would require a substantial drop in temperature of the

electrons. No clear sign of this has been identified in the data, although our current temperature estimates for the warm electron population derive from spacecraft potential measurements (specifically, the fact that it is substantially negative) and only give an order of magnitude estimation. However, it is difficult to come up with a mechanism that could produce such a sharp drop in temperature as required across the boundary.

3.5.6 Inner shock

Canonical model

Because of the effective cooling of ions and electrons due to collisions with neutrals in the dense innermost part of the coma, inside the diamagnetic cavity, the ion acoustic speed is low ($\sim$0.35 km/s, Gombosi, 2015) and the flow will be supersonic close to the nucleus. However, the plasma will clearly be subsonic at the stagnation point just outside of the cometary ionopause. Therefore, an *inner shock*, analogous to the bow shock discussed in Section 3.5.1, is expected to form somewhere inside the ionopause, where the transition from supersonic to subsonic flow occurs. The existence and nature of this shock remains unclear. Goldstein et al. (1989) observed a thin density spike at the inner edge of the ionopause of comet 1P/Halley where recombination was the primary loss mechanism limiting the maximum density and it has been suggested (Cravens, 1989) that this so called *recombination layer* could fill the function of an inner shock, but this is far from being generally accepted.

Intermediately active comet

An inner shock is observed to form in the hybrid simulations of Koenders et al. (2015), see Figure 3.12. On account of the low electron temperature inside the diamagnetic cavity (and in the inner coma in general, see Figure 3.3(a)) in these simulations, the ion-acoustic speed is low and the outflowing ions are supersonic already at the velocity of the neutral gas ($\sim$1 km/s), at which they are born and to which they are collisionally coupled in the inner parts of the cavity. Their velocity decreases as they begin to stagnate closer to the contact surface, and eventually the transition to subsonic flow occurs, giving rise to the inner shock (dashed black line in Figure 3.12). Thus, these simulation results conform rather well to the canonical case described above.

No clear evidence of an inner shock has so far been found in the Rosetta data. The presence of a warm ($\sim$5 eV) electron population throughout the parts of the inner coma probed by Rosetta, even inside the diamagnetic cavity, gives an ion acoustic speed well in excess of the neutral outflow velocity, or indeed the $\sim$4 km/s speed the ions were observed to obtain inside the cavity (c.f. Paper III). This means that they were in fact subsonic throughout the cavity, or at least the parts of it reached by Rosetta. Also, no stagnation of the ions was observed at the cavity boundary, although these measurements

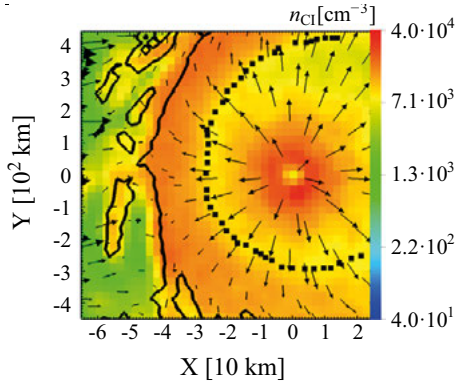

Figure 3.12. Contact surface (solid black line) and inner shock (dashed black line) in hybrid simulations. Color denotes cometary ion density and the arrows show the magnitude (arrow length) and direction (arrow orientation) of the ion flow velocity. *(Adapted from Koenders et al., 2015. Reprinted with permission from the publishers.)*

gave no indication of the flow direction of the ions, so a stagnation in the radial component of the velocity cannot be conclusively ruled out. An inner region of efficient electron cooling, predicted by theory (Gombosi, 2015; Engelhardt et al., 2018) and invoked in order to explain the presence of the cold electron population (c.f. Section 3.4.1) could have lower ion acoustic velocity and supersonic ions. The inner shock would then appear in connection with the electron-neutral decoupling distance (Gombosi, 2015), where the electrons collisionally decouple from the neutrals and a warm electron population can persist, giving an ion-acoustic velocity well in excess of the outflowing ions. However, such a region appears to have been beyond the reach of Rosetta.

4. Outlook

The observations by Rosetta during its more than two-year long stay at comet 67P/Churyumov-Gerasimenko revealed a plasma environment in many respects much different from the ones found by previous missions to comets and predicted by simulations. In spite of (or sometimes as a result of) the significant efforts and progress that have been made in understanding the cometary plasma environment from Rosetta observations, many unresolved questions still remain. Here follows a (non-exhaustive) selection for the interested reader.

1. What is the dynamics of the ions outside the diamagnetic cavity? We have found (Paper III) that the cometary ions decouple from the neutrals already inside the cavity, and found no sign of stagnation outside the cavity boundary, although the non-directional nature of our measurements means that we cannot rule out a change in flow direction, producing an effective stagnation in the radial component of the ion motion. Inside the the cavity, our (few) wake observations suggest a radial, supersonic flow (at least w.r.t. the transverse ion temperature), and similar wake effects have been observed in the region surrounding the cavity, albeit much less consistently. We have preferred to attribute the inconsistency of the wake effects on the outside of the cavity as due to a variability of the extent of the wake in the highly variable and dynamic plasma surrounding the cavity, causing e.g. substantial variations in the spacecraft potential, as opposed to an effect of a variable ion flow direction. However, this point should be examined further in the future. Both LAP and ICA low-energy ion measurements are subject to disturbances due to spacecraft-plasma interaction in general, and spacecraft charging in particular, which complicate the measurements and limit what conclusions and interpretations may be drawn from them. E.g., the directions of observed low-energy ions cannot be reliably determined by ICA in the region surrounding the diamagnetic cavity, on account of the strongly negative spacecraft potential there. The spacecraft-plasma interaction, and its influence on the measurements, specifically the low-energy cometary ions, require further investigation. Such work is ongoing, within both the LAP and ICA teams, primarily by means of PIC simulations using the Spacecraft Plasma Interaction System (SPIS)), and will hopefully contribute to a better understanding of the measurements and the ion environment in the inner coma in a not too distant future.

2. What is the nature of the plasma and magnetic field enhancements in the region surrounding the cavity? Are they steepened waves travelling inwards towards the cavity? Or are they pulse-like structures detaching from the inner

region and moving outwards? Or do they represent temporal variations of the entire inner plasma environment of the comet? Little is known at this time and much remains to be done. Hopefully, resolving 1. above should provide measurements that can offer some clues.

3. How is the diamagnetic cavity formed? The observed (and modelled, Vigren and Eriksson, 2017) decoupling and acceleration of the cometary ions already inside the diamagnetic cavity is inconsistent with the idea of the ion-neutral drag force as the main source of outward pressure to balance the inward pressure of the piled-up solar wind magnetic field. The ubiquitous warm electron population has more than enough thermal pressure to be responsible for this, but since the density is consistently higher on the outside of the cavity than on the inside, the pressure difference appears to be in the wrong direction, unless there is a substantial drop in electron temperature across the cavity boundary. Our electron temperature measurements are not yet sufficiently well understood to conclusively rule this out, but it is hard to imagine a physical mechanism that could produce such a sharp, localized drop in electron temperature in the absence of any significant variations in the neutral gas, which varies smoothly across the boundary. The decoupling and acceleration of the cometary ions give them a dynamic pressure also of the right order to balance the outside magnetic pressure at the cavity boundary. However, here we are again faced with the problem of the elevated density on the outside of the cavity. We would require a substantial drop in at least the radial component of the ion velocity across the boundary, which ties this issue together with point 1) above. Perhaps the diamagnetic cavity is a dynamical phenomenon and there is no pressure balance at the cavity boundary,. However, this would still require some outward force to expel the magnetic field from the inner region, even if this does not result in a static equilibrium.

4. What is the nature of the diamagnetic cavity boundary? Closely related to point 1., 2. and 3. above, we aspire to understand better the physics of the cavity boundary itself. The Chapman-Ferraro model for the Earth's magnetopause has been invoked in this context. Perhaps this is a good starting point for further modeling efforts on this topic, including also PIC simulations (which would likely have to be limited to the boundary itself, not the entire cavity for computational reasons, see also point 5. below). Probably, resolving point 1. (and possibly also point 2.) above will be required before a good understanding of the nature of the cavity boundary can be achieved.

5. What is the dynamics of the cold electron population, found to be intermittently interspersed within the ubiquitous population of warm electrons? We have found (Paper III) that this population is likely pervasive inside the diamagnetic cavity, and that its intermittency begins at or near the cavity boundary. Hybrid simulations (e.g. Koenders et al., 2015) exhibit strong filamentation of the plasma at the boundary of the diamagnetic cavity, which has been invoked as a sample specimen of the kind of filamentation suggested for the cold electrons. However, the hybrid simulations do not include multiple

electron populations and fail to reproduce some of the more detailed features observed in relation to the cavity, e.g. its highly dynamic extent and the decoupling of ions and neutrals. Thus, its reliability for modeling the (cold) electron dynamics is limited. A more detailed mapping of the occurrence of the cold electrons, both by LAP and MIP, should be done, and relationships sought to other observed quantities (e.g. the ion velocity and the magnetic field). A global survey of the occurrence of cold electrons has already been performed (Engelhardt et al., 2018), but their dynamics in the region surrounding the cavity has yet to be thoroughly examined. This likely also requires a better understanding of the spacecraft-plasma interaction, since this may affect at least the LAP observations of such cold electrons. Further efforts to quantify the relative abundance of the cold electrons, when observed, is ongoing, at least within the MIP team, and may provide some insights.

6. How does electron cooling work in the inner coma? The cold electron population testifies to the existence of a region of substantial electron cooling in the innermost parts of the coma, beyond the reach of Rosetta. Simple models assuming radial transport of newly born electrons in the inner coma have a hard time accounting for the required amount of cooling. The presence of an ambipolar electric field that holds back these electrons and keeps them in the region of dense neutral gas and efficient cooling close to the nucleus for longer times may be a part of the explanation. Further modeling is required, and to some extent ongoing, to better understand the electron kinetics in the inner coma. PIC simulations have been performed (Deca et al., 2017), but will have a hard time including the entire inner coma region (up to and beyond the diamagnetic cavity boundary) for the foreseeable future. Perhaps kinetic electron transport code developed e.g. for Titan (Galand et al., 1999) can be adapted to the environment of 67P to provide some insight.

7. Why was no bow shock observed, even during the spacecraft excursion undertaken specifically for that purpose? Hybrid simulations indicated that this excursion should be sufficient to reach the bow shock, yet it was not observed. What physics, not included in the hybrid models, was responsible for pushing the bow shock out so far? Has it anything to do with the electron dynamics, not accurately captured by the hybrid models? Or was the bow shock in fact observed after all, only it has yet to identified in the data? While there was no *obvious* sign of a bow shock in the data, data quantities are large and have yet to be exhaustively probed in detail. Further analysis is required and may reveal less conspicuous signs of a bow shock thus far overlooked.

8. The role of waves and instabilities for transferring energy between different particle populations, and possibly reshaping the plasma environment of the comet, will be further investigated in the (near) future. One example is the waves found outside the diamagnetic cavity in Paper IV. Further studies should be undertaken to investigate their nature; the interpretations presented thus far are mostly limited to the theoretical framework of waves in a homogeneous plasma. Possible effects due to the inhomogeneous nature of the

plasma surrounding the cavity should be examined further, by theoretical considerations and numerical models (e.g. the numerical plasma dispersion solver WHAMP (Waves in Homogeneous Anisotropic Magnetized Plasma, Roennmark, 1982)), as well as what effects the waves have on their environment. The instability proposed for their generation (the drift cyclotron instability) should also be further examined accounting for the specifics of the plasma environment surrounding the cavity (thus related to points 1. and 2. above). Can some other candidate generation mechanism be found that is more favorable for wave generation in this environment? Finally, lower hybrid waves have also been observed at the comet, likely driven by a lower hybrid drift instability. What is their role for shaping the plasma environment of the comet? This will be further investigated in the near future.

5. Summary of publications

5.1 Paper I

Evolution of the plasma environment of comet 67P from spacecraft potential measurements by the Rosetta Langmuir probe instrument

Authors
E. Odelstad, A. I. Eriksson, N. J. T. Edberg, F. Johansson, E. Vigren, M. André , C.-Y. Tzou, C. Carr, and E. Cupido

Journal
Geophysical Research Letters (GRL)

Details
Volume 42, Issue 23, Dec 2015, Pages 10,126-10,134

My contribution
I planned the study, performed the data analysis and wrote the paper, with valuable contributions from the co-authors in the form of data contribution and preprocessing, productive discussions and comments on the original manuscript.

Summary

In general, it has been difficult to obtain consistent, reliable and accurate estimates of plasma densities and temperatures by the Langmuir probes on Rosetta (RPC-LAP) in the highly variable and dynamic plasma environment of 67P and in the presence of a strongly charged spacecraft. Over longer periods of time, the most consistent and reliable measurements were actually the spacecraft potential obtained from the photoelectron knee in the Langmuir probe sweeps (c.f. Section 2 of I). The spacecraft potential is set by the balance of currents due to impacting plasma electrons and emitted photoelectrons; this is illustrated in 5.1(a). This means that the spacecraft potential is highly sen-

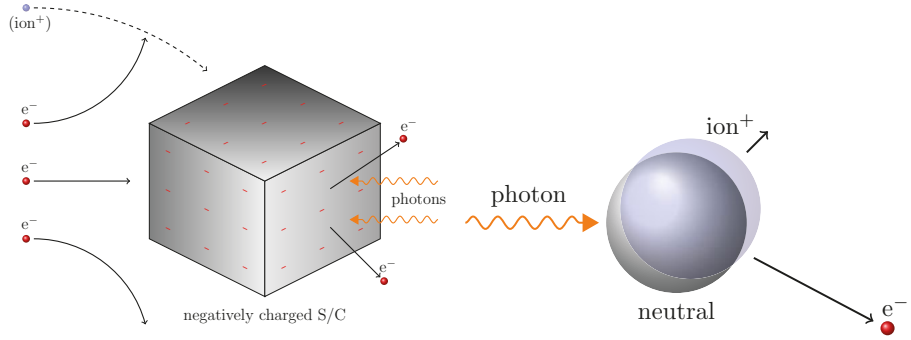

(a) The spacecraft potential is set by the balance of currents due to impacting plasma electrons and emitted photoelectrons, giving $V_{S/C} \propto n_e\sqrt{T_e}$ (for $V_{S/C} < 0$). Thus $V_{S/C}$ can be used to monitor the plasma environment.

(b) Photoionization produces warm (∼10 eV) electrons (and cold ions); due to conservation of energy and momentum the much lighter electron comes away with virtually all the excess energy of the reaction.

Figure 5.1. Paper I: Using the spacecraft potential to monitor the evolution of the cometary plasma environment.

sitive to the electron density and temperature in the surrounding plasma and can be used to monitor the plasma environment of the comet. In this Paper, we used measurements of the spacecraft potential to study the evolution of the plasma environment in the inner coma of comet 67P, at cometocentric distances generally between 10 and 150 km, during the time period from early September 2014 to late March 2015, corresponding to heliocentric distances from about 3.5 AU to 2.1 AU. The spacecraft potential was found top be persistently negative within about 50 km of the nucleus throughout this period. This was attributed to a high electron temperature of around 5 – 10 eV, resulting from the low electron-neutral collision rate in the tenuous neutral gas being insufficient to effectively cool the coma photoelectrons, which are born with typical energies around 10 eV (illustrated in 5.1(b)).

During the investigated period, the comet spin axis was tilted w.r.t. the comet orbital plane so that the northern hemisphere of the nucleus had summer conditions. As a consequence, the highest electron fluxes and the most negative spacecraft potentials were found in the northern hemisphere. Here, there was also a clear variation of spacecraft potential with comet longitude, exactly as seen for the neutral gas: Recurring peaks in density and concurrent dips in spacecraft potential were observed with a period of approximately 6 h, corresponding to half the rotation period of the nucleus (see Figure 5.2). This was found to coincide with sunlit parts of the neck region of the nucleus being in view of the spacecraft.

The clear covariation of spacecraft potential with the neutral density as measured by the ROSINA Comet Pressure Sensor (COPS) showed that the neutral gas and the plasma were closely coupled. While this is well known for a fully developed comet like 1P/Halley, it was not obvious that it would be

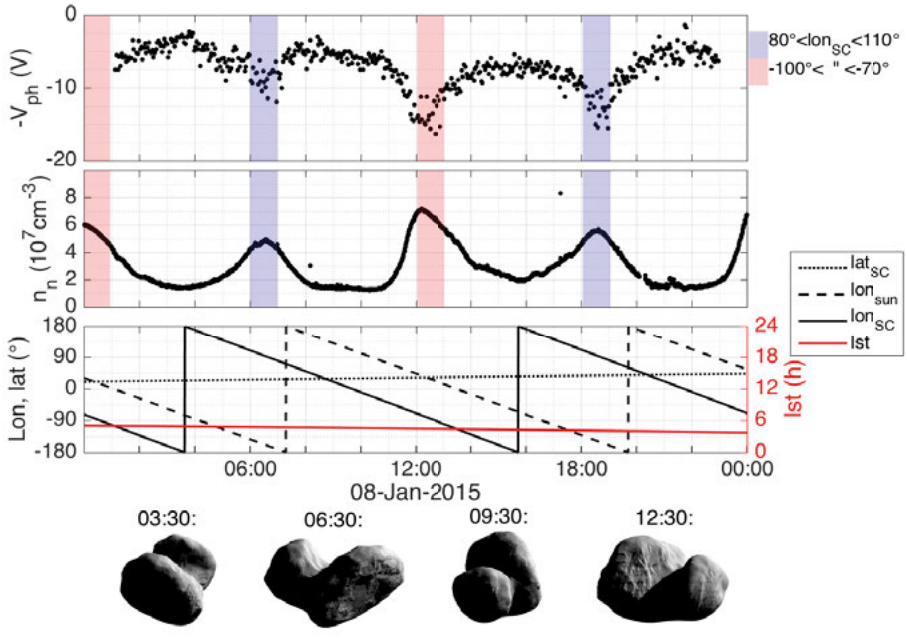

Figure 5.2. Paper I: Covariation of RPC-LAP spacecraft potential (upper panel) and ROSINA-COPS neutral gas density (middle panel) measurements on January 8, 2015, at 28 km from the nucleus. Also shown are the latitude and longitude of the spacecraft and the longitude of the Sun, in comet-fixed coordinates, as well as the local solar time (bottom panel). Blue and red colored patches indicate times when the longitude of the spacecraft was between 80° and 110° and -100° and -70°, respectively, corresponding to sunlit parts of the neck region being in view of the spacecraft. Spacecraft perspectives of the partially illuminated nucleus are shown for four different times below the bottom panel. *(Reprinted from Paper I, with permission from the publishers.)*

the case for the much weaker 67P, particularly early in the mission before any strong boundary layers had formed. The longitudinal modulation of the spacecraft potential and neutral gas was evident already in mid-September 2014, at 3.5 AU heliocentric distance and 30 km from the nucleus. In this sense, 67P had a clear ionosphere of its own, where the local plasma dominated over the solar wind, already at this large distance from the Sun.

Since the publication of this study, the main additions to its topic have been the extension of the statistics to the full mission in Paper II, and the improved calibrations presented therein. The importance of the spacecraft potential for all plasma measurements is indicated by the fact that the paper as yet has 28 citations in the SAO/NASA Astrophysics Data System (ADS).

5.2 Paper II

Measurements of the electrostatic potential of Rosetta at comet 67P

Authors
E. Odelstad, G.Stenberg-Wieser, M. Wieser, A. I. Eriksson, H. Nilsson and F. L. Johansson

Journal
Monthly Notices of the Royal Astronomical Society (MNRAS)

Details
Volume 469, Issue Suppl_2, 21 July 2017, Pages S568–S581

My contribution
I planned the study, performed the data analysis and wrote the paper, with valuable contributions from the co-authors in the form of data contribution and preprocessing, productive discussions and comments on the original manuscript.

Summary

The charged spacecraft perturbs the potential of the surrounding plasma, possibly disturbing the Langmuir probe (RPC-LAP) measurements. The booms of lengths $\sim$1.5 – 2 m on which the probes were mounted were smaller than or comparable to typical Debye lengths of the warm electrons during large parts of the mission (e.g. $\sim$1 – 10 m for most of the early mission). Therefore, the LAP spacecraft potential measurements only picked up some fraction of the full spacecraft potential; this is illustrated in Figure 5.3(a). Simulations conducted before the arrival of Rosetta at the comet indicated that, for LAP:s probe 1 (LAP1) in a tenuous solar wind environment, the fraction of the spacecraft potential measured would be on the order $1/2$ to $2/3$ (Sjögren et al., 2012).

The spacecraft potential can also be estimated from the ion energy spectra obtained by the Ion Composition Analyzer (RPC-ICA), located on the main spacecraft body. Ions entering the instrument have been accelerated by the spacecraft potential and the lowest observed ion energy thus gives an estimate of the spacecraft potential; this is illustrated in Figure 5.3(b). However, the ICA ion energy spectra suffer from an unknown energy offset, that furthermore depends on the sensor temperature (which was not well measured

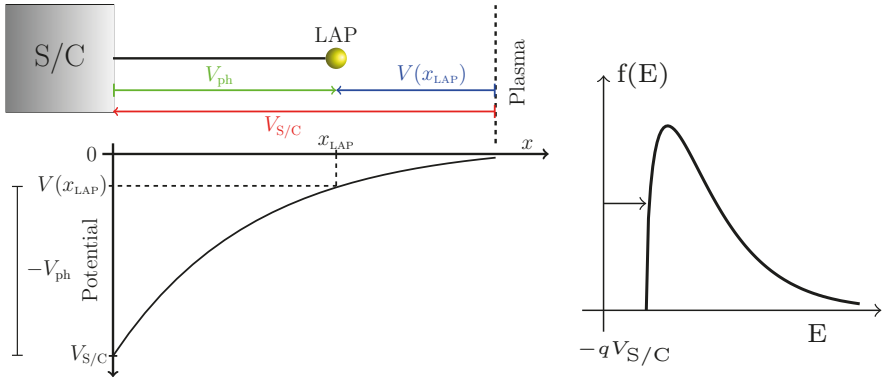

(a) Illustration of the potential structure around a (negatively) charged spacecraft. The local plasma potential observed by LAP at a distance x_{LAP} from the spacecraft main body differs by an amount $V(x_{LAP})$ from the plasma potential at infinity due to the residual potential field of the spacecraft.

(b) Shift of ICA energy spectra due to pre-acceleration of ions in S/C potential field.

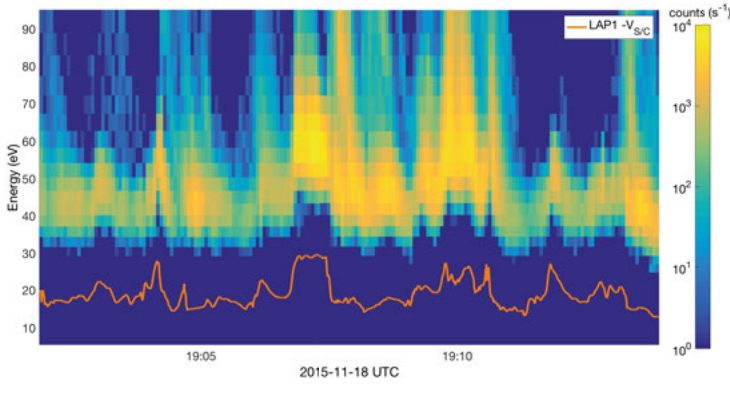

(c) Comparison of ICA energy spectra and LAP1 $V_{S/C}$ measurements (orange line), under stable ICA sensor temperature. ICA spectra have a shift in energy of -$V_{S/C}$ and an unknown energy offset.

Figure 5.3. Paper II: Determining the fraction of $V_{S/C}$ picked up by LAP and the energy offset in ICA ion spectra by combining measurements from both instruments.

onboard). Thus, while LAP measured only a proportion of the full spacecraft potential, ICA measured the full spacecraft potential, but with an unknown additive offset. In this Paper we combined measurements from both instruments to allow accurate determination of the full spacecraft potential, how large a fraction of it that was observed by LAP1 and estimated the energy offset of ICA.

We found that the correlation was generally very good between the spacecraft potential estimates obtained from the two instruments, see Figure 5.3(c), showing clearly that the instruments accurately measured the spacecraft poten-

tial. We also found intermittent intervals where the correlation became weaker, typically coinciding with a reduction in the total ion flux observed by ICA and many times also with a drop in the spacecraft potential observed by LAP (not shown). We interpreted this as a temporary loss of local ionization, in the ambient plasma or at least in the ICA field of view. Our cross-calibration was limited by the fact that ICA needed to be in high-time-resolution mode (4 s time resolution instead of the nominal 192 s), which was only run very intermittently throughout the mission. Thus our study was by necessity limited to those intervals. In general, we found that the fraction of the spacecraft potential picked up by LAP1 was between about 0.7 and 1. Thus, a correction factor between about 1 and 1.4 should be applied to the LAP1 measurements to obtain the full $V_{S/C}$. However no clear correlation with well-determined extraneous parameters (e.g. cometocentric distance, heliocentric distance, latitude etc.) was found that could be used to further constrain this fraction outside the studied intervals. The ICA energy offset was estimated to 13.7 eV, with a 95 per cent confidence interval between 12.5 and 15.0 eV.

We also presented LAP measurements of the spacecraft potential throughout the entire stay of Rosetta at 67P. $V_{S/C}$ was mostly negative, often below -10 V and sometimes below -20 V. As in Paper I, we attributed this to a warm ($\sim$5 – 10 eV) population of coma photoelectrons that were present because the neutral gas was insufficiently dense for them to be effectively cooled by collisions with neutrals. Positive spacecraft potentials (0-5 V) were only observed in regions far from the nucleus, or above the more inactive areas on it, where the electron density was very low ($\sim$10 cm^{-3}) and where significant electron cooling by neutrals was not possible. Thus we concluded that the thermal flux of electrons in the cometary plasma, at the position of the spacecraft, was dominated by these warm, uncooled electrons throughout Rosetta's stay at the comet, notably also at and around perihelion where strongly negative spacecraft potentials were observed. The prevalence of these warm electrons correlated well with diurnal and seasonal variations that drove the neutral outgassing (c.f. Paper I and Hansen et al. 2016), consistent with these electrons being predominantly produced at or inside the position of the spacecraft.

As the spacecraft potential influences all the RPC plasma measurements (possibly with the exception of the MIP density measurements), the ion mode measurements of ROSINA-DFMS and the ability of charged dust grains to reach the Rosetta dust detectors GIADA, COSIMA and MIDAS, the mission map of spacecraft potential should be useful in forthcoming studies. The offset calibration of ICA energy should be useful for all studies of low energy ions using this instrument, and the inference of the presence of warm electrons is an observation of direct interest to cometary plasma physics. Further studies should include better modeling of the Rosetta spacecraft potential for a given set of plasma parameters, and improved simulations of the spacecraft-plasma interaction, e.g. using the Spacecraft Plasma Interaction System (SPIS) as in Sjögren et al. (2012) (ongoing).

5.3 Paper III

Ion velocity and electron temperature inside and around the diamagnetic cavity of comet 67P

Authors
E. Odelstad, A. I. Eriksson, F. L. Johansson, E. Vigren, P. Henri, N. Gilet, K. L. Heritier, X. Vallières, M. Rubin, and M. André

Journal
Journal of Geophysical Research: Space Physics

Details
Volume 123, Article published in Early View on 25 July, 2018

My contribution
I planned the study, performed the data analysis and wrote the paper, with valuable contributions from the co-authors in the form of data contribution and preprocessing, productive discussions and comments on the original manuscript.

Summary

In this Paper, we combined two Rosetta plasma instruments, Langmuir probe sweeps from LAP and plasma density measurements from MIP, to obtain estimates of the ion velocity and electron temperature in and around the diamagnetic cavity of 67P. The ion velocity (both bulk drift and thermal motion) is an important parameter for understanding the structure and dynamics of the cometary plasma environment. Important insights into the effectiveness of ion-neutral collisions, transport processes of ionospheric plasma and the existence and pervasiveness of electric fields in the inner coma can be gained from constraining the velocity of the ions. The electron temperature is important for dust charging and dynamics, as well as production and loss of plasma by electron impact ionization and recombination. It also strongly influences the plasma dynamics, e.g. the presence of an ambipolar electric field.

A major point of interest in cometary plasma physics has also been the existence, extent and formation mechanism of the diamagnetic cavity, a region in the inner-most part of the coma into which the interplanetary magnetic field cannot reach and which, in the absence of an intrinsic magnetic field of the nucleus, will be magnetic-field-free. Current understanding of this phenomenon derives predominantly from observations from Halley, and is based

on the premise that the newly formed cometary ions are collisionally coupled to the neutral gas inside the diamagnetic cavity. The outward-radial ion flow then stagnates when meeting the magnetized plasma at the cavity boundary, and the magnetic pressure on the outside is balanced from the inside by the ion-neutral drag force on the ions, sustaining a field-free cavity. However, it is far from clear that this process holds at a less active comet like 67P, where the ion-neutral collisional coupling in the more tenuous coma is more uncertain.

As pointed out already in the context of Paper I, Langmuir probe measurements in the highly variable and dynamic plasma environment of 67P and close to a large, negatively charged spacecraft are difficult and come with substantial uncertainty. In general, supplementary input is required to complement and validate the measurements. In Paper III, measurements of the plasma density by MIP, not yet regularly available from LAP alone, complements the LAP Langmuir probe sweeps (specifically the *ion and electron slopes*, c.f. Sections 2.1.3. and Appendix A of Paper III) so that sufficiently reliable measurements of the ion velocity, and at least order-of-magnitude estimates of the electron temperature, could be obtained. We applied this to data obtained inside the cavity and, during a select period, the surrounding region as well. The resulting ion velocity estimates cannot distinguish between thermal and bulk motion, but will represent a combination of the two. Also, some uncertainty remains due to possible spacecraft-plasma interaction and potentially very out-of-equilibrium velocity distributions (Vigren and Eriksson, 2017). To constrain the uncertainty and validate our measurements, we compared our results to a simple analytic flux conservation model (Vigren, 2018) assuming steady radial flow (and neglecting recombination) inside the cavity. The model was driven by photoionization using daily averaged photo-ionization frequencies for H_2O, computed at the location of 67P from the Timed SEE L3 v12 database, corrected for phase shift and heliocentric distance (Heritier et al., 2018).

Inside the diamagnetic cavity, we found ion velocities generally in the range 2 – 4 km/s, c.f. Figure 5.4(a). The effective ion drift speeds from the flux conservation model were in good agreement with the values obtained from combining LAP and MIP throughout the cavity. We also observed at least one case of clear regime change in the current collection of LAP2 in connection with a spacecraft slew inside the cavity, suggesting the existence of a spacecraft wake. This is a strong indication that the ion flow was supersonic inside the cavity and therefore that our ion velocity measurements should be interpreted primarily as a bulk drift speed. The geometry of the slew and the associated regime change were consistent with an outward-radial flow direction, justifying the assumptions behind the flux conservation model and the good agreement between it and the values obtained from combining LAP and MIP. **Most importantly:** *These velocities were significantly above the expected neutral velocity $\lesssim$1 km/s, showing that the ions were, at least partially, decoupled*

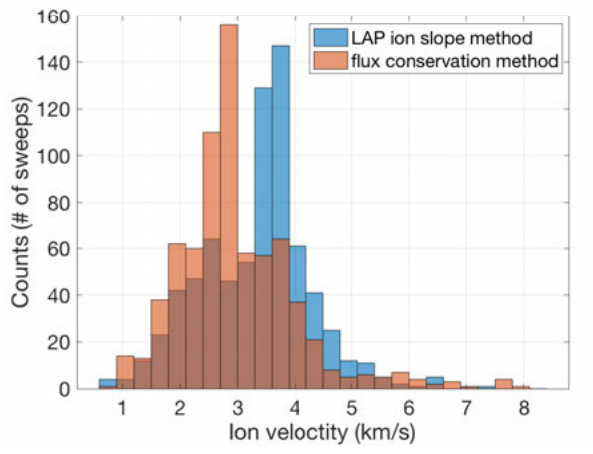

(a) Histograms of the ion velocity derived from LAP ion slopes and MIP density measurements inside the diamagnetic cavity, together with effective ion drift speeds derived from a flux-conservation based model.

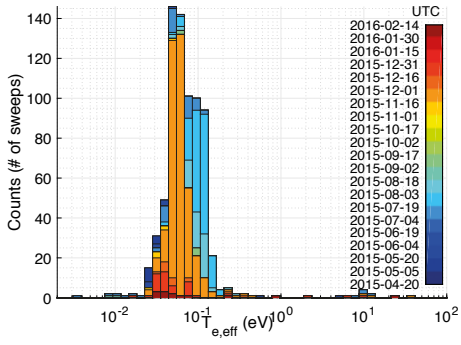

(b) Histograms of the electron temperature (of the cold component!) derived from LAP electron slopes and MIP density measurements inside the diamagnetic cavity.

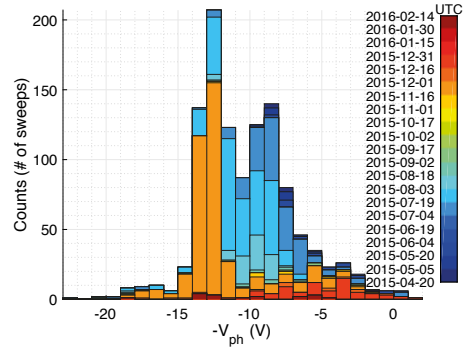

(c) Histograms of the spacecraft potential observed by LAP inside the diamagnetic cavity. The persistently negative values attest to the pervasiveness of a population of warm electrons, not substantially cooled by collisions with neutrals, throughout the parts of the cavity reached by Rosetta.

Figure 5.4. Paper III: Ion velocity and electron temperature inside the diamagnetic cavity of 67P.

from the neutrals. This implies that ion-neutral drag force was not *responsible for balancing the outside magnetic pressure at the cavity boundary.*

The electron temperatures obtained from combining LAP and MIP demonstrated the ubiquitous presence of a population of cold electrons inside the cavity, with temperatures $\lesssim$0.2 eV, consistent with expectations for collision-

ally cooled coma electrons, c.f. Figure 5.4(b). Such a population had previously been observed intermittently outside the cavity (Eriksson et al., 2017), in addition to the warm bulk population inferred from spacecraft potential measurements in Papers I and II. In fact, immediately outside the cavity, LAP sweeps without clear signatures of such cold electrons began to turn up intermittently, suggesting that the filamentation of these cold electrons, proposed to explain their intermittent nature outside the cavity (Eriksson et al., 2017), began at or near the cavity boundary and was possibly related to an instability of this boundary. It also reinforced the notion of previous authors (Henri et al., 2017) that the formation and extent of the cavity as related to electron-neutral collisionality, if not directly by electron-neutral collisional drag at the cavity boundary, then perhaps indirectly through its effect on the electron dynamics and electric fields (e.g. an ambipolar field) inside the cavity.

We here also made a detailed examination of the spacecraft potential measurements inside the cavity (more detailed than the global survey in Paper II), finding it to be consistently $\lesssim$-5 V, c.f. Figure 5.4(c). This proved that the population of warm ($\sim$5 – 10 eV) electrons was also present throughout the parts of the cavity probed by Rosetta, and showed that Rosetta never entered the region of collisionally coupled electrons presumed to exist in the innermost part of the coma, not even during any of the passes through the diamagnetic cavity.

The main results of this Paper, that the ions are not collisionally coupled to the neutrals and that the pressure balance at the cavity boundary is not maintained by the ion-neutral drag force, have already caused quite a stir in the Rosetta plasma community, forcing reevaluation of the physics governing the formation and extent of the diamagnetic cavity, as well as the premises on which most current chemical transport models of the cometary ionosphere are based (e.g. Vigren, 2018; Heritier et al., 2018; Heritier et al., 2017; Galand et al., 2016; Vigren et al., 2015; Vigren and Galand, 2013, etc). Some uncertainties remain (e.g. the exact influence of the spacecraft space-charge sheath on the ion velocity measurements), and should be addressed in the future (ongoing, e.g. by means of simulations using the Spacecraft Plasma Interaction System (SPIS)). Much also remains to be done regarding the plasma dynamics in the region surrounding the cavity, where results from this Paper (e.g. the different preponderance of cold and warm electrons inside and outside the cavity) offer a promising set of starting points. Not the least, the ion motion in this very variable and dynamic region where flow directions and regimes are yet highly uncertain, should be further investigated in future work.

5.4 Paper IV

Plasma density and magnetic field fluctuations in the ion gyro-frequency range near the diamagnetic cavity of comet 67P

Authors

E. Odelstad, A. I. Eriksson, M. André, D. Graham, H. Breuillard, C. Goetz, E. Vigren, K. Masunaga, H. Nilsson and P. Henri

Details

Manuscript in preparation

My contribution

I planned the study, performed the data analysis and wrote the manuscript, with valuable contributions from the co-authors in the form of data contribution and preprocessing, productive discussions and comments on the original manuscript.

Summary

A plasma can support a plethora of different wave phenomena, which can play an important role for transferring energy between different particle populations and may contribute to shaping the plasma environment of the comet. In particular the region surrounding the diamagnetic cavity has been found to be very dynamic. It is characterized by the formation of large-amplitude plasma and magnetic field enhancements ($\delta n/n > 1$ and $\delta B/B > 1$), of typical duration of a few minutes, that are highly asymmetric: the density and magnetic field increase much more rapidly up to their peak values than the rate at which they decrease afterwards (Hajra et al., 2018; Henri et al., 2017; Goetz et al., 2016b), see Figure 5.5. The nature of this phenomenon is yet unknown and has been the subject of much discussion within the Rosetta plasma community. A novel observation in this context, on which this Paper is based, is the intermittent occurrence of a different set of large-amplitude ($\delta n/n \sim 1$) plasma density fluctuations on much shorter time scales, that occur on the descending slopes of these enhancements.

These fluctuations turn out to be quasi-harmonic oscillations with typical frequencies of $\sim$0.1 Hz, about 10 times the water ion cyclotron frequency and less than half the proton cyclotron frequency. We also find that they, at least occasionally, have associated fluctuations in the magnetic field, albeit much weaker ($\delta B/B \lesssim 0.1$). We have performed minimum-variance and

spectral polarization analyses on these magnetic fluctuations, finding that they are generally elliptically polarized (ellipticity $\sim$0.5) and propagate (close to) perpendicular to the background magnetic field. The principal component of polarization is almost (anti-)[1]parallel to the background field (i.e. it is "magnetically compressive") and consistently lags the density oscillations by $\sim$90°.

We have considered water-proton ion-ion hybrid (Buchsbaum) waves as a possible mechanism behind the fluctuations, giving frequencies potentially in the right range for a relative proton abundance $\gtrsim$25%. However, neither models nor measurements currently support such a high ratio of protons in this part of the coma, which is beyond the reach of protons of solar wind origin (Behar et al., 2017). We also disfavor whistler mode waves, which may also occur at these frequencies, on account of their considerable group velocity, which would provide an efficient escape of energy and likely require an excessive amount of free energy to sustain such strong waves as we observe here. As a possible explanation for the waves, we have instead proposed ion Bernstein waves, possibly generated by a drift-cyclotron instability in the strongly inhomogeneous plasma near the cavity. Such waves, while often denoted as electrostatic since their dispersion relation can be accurately derived in neglect of magnetic field perturbations, do in fact exhibit magnetic field perturbations, even when their wave vector is perpendicular to the background field. They have also been found to develop strong magnetic compression in high-β plasmas as shown e.g. by Denton et al. (2010). The plasma β is $\gtrsim 3$ in the plasma surrounding the cavity; Denton et al. had $\beta \lesssim 2$. Thus this kind of waves appear to be consistent with our observations.

To our knowledge, this is the first time this kind of waves have been observed in the plasma near a comet. Future studies should further examine the exact polarization and other properties developed by such waves in the kind of very inhomogeneous plasma encountered outside the diamagnetic cavity of 67P, for more detailed comparison to our observations. For example, one could use the numerical plasma dispersion solver WHAMP (Waves in Homogeneous Anisotropic Magnetized Plasma, Roennmark, 1982) with distribution functions adapted to give a perpendicular current as similar to the polarization current in the inhomogeneous plasma as possible, in a manner similar to the analytical treatment of lower hybrid waves on density gradients in André et al. (2017). In addition to the general importance of understanding plasma wave phenomena mentioned above, understanding these waves in particular, and the mechanism that generates them, should provide important clues into the nature of the large-amplitude plasma and magnetic field enhancements observed near the diamagnetic cavity. For instance, it is as yet unclear whether these enhancements represent primarily temporal or spatial dynamics. Perhaps eventually, it may even contribute to forming a better understanding of the for-

[1]In the absence of reliable electric field measurements, our analysis cannot unambiguously determine the sign of the wave vector.

mation and dynamics of the cavity itself, one of the major points of interest in modern cometary plasma physics.

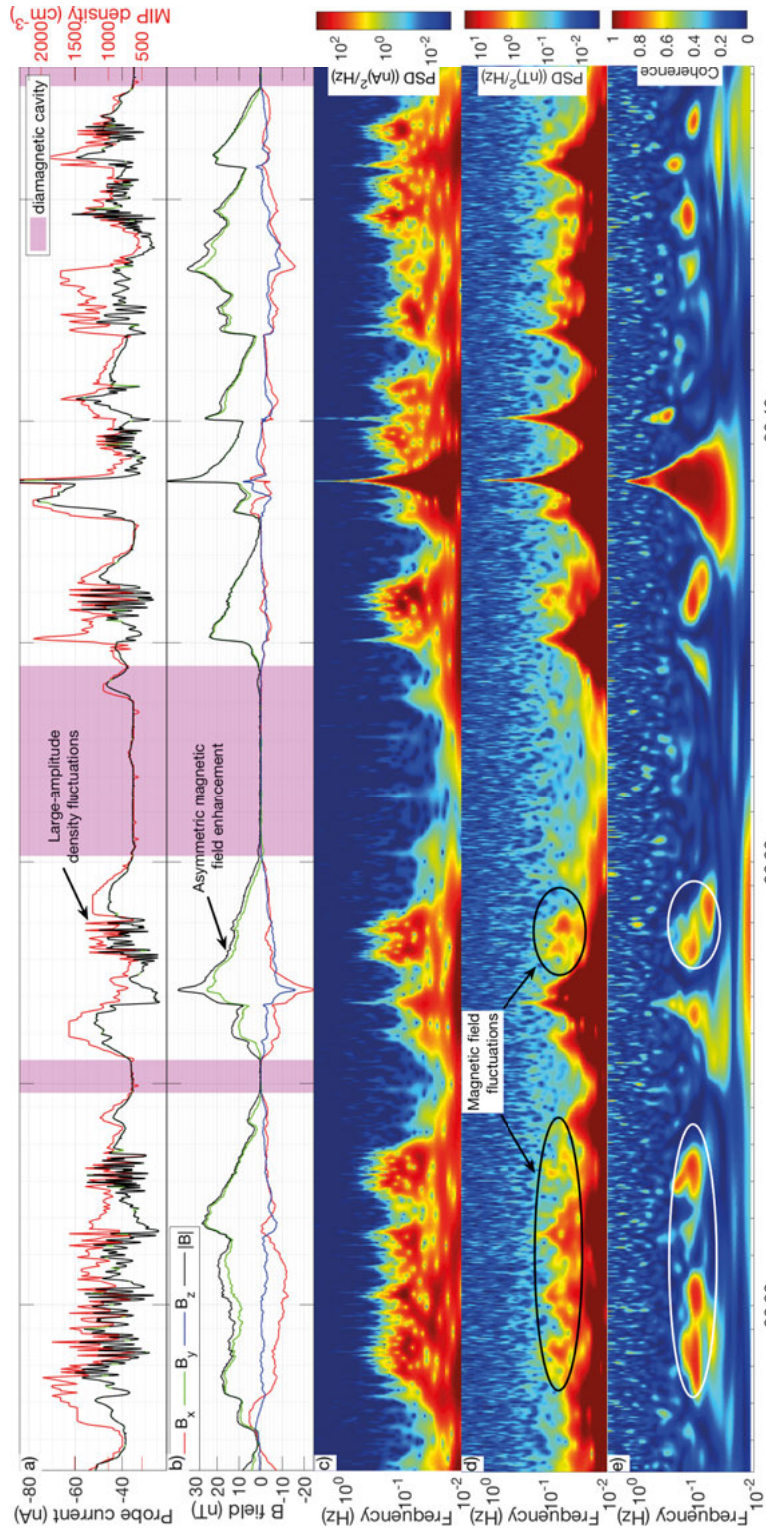

Figure 5.5. Paper IV: Wave observations near the diamagnetic cavity on Nov 20, 2015. a) MIP plasma density (red) and LAP probe current (black), b) magnetic field, c) wavelet scalogram of LAP1 current, d) wavelet scalogram of magnetic field e) wavelet coherence between LAP1 current and magnetic field (see Paper IV for explanation).

6. Sammanfattning på svenska
Summary in Swedish

Rymdsonden Rosetta var den europeiska rymdorganisationens (ESA) kometjägare. Under drygt två års tid åren 2014 – 2016 följde Rosetta kometen 67P/Churyumov-Gerasimenko på nära håll i dess bana runt solen, typiskt något tiotal till hundratal kilometer från kometkärnan. Detta gav en aldrig tidigare skådad möjlighet att närstudera en komet under en längre tid. Tidigare expeditioner till kometer, som t. ex. ESAs rymdsond Giotto som besökte Halleys komet 1986, var alla kortvariga förbiflygningar på stora avstånd, som minst runt 500 km. Med ombord på Rosetta fanns bland annat en uppsättning på fem instrument avsedda för observationer av plasmamiljön runt kometen, det s.k. Rosetta Plasma Consortium (RPC). Två av dessa instrument, Langmuirprobsinstrumentet (LAP) och en jonspektrometer (Ion Composition Analyzer, ICA), levererades och sköttes av svenska forskningsgrupper vid Institutet för Rymdfysik i Uppsala respektive Kiruna. Dessa två instrument, tillsammans med de övriga instrumenten i RPC och en neutralgasanalysator (ROSINA) har i denna avhandling använts för att studera plasmamiljön runt kometen.

Plasma är en gas i vilken elektroner separerats från sina atomkärnor, så att den består (åtminstone delvis) av elektriskt laddade partiklar: joner och elektroner. Plasma är således ett möjligt aggregationstillstånd (eller *fas*) hos materia, och alltså inte ett specifikt ämne. Jonisering av gas, så att plasma bildas, sker naturligt t. ex. vid blixtnedslag och (i begränsad omfattning) i eldslågor. Det kan också ske artificiellt, t. ex. i lysrör, plasmaskärmar och, förstås, i experimentella fusionsreaktorer, där de höga temperaturer som krävs för fusion innebär att plasma bildas. Teknik baserad på plasma används också allt oftare inom industrin, t. ex. vid olika typer av ytbehandlingar. Till skillnad från dessa tämligen begränsade exempel från jorden, är plasmatillståndet det vanligaste tillståndet för den materia vi kan observera ute i rymden. Solen består t. ex. huvudsakligen av plasma, och dess övre atmosfär läcker ständigt plasma som strömmar ut genom solsystemet i form av den s.k. solvinden. Solens UV-strålning bidrar också till jonisation av gas, t. ex. i de övre lagren av atmosfären runt jorden, den s.k. jonosfären, liksom runt många av de övriga planeterna, så att plasma bildas. Kometer är här inget undantag: De består av en blandning av is och stoft som blev över efter bildandet av de yttre planeterna (Jupiter, Saturnus, Uranus och Neptunus) och rör sig vanligtvis längs banor i solsystemets kalla ytterkanter, där de förblivit nedfrusna under miljarder år. Vissa av dem kan dock ibland komma på avvägar och passera genom det inre solsystemet,

där den ökade solstrålningen leder till sublimering (direkt avdunstning av fast materia, utan att först anta flytande form) av isen och bildandet av en flyktig atmosfär av gas och stoft, den s.k. koman; kometen sägs då ha blivit aktiv. Gasen i koman joniseras sedan (åtminstone delvis) av solens UV-strålning så att en jonosfärsliknande omgivning uppstår runt kometen, där plasma från kometen växelverkar med plasmat i solvinden.

Denna plasmamljö är unik i flera avseenden. Kometers ringa storlek (typiskt några hundra meter till några kilometer i diameter), och därmed svaga gravitationskraft, innebär att de inte kan hålla kvar sin atmosfär, som därför hela tiden läcker ut i rymden och skulle sina om den inte hela tiden fylldes på av nytt material som släpps ut från kometens yta. Detta ger upphov till en väldigt utsträckt och diffus jonosfär, vars växelverkan med solvinden sker över mycket stora avstånd (upp till flera hundratusen kilometer), mycket större än vad som typiskt är fallet vid planeterna och vissa av deras månar. Kometers avlånga banor runt solen gör också att de utsätts för mycket varierande mängd solinstrålning och därmed stora variationer i hur mycket gas och stoft som lämnar kometkärnan och bidrar till koman. Detta innebär att en långtidsstudie av det slag som Rosetta genomfört gör det möjligt att studera inte bara en, utan en hel följd av varierande plasmamiljöer som uppstår allteftersom kometen rör sig i sin bana runt solen.

Inom ramen för denna avhandling har vi bland annat använt mätningar av den elektrostatiska potentialen hos rymdfarkosten gentemot det omgivande plasmat för att studera elektrontemperatur och plasmatäthet i koman under expeditionens gång. Dessa har hittills överlag visat sig vara mycket lättare att tolka än mer direkta mätningar av täthet och elektrontemperatur med LAP, som dock också är möjliga och kommit till användning i vissa fall. Denna s.k. *rymdfarkostpotential* beror starkt på elektrontemperatur och täthet i det omgivande plasmat och kan därmed användas för få att åtminstone en grov uppskattning av dessa parametrar och deras utveckling över tid. Vi har funnit att rymdfarkostpotentialen mestadels är negativ under expeditionen, inte sällan med tiotals volt, vilket varslar om närvaron av ett bestånd av varma (runt 5 elektronvolt (eV), eller 50 000 K) elektroner i koman, även i de inre delarna (så långt in som Rosetta nådde). Detta skiljer sig från förutsägelser baserade på modeller från Halleys komet, där elektronerna var mycket kallare (0.01 – 0.1 eV, eller ca 100 – 1000 K). Skillnaden beror på att elektronkylningen, som huvudsakligen sker genom kollisioner med neutrala molekyler i den omgivande gasen, är mycket mindre effektiv vid 67P än vid den mycket mera aktivt utgasande Halley. Dock har även ett återkommande bestånd av kalla elektroner observerats, som tidvis samexisterar med det varma beståndet. Detta tyder på att effektiv elektronkylning trots allt pågick tidvis någonstans i koman innanför Rosetta, varpå de nedkylda elektronerna ibland lämnade detta allra innersta område och blandade sig med de varma elektronerna längre ut. Hur detta exakt går till är ännu inte helt klarlagt.

Vi fann också att den negativa rymdfarkostpotentialen relativt väl följde neutralgastätheten, åtminstone på tidsskalor motsvarande några timmar och längre, som i sin tur var tämligen variabel på grund av dygns- och säsongsmässiga variationer i utgasning över kometens yta, bl. a. en följd av dess oregelbundna form och lutande rotationsaxel gentemot banplanet. Detta vittnar om att plasmadynamiken på dessa lite längre tids- och rumsskalor dominerades av lokal produktion och radiell transport. På kortare tidsskalor, några minuter eller mindre, uppvisade plasmat dock mycket mer dynamik, som inte observerades i den neutrala gasen, och därmed får hänföras till komplicerad inre dynamik och kollektiv växelverkan (t. ex. turbulens och vågor) i plasmat självt, som vi ännu bara precis börjat förstå oss på.

En utmärkande egenskap hos rymplasma i allmänhet, och plasmamiljön runt kometer i synnerhet, är de komplicerade strukturer som uppstår i växelverkan mellan solvinden, dess magnetfält och plasmat som bildas lokalt genom jonisation av atmosfärisk gas. Ett typiskt exempel på detta är den så kallade *bogchocken*, som uppstår då ett supersoniskt flöde av gas (eller vätska) övergår till subsonisk hastighet till följd av inbromsning framför någon typ av hinder, t. ex. en komet eller annan himlakropp. Detta sker också t. ex. framför ett flygplan som färdas i överljudsfart; den karakteristiska "ljudbangen" som då uppstår är ett exempel på en bogchock, i detta fall i den neutrala gasen i jordens atmosfär. Bogchocken är ett exempel på ett s.k. *gränsskikt*, en tunn övergångszon som åtskiljer två områden med väsentligt olika egenskaper (supersoniskt jämte subsoniskt flöde i exemplet med bogchocken). Vid sådana gränsskikt sker ofta fysikaliska processer av mycket stort intresse, eftersom de i allmänhet betydligt mera överskådliga förhållanden som råder på vardera sidan om skiktet här bryter samman och uppdagar ny, ofta mer fundamental, fysik.

Ett annat gränsskikt som uppstår vid kometen, och helt saknar motsvarighet i vår vardag här på jorden, är den s.k. *diamagnetiska kaviteten*, ett område i komans innersta delar dit solvinden, och dess magnetfält, inte når och som därmed förblir i princip helt omagnetiserat. Dess existens förutsades teoretiskt redan på 1960-talet, men den enda observationen innan Rosettas ankomst till 67P var från Halleys komet, och ledde till en revidering av mekanismen bakom dess uppkomst: de teoretiska modellerna förutsåg att det dynamiska trycket från de utåt strömmande nybildade kometjonerna i den inre koman balanserade det magnetiska tryck som den magnetiserade solvinden bar med sig och på så vis skärmade av detta område och gav upphov till kaviteten. Vid Halley fann man att jonernas egna dynamiska tryck var otillräckligt för att bilda en kavitet av den ansenliga storlek man där observerade. Istället kom man fram till att det var trycket från den utströmmande ännu ej joniserade neutrala gasen som, via kollisioner med de vid kavitetsgränsen stagnerade kometjonerna, bidrog till att hålla emot solvinden och skärma av den innersta delen av koman från dess magnetfält.

En diamagnetisk kavitet har också observerats av Rosetta vid 67P, och en viktig fråga var huruvida den uppstod och betedde sig på samma sätt som vid Halley, med tanke på att 67P är en mycket mindre aktiv komet. Det visade sig att så inte alls var fallet. Kaviteten var i detta fall mycket mer dynamisk och nyckfull än vid Halley, och nådde vid åtskilliga tillfällen mycket längre ut än vad som verkade kunna förklaras av neutralgasens tryck på jonerna (även om det till viss del råder delade meningar om detta). Inom ramen för denna avhandling har vi använt Langmuirprobsinstrumentet (LAP), tillsammans med andra plasmainstrument ombord, för att undersöka flödeshastigheten hos kometjonerna i och omkring den diamagnetiska kaviteten. Vi fann typiska hastigheter (radiellt utåt från kometen) på ca 2 – 4 km/s, märkbart snabbare än neutralgasen, som bedömts röra sig med maximalt 1 km/s, troligen lägre (möjligen så lågt som ner mot 500 m/s). Detta visar att kopplingen mellan joner och neutraler, via kollisioner dem emellan, inte alls var så stark som väntat, och som krävts för att förklara kaviteten som en följd av neutralgasens tryck på jonerna. Då skulle man förvänta sig att jonerna flödade tillsammans med gasen, med samma hastighet. Dessutom rörde sig ju jonerna snabbare utåt än neutralerna, så ett eventuellt tryck från de senare skulle i så fall verka i fel riktning (inåt) för att kunna bidra till en eventuell tryckbalans mot magnetfältet vid kavtitetsgränsen. Vi har således visat att andra förklaringsmodeller måste till för att klargöra mekanismen bakom den diamagnetiska kaviteten vid 67P.

Vi har också studerat utpräglade vågor vi funnit i plasmat alldeles utanför kaviteten. Detta område är mycket dynamiskt och domineras av kraftiga återkommande (med några minuters mellanrum) förtätningar av plasmat och förstärkningar av magnetfältet, som orsakat mycket huvudbry. Vi har nyligen upptäckt kraftiga täthetsfluktuationer, mycket snabbare än dessa förtätningar, som typiskt förekommer under deras avtagande fas. Vi har studerat dessa i hopp om att utröna vad de är för något, hur de uppstår, och hur de påverkar det omgivande plasmat. Vi har använt moderna metoder för analys av plasmavågor för att klargöra deras egenskaper och föreslagit möjliga mekanismer bakom deras uppkomst och utbredning. Plasmavågor i allmänhet kan omfördela energi mellan olika partikelbestånd i plasmat och bidra till att forma plasmamiljön runt kometen, så varje observerat vågfenomen är av stort intresse och potentiellt värdefullt för att förstå kometplasmat, dess struktur och dynamik. Vi hoppas till exempel att eventuella insikter om vilka mekanismer som ligger bakom dessa vågor kan bidra till ökad förståelse av beskaffenheten hos detta, hittills dåligt förstådda, plasma som omgärdar kaviteten och där dessa vågor uppstår.

Bibliography

Alfven, H. (1957). "On the theory of comet tails." *Tellus* 9 (Cited on pages 30, 52, 53).

André, M. et al. (2017). "Lower hybrid waves at comet 67P/Churyumov-Gerasimenko". MNRAS 469, S29–S38.
DOI: 10.1093/mnras/stx868 (Cited on pages 44, 75).

Bagdonat, T. and U. Motschmann (2002). "From a Weak to a Strong Comet - 3d Global Hybrid Simulation Studies". *Earth Moon and Planets* 90, pp. 305–321.
DOI: 10.1023/A:1021578232282 (Cited on page 17).

Balogh, André and Rudolf A. Treumann (2013a). "Planetary Bow Shocks". In: *Physics of Collisionless Shocks: Space Plasma Shock Waves*. New York, NY: Springer New York, pp. 411–461. ISBN: 978-1-4614-6099-2.
DOI: 10.1007/978-1-4614-6099-2_10 (Cited on page 17).

Balogh, André and Rudolf A. Treumann (2013b). "The Heliospheric Termination Shock". In: *Physics of Collisionless Shocks: Space Plasma Shock Waves*. New York, NY: Springer New York, pp. 463–494. ISBN: 978-1-4614-6099-2.
DOI: 10.1007/978-1-4614-6099-2_11 (Cited on page 18).

Balsiger, H. et al. (1986). "Ion composition and dynamics at comet Halley". *Nature* 321, pp. 330–334.
DOI: 10.1038/321330a0 (Cited on pages 36, 38).

Balsiger, H. et al. (2007). "Rosina Rosetta Orbiter Spectrometer for Ion and Neutral Analysis". Space Sci. Rev. 128, pp. 745–801.
DOI: 10.1007/s11214-006-8335-3 (Cited on pages 21, 26).

Behar, E. et al. (2016). "Mass loading at 67P/Churyumov-Gerasimenko: A case study". Geophys. Res. Lett. 43, pp. 1411–1418.
DOI: 10.1002/2015GL067436 (Cited on page 41).

Behar, E. et al. (2017). "The birth and growth of a solar wind cavity around a comet - Rosetta observations". MNRAS 469, S396–S403.
DOI: 10.1093/mnras/stx1871 (Cited on pages 41, 43, 44, 48, 49, 75).

Berčič, L. et al. (2018). "Cometary ion dynamics observed in the close vicinity of comet 67P/Churyumov-Gerasimenko during the intermediate activity period". A&A 613, A57, A57.
DOI: 10.1051/0004-6361/201732082 (Cited on pages 44–46).

Beth, A. et al. (2018). "Comparative study of photo-produced ionosphere in the close environment of comets". A&A submitted (Cited on page 35).

Bieler, A. et al. (2015). "Abundant molecular oxygen in the coma of comet 67P/Churyumov-Gerasimenko". Nature 526, pp. 678–681.
DOI: 10.1038/nature15707 (Cited on page 27).

Biermann, L. (1951). "Kometenschweife und solare Korpuskularstrahlung". *Zeitschrift für Astrophysik* 29, p. 274 (Cited on page 30).

Biermann, L. et al. (1967). "The interactions of the solar wind with a comet". Sol. Phys. 1, pp. 254–284.
DOI: 10.1007/BF00150860 (Cited on pages 46, 55, 57).

Bockelee-Morvan, D. et al. (2004). "The composition of cometary volatiles". In: *Comets II*. Ed. by M. Festou et al. Univ. of Arizona Press, Tucson, pp. 391–423 (Cited on page 27).

Broiles, T. W. et al. (2016). "Statistical analysis of suprathermal electron drivers at 67P/Churyumov-Gerasimenko". MNRAS 462, S312–S322.
DOI: 10.1093/mnras/stw2942 (Cited on pages 24, 44).

Burch, J. L. et al. (2007). "RPC-IES: The Ion and Electron Sensor of the Rosetta Plasma Consortium". Space Sci. Rev. 128, pp. 697–712.
DOI: 10.1007/s11214-006-9002-4 (Cited on page 24).

Carr, C. et al. (2007). "RPC: The Rosetta Plasma Consortium". Space Sci. Rev. 128, pp. 629–647.
DOI: 10.1007/s11214-006-9136-4 (Cited on page 21).

Clark, G. et al. (2015). "Suprathermal electron environment of comet 67P/Churyumov-Gerasimenko: Observations from the Rosetta Ion and Electron Sensor". A&A 583, A24, A24.
DOI: 10.1051/0004-6361/201526351 (Cited on page 44).

Coates, A. J. (2017). "Pickup Particle Acceleration at Comets, Moons and Magnetospheres". In: *Journal of Physics Conference Series*. Vol. 900. Journal of Physics Conference Series, p. 012002.
DOI: 10.1088/1742-6596/900/1/012002 (Cited on page 40).

Coates, A. J. and G. H. Jones (2009). "Plasma environment of Jupiter family comets". Planet. Space Sci. 57, pp. 1175–1191.
DOI: 10.1016/j.pss.2009.04.009 (Cited on page 40).

Coates, A J et al. (2015). "Ion pickup observed at comet 67P with the Rosetta Plasma Consortium (RPC) particle sensors: similarities with previous observations and AMPTE releases, and effects of increasing activity". *Journal of Physics: Conference Series* 642.1, p. 012005 (Cited on page 40).

Coates, AJ (1995). "Heavy ion effects on cometary shocks". *Advances in Space Research* 15.8, pp. 403–413 (Cited on page 47).

Colangeli, L. et al. (2007). "The Grain Impact Analyser and Dust Accumulator (GIADA) Experiment for the Rosetta Mission: Design, Performances and First Results". Space Sci. Rev. 128, pp. 803–821.
DOI: 10.1007/s11214-006-9038-5 (Cited on page 21).

Cravens, T. E. (1986). "The physics of the cometary contact surface". In: *ESLAB Symposium on the Exploration of Halley's Comet*. Ed. by B. Battrick et al. Vol. 250. ESA Special Publication (Cited on pages 34, 35, 55).

Cravens, T. E. (1987). "Theory and observations of cometary ionospheres". *Advances in Space Research* 7, pp. 147–158.
DOI: 10.1016/0273-1177(87)90212-2 (Cited on pages 34, 35, 55).

Cravens, T. E. (1989). "A magnetohydrodynamical model of the inner coma of Comet Halley". J. Geophys. Res. 94, pp. 15025–15040.
DOI: 10.1029/JA094iA11p15025 (Cited on page 58).

Cravens, T. E. (1991). "Plasma processes in the inner coma". In: *IAU Colloq. 116: Comets in the post-Halley era*. Ed. by R. L. Newburn Jr. et al. Vol. 167. Astrophysics and Space Science Library, pp. 1211–1255.
DOI: 10.1007/978-0-7923-1165-2_50 (Cited on page 48).

Cravens, T. E. (2004). *Physics of solar system plasmas*. Cambridge University Press (Cited on pages 31, 32).

Deca, J. et al. (2017). "Electron and Ion Dynamics of the Solar Wind Interaction with a Weakly Outgassing Comet". Phys. Rev. Lett. 118.20, 205101, p. 205101.
DOI: 10.1103/PhysRevLett.118.205101 (Cited on pages 36, 51, 62).

Dello Russo, N. et al. (2000). "Water Production and Release in Comet C/1995 O1 Hale-Bopp". Icarus 143, pp. 324–337.
DOI: 10.1006/icar.1999.6268 (Cited on page 23).

Denton, R. E. et al. (2010). "Multiple harmonic ULF waves in the plasma sheet boundary layer: Instability analysis". J. Geophys. Res. Space Physics 115.A14, A12224, A12224.
DOI: 10.1029/2010JA015928 (Cited on page 75).

Eberhardt, P. and D. Krankowsky (1995). "The electron temperature in the inner coma of comet P/Halley." A&A 295, p. 795 (Cited on page 18).

Edberg, N. J. T. et al. (2015). "Spatial distribution of low-energy plasma around comet 67P/CG from Rosetta measurements". Geophys. Res. Lett. 42, 4263–4269.
DOI: 10.1002/2015GL064233 (Cited on pages 37, 38).

Edberg, N. J. T. et al. (2016a). "CME impact on comet 67P/Churyumov-Gerasimenko". MNRAS 462, S45–S56.
DOI: 10.1093/mnras/stw2112 (Cited on page 48).

Edberg, N. J. T. et al. (2016b). "Solar wind interaction with comet 67P: Impacts of corotating interaction regions". J. Geophys. Res. Space Physics 121, pp. 949–965.
DOI: 10.1002/2015JA022147 (Cited on pages 44, 54).

Elphic, R. C. et al. (1980). "The location of the dayside ionopause of Venus - Pioneer Venus Orbiter magnetometer observations". Geophys. Res. Lett. 7, pp. 561–564.
DOI: 10.1029/GL007i008p00561 (Cited on page 17).

Engelhardt, I. A. D. et al. (2018). "Cold electrons at comet 67P/Churyumov-Gerasimenko". *ArXiv e-prints* (Cited on pages 42, 44, 59, 62).

Eriksson, A. I. et al. (2007). "RPC-LAP: The Rosetta Langmuir Probe Instrument". Space Sci. Rev. 128, pp. 729–744.
DOI: 10.1007/s11214-006-9003-3 (Cited on page 24).

Eriksson, A. I. et al. (2017). "Cold and warm electrons at comet 67P/Churyumov-Gerasimenko". A&A 605, A15, A15.
DOI: 10.1051/0004-6361/201630159 (Cited on pages 24, 42, 73).

Flammer, K. R. and D. A. Mendis (1991). "A note on the mass-loaded MHD flow of the solar wind towards a cometary nucleus". Ap&SS 182, pp. 155–162.
DOI: 10.1007/BF00646450 (Cited on page 46).

Galand, M. et al. (1999). "The Ionosphere of Titan: Ideal Diurnal and Nocturnal Cases". Icarus 140, pp. 92–105.
DOI: 10.1006/icar.1999.6113 (Cited on page 62).

Galand, M. et al. (2016). "Ionospheric plasma of comet 67P probed by Rosetta at 3 au from the Sun". MNRAS 462, S331–S351.
DOI: 10.1093/mnras/stw2891 (Cited on page 73).

Gan, L. and T. E. Cravens (1990). "Electron energetics in the inner coma of comet Halley." J. Geophys. Res. 95, pp. 6285–6304 (Cited on page 18).

Gilet, N. et al. (2017). "Electrostatic Potential Radiated by a Pulsating Charge in a Two-Electron Temperature Plasma". *Radio Science* 52, pp. 1432–1448.
DOI: 10.1002/2017RS006294 (Cited on pages 24, 42).

Glassmeier, K.-H. et al. (2007a). "RPC-MAG The Fluxgate Magnetometer in the ROSETTA Plasma Consortium". Space Sci. Rev. 128, pp. 649–670.
DOI: 10.1007/s11214-006-9114-x (Cited on page 24).

Glassmeier, K.-H. et al. (2007b). "The Rosetta Mission: Flying Towards the Origin of the Solar System". Space Sci. Rev. 128, pp. 1–21.
DOI: 10.1007/s11214-006-9140-8 (Cited on page 20).

Goetz, C. et al. (2016a). "First detection of a diamagnetic cavity at comet 67P/Churyumov-Gerasimenko". A&A 588, A24, A24.
DOI: 10.1051/0004-6361/201527728 (Cited on page 57).

Goetz, C. et al. (2016b). "Structure and evolution of the diamagnetic cavity at comet 67P/Churyumov-Gerasimenko". MNRAS 462, S459–S467.
DOI: 10.1093/mnras/stw3148 (Cited on page 74).

Goetz, C. et al. (2017). "Evolution of the magnetic field at comet 67P/Churyumov-Gerasimenko". MNRAS 469, S268–S275.
DOI: 10.1093/mnras/stx1570 (Cited on pages 51, 54).

Goldstein, B. E. et al. (1989). "Observations of a shock and a recombination layer at the contact surface of Comet Halley". J. Geophys. Res. 94, pp. 17251–17257.
DOI: 10.1029/JA094iA12p17251 (Cited on page 58).

Gombosi, T. I. (2015). "Physics of Cometary Magnetospheres". In: *Magnetotails in the Solar System*. Ed. by A. Keiling et al. Vol. 207. Washington DC American Geophysical Union Geophysical Monograph Series, pp. 169–

188.
DOI: 10.1002/9781118842324.ch10 (Cited on pages 17, 34, 35, 58, 59).
Grasset, O. et al. (2013). "JUpiter ICy moons Explorer (JUICE): An ESA mission to orbit Ganymede and to characterise the Jupiter system". Planet. Space Sci. 78, pp. 1–21.
DOI: 10.1016/j.pss.2012.12.002 (Cited on page 19).
Grensemann, M. G. and G. Schwehm (1993). "Giotto's second encounter: The mission to comet P/Grigg-Skjellerup". J. Geophys. Res. 98, p. 20.
DOI: 10.1029/93JA02528 (Cited on page 17).
Gulkis, S. et al. (2007). "MIRO: Microwave Instrument for Rosetta Orbiter". Space Sci. Rev. 128, pp. 561–597.
DOI: 10.1007/s11214-006-9032-y (Cited on page 21).
Haerendel, G. (1987). "Plasma transport near the magnetic cavity surrounding comet Halley". Geophys. Res. Lett. 14, pp. 673–676.
DOI: 10.1029/GL014i007p00673 (Cited on page 55).
Hajra, R. et al. (2018). "Dynamic unmagnetized plasma in the diamagnetic cavity around comet 67P/Churyumov-Gerasimenko". MNRAS 475, 4140–4147.
DOI: 10.1093/mnras/sty094 (Cited on page 74).
Hanner, M. S. and J. P. Bradley (2004). "Composition and mineralogy of cometary dust". In: *Comets II*. Ed. by M. Festou et al. Univ. of Arizona Press, Tucson, pp. 555–564 (Cited on page 27).
Hansen, K. C. et al. (2016). "Evolution of water production of 67P/Churyumov-Gerasimenko: An empirical model and a multi-instrument study". MNRAS 462, S491–S506.
DOI: 10.1093/mnras/stw2413 (Cited on pages 23, 69).
Hässig, M et al. (2015). "Time variability and heterogeneity in the coma of 67P/Churyumov-Gerasimenko". *Science* 347.6220, aaa0276 (Cited on page 23).
Henri, P. et al. (2017). "Diamagnetic region(s): structure of the unmagnetized plasma around Comet 67P/CG". MNRAS 469, S372–S379.
DOI: 10.1093/mnras/stx1540 (Cited on pages 73, 74).
Heritier, K. L. et al. (2017). "Ion composition at comet 67P near perihelion: Rosetta observations and model-based interpretation". MNRAS 469, S427–S442.
DOI: 10.1093/mnras/stx1912 (Cited on page 73).
Heritier, K. L. et al. (2018). "Plasma source and loss at comet 67P during the Rosetta mission". A&A Forthcoming article.
DOI: 10.1051/0004-6361/201832881 (Cited on pages 71, 73).
Hirao, K. and T. Itoh (1987). "The Sakigake / Suisei Encounter with Comet P/Halley". A&A 187, p. 39 (Cited on page 17).
Ip, W. H. and W. I. Axford (1990). "The plasma." In: *Physics and Chemistry of Comets*. Ed. by W. F. Huebner, pp. 177–232 (Cited on page 55).

Ip, W.-H. and W. I. Axford (1987). "The formation of a magnetic-field-free cavity at Comet Halley". *Nature* 325, p. 418.
DOI: 10.1038/325418a0 (Cited on page 55).

Israelevich, P. L. et al. (1992). "On the flow around the diamagnetic cavity of Comet Halley". J. Geophys. Res. 97, p. 17.
DOI: 10.1029/92JA01209 (Cited on page 55).

Itikawa, Y. and N. Mason (2005). "Cross Sections for Electron Collisions with Water Molecules". *Journal of Physical and Chemical Reference Data* 34, pp. 1–22.
DOI: 10.1063/1.1799251 (Cited on page 31).

Jia, Y. D. et al. (2009). "Study of the 2007 April 20 CME-Comet Interaction Event with an MHD Model". ApJ 696.1, p. L56 (Cited on page 54).

Karlsson, T. et al. (2017). "Rosetta measurements of lower hybrid frequency range electric field oscillations in the plasma environment of comet 67P". Geophys. Res. Lett. 44, pp. 1641–1651.
DOI: 10.1002/2016GL072419 (Cited on page 44).

Keller, H. U. et al. (2007). "OSIRIS The Scientific Camera System Onboard Rosetta". Space Sci. Rev. 128, pp. 433–506.
DOI: 10.1007/s11214-006-9128-4 (Cited on page 21).

Kissel, J. et al. (2007). "Cosima High Resolution Time-of-Flight Secondary Ion Mass Spectrometer for the Analysis of Cometary Dust Particles onboard Rosetta". Space Sci. Rev. 128, pp. 823–867.
DOI: 10.1007/s11214-006-9083-0 (Cited on page 21).

Koenders, C. et al. (2013). "Revisiting cometary bow shock positions". Planet. Space Sci. 87, pp. 85–95. ISSN: 0032-0633.
DOI: http://dx.doi.org/10.1016/j.pss.2013.08.009 (Cited on pages 17, 47).

Koenders, C. et al. (2015). "Dynamical features and spatial structures of the plasma interaction region of 67P/Churyumov-Gerasimenko and the solar wind". Planet. Space Sci. 105, pp. 101–116.
DOI: 10.1016/j.pss.2014.11.014 (Cited on pages 43, 44, 46, 51, 52, 55, 58, 59, 61).

Koenders, C. et al. (2016). "Magnetic field pile-up and draping at intermediately active comets: results from comet 67P/Churyumov-Gerasimenko at 2.0 AU". MNRAS 462, S235–S241.
DOI: 10.1093/mnras/stw2480 (Cited on pages 53, 54).

Kofman, W. et al. (2007). "The Comet Nucleus Sounding Experiment by Radiowave Transmission (CONSERT): A Short Description of the Instrument and of the Commissioning Stages". Space Sci. Rev. 128, pp. 413–432.
DOI: 10.1007/s11214-006-9034-9 (Cited on page 21).

Krankowsky, D. et al. (1986). "In situ gas and ion measurements at comet Halley". Nature 321, pp. 326–329.
DOI: 10.1038/321326a0 (Cited on page 23).

Lisse, C. M. et al. (2004). "X-ray and extreme ultraviolet emission from comets". In: *Comets II*. Ed. by M. Festou et al. Univ. of Arizona Press, Tucson, pp. 631–643 (Cited on page 31).

Mauk, B. H. et al. (2009). "Fundamental Plasma Processes in Saturn's Magnetosphere". In: *Saturn from Cassini-Huygens*. Ed. by Michele K. Dougherty et al. Dordrecht: Springer Netherlands, pp. 281–331. ISBN: 978-1-4020-9217-6.
DOI: 10.1007/978-1-4020-9217-6_11 (Cited on page 53).

McComas, D. J. et al. (2012). "The Heliosphere's Interstellar Interaction: No Bow Shock". *Science* 336, p. 1291.
DOI: 10.1126/science.1221054 (Cited on page 18).

Mendis, D. A. (1988). "A postencounter view of comets". *Annual review of astronomy and astrophysics* 26, pp. 11–49.
DOI: 10.1146/annurev.aa.26.090188.000303 (Cited on page 46).

Neubauer, F. M. et al. (1986). "First results from the Giotto magnetometer experiment at comet Halley". *Nature* 321, pp. 352–355.
DOI: 10.1038/321352a0 (Cited on pages 56, 57).

Nilsson, H. et al. (2007). "RPC-ICA: The Ion Composition Analyzer of the Rosetta Plasma Consortium". Space Sci. Rev. 128, pp. 671–695.
DOI: 10.1007/s11214-006-9031-z (Cited on page 24).

Nilsson, H. et al. (2015a). "Birth of a comet magnetosphere: A spring of water ions". *Science* 347.1, aaa0571, aaa0571.
DOI: 10.1126/science.aaa0571 (Cited on pages 41, 42, 45).

Nilsson, H. et al. (2015b). "Evolution of the ion environment of comet 67P/Churyumov-Gerasimenko. Observations between 3.6 and 2.0 AU". A&A 583, A20, A20.
DOI: 10.1051/0004-6361/201526142 (Cited on page 45).

Nilsson, H. et al. (2017). "Evolution of the ion environment of comet 67P during the Rosetta mission as seen by RPC-ICA". MNRAS 469, S252–S261.
DOI: 10.1093/mnras/stx1491 (Cited on pages 45, 48, 49, 51).

Omidi, N. et al. (1986). "The effect of heavy ions on the formation and structure of cometary bow shocks". Icarus 66, pp. 165–180.
DOI: 10.1016/0019-1035(86)90016-3 (Cited on page 40).

Reinhard, R. (1986). "The Giotto encounter with comet Halley". *Nature* 321, pp. 313–318.
DOI: 10.1038/321313a0 (Cited on page 17).

Richter, I. et al. (2011). "Deep Space 1 at comet 19P/Borrelly: Magnetic field and plasma observations". Planet. Space Sci. 59, pp. 691–698.
DOI: 10.1016/j.pss.2011.02.001 (Cited on page 17).

Riedler, W. et al. (2007). "MIDAS The Micro-Imaging Dust Analysis System for the Rosetta Mission". Space Sci. Rev. 128, pp. 869–904.
DOI: 10.1007/s11214-006-9040-y (Cited on page 21).

Roennmark, K. (1982). *Waves in homogeneous, anisotropic multicomponent plasmas (WHAMP)*. Tech. rep. (Cited on pages 63, 75).

Russell, C. T. (2013). "Planetary Bow Shocks". In: *Collisionless Shocks in the Heliosphere: Reviews of Current Research*. American Geophysical Union (AGU), pp. 109–130. ISBN: 9781118664179.
DOI: 10.1029/GM035p0109 (Cited on page 17).

Russell, C. T. et al. (1986). "Near-tail reconnection as the cause of cometary tail disconnections". J. Geophys. Res. 91, pp. 1417–1423.
DOI: 10.1029/JA091iA02p01417 (Cited on page 54).

Sagdeev, R. Z. et al. (1987). "Vega 1 and Vega 2 spacecraft encounters with comet Halley." *Soviet Astronomy Letters* 12, pp. 243–247 (Cited on page 17).

Schunk, Robert and Andrew Nagy (2009). *Ionospheres: physics, plasma physics, and chemistry*. Cambridge university press (Cited on page 31).

Sierks, Holger et al. (2015). "On the nucleus structure and activity of comet 67P/Churyumov-Gerasimenko". *Science* 347.6220, aaa1044 (Cited on page 23).

Sjögren, A. et al. (2012). "Simulation of Potential Measurements Around a Photoemitting Spacecraft in a Flowing Plasma". *IEEE Transactions on Plasma Science* 40, pp. 1257–1261.
DOI: 10.1109/TPS.2012.2186616 (Cited on pages 67, 69).

Stenberg Wieser, G. et al. (2017). "Investigating short-time-scale variations in cometary ions around comet 67P". MNRAS 469, S522–S534.
DOI: 10.1093/mnras/stx2133 (Cited on pages 24, 25).

Stern, S. A. et al. (2007). "Alice: The rosetta Ultraviolet Imaging Spectrograph". Space Sci. Rev. 128, pp. 507–527.
DOI: 10.1007/s11214-006-9035-8 (Cited on page 21).

Szegö, K. et al. (2000). "Physics of Mass Loaded Plasmas". Space Sci. Rev. 94, pp. 429–671 (Cited on page 19).

Taylor, M. G. G. T. et al. (2017). "The Rosetta mission orbiter science overview: the comet phase". *Philosophical Transactions of the Royal Society of London Series A* 375, 20160262, p. 20160262.
DOI: 10.1098/rsta.2016.0262 (Cited on page 20).

Tenishev, V. et al. (2008). "A Global Kinetic Model for Cometary Comae: The Evolution of the Coma of the Rosetta Target Comet Churyumov-Gerasimenko throughout the Mission". ApJ 685, pp. 659–677.
DOI: 10.1086/590376 (Cited on pages 29, 34).

Trotignon, J. G. et al. (2007). "RPC-MIP: the Mutual Impedance Probe of the Rosetta Plasma Consortium". Space Sci. Rev. 128, pp. 713–728.
DOI: 10.1007/s11214-006-9005-1 (Cited on page 24).

Tsurutani, B. T. (1991). "Comets - A laboratory for plasma waves and instabilities". *Washington DC American Geophysical Union Geophysical Monograph Series* 61, pp. 189–209 (Cited on page 40).

van Buren, D. (1993). “Stellar Wind Bow Shocks”. In: *Massive Stars: Their Lives in the Interstellar Medium*. Ed. by J. P. Cassinelli and E. B. Churchwell. Vol. 35. Astronomical Society of the Pacific Conference Series, p. 315 (Cited on page 16).

Vigren, E. (2018). “Analytic model of comet ionosphere chemistry”. A&A Forthcoming article.
DOI: 10.1051/0004-6361/201832704 (Cited on pages 71, 73).

Vigren, E. and A. I. Eriksson (2017). “A 1D Model of Radial Ion Motion Interrupted by Ion-Neutral Interactions in a Cometary Coma”. ApJ 153, 150, p. 150.
DOI: 10.3847/1538-3881/aa6006 (Cited on pages 35, 46, 61, 71).

Vigren, E. and A. I. Eriksson (2018). “On the Ion-Neutral Coupling in Cometary Comae”. MNRAS in review (Cited on page 35).

Vigren, E. and M. Galand (2013). “Predictions of Ion Production Rates and Ion Number Densities within the Diamagnetic Cavity of Comet 67P/Churyumov-Gerasimenko at Perihelion”. ApJ 772, 33, p. 33.
DOI: 10.1088/0004-637X/772/1/33 (Cited on page 73).

Vigren, E. et al. (2015). “On the Electron-to-Neutral Number Density Ratio in the Coma of Comet 67P/Churyumov-Gerasimenko: Guiding Expression and Sources for Deviations”. ApJ 812, 54, p. 54.
DOI: 10.1088/0004-637X/812/1/54 (Cited on pages 36, 37, 73).

Vigren, E. et al. (2017). “Effective ion speeds at 200-250 km from comet 67P/Churyumov-Gerasimenko near perihelion”. MNRAS 469, S142–S148.
DOI: 10.1093/mnras/stx1472 (Cited on pages 35, 46).

Voelzke, M. R. (2005). “Disconnection Events Processes in Cometary Tails”. *Earth Moon and Planets* 97, pp. 399–409.
DOI: 10.1007/s11038-006-9073-y (Cited on page 54).

von Rosenvinge, T. T. et al. (1986). “The International Cometary Explorer Mission to Comet Giacobini-Zinner”. *Science* 232, pp. 353–356.
DOI: 10.1126/science.232.4748.353 (Cited on page 17).

Whipple, F. L. (1950). “A comet model. I. The acceleration of Comet Encke”. ApJ 111, pp. 375–394.
DOI: 10.1086/145272 (Cited on page 27).

Yang, L. et al. (2016). “Observations of high-plasma density region in the inner coma of 67P/Churyumov-Gerasimenko during early activity”. MNRAS 462, S33–S44.
DOI: 10.1093/mnras/stw2046 (Cited on page 42).

Acta Universitatis Upsaliensis

Digital Comprehensive Summaries of Uppsala Dissertations from the Faculty of Science and Technology 1694

Editor: The Dean of the Faculty of Science and Technology

A doctoral dissertation from the Faculty of Science and Technology, Uppsala University, is usually a summary of a number of papers. A few copies of the complete dissertation are kept at major Swedish research libraries, while the summary alone is distributed internationally through the series Digital Comprehensive Summaries of Uppsala Dissertations from the Faculty of Science and Technology. (Prior to January, 2005, the series was published under the title "Comprehensive Summaries of Uppsala Dissertations from the Faculty of Science and Technology".)

Distribution: publications.uu.se
urn:nbn:se:uu:diva-356426

ACTA
UNIVERSITATIS
UPSALIENSIS
UPPSALA
2018